Boundary layer reattachment in hypersonic flow.

Roger Kingsford Fancett.

B.Sc.(Eng).

January 1968.

A thesis submitted for the Degree of Doctor of Philosophy in the Faculty of Engineering of the University of London.

Abstract

The thesis describes a detailed experimental study of wedge and step separated flows performed in a hypersonic gun tunnel. Reattachment pressure and heat transfer distributions and pressures within the shear layer have been measured at Mach numbers of 8.2 and 9.7 using conical and contoured nozzle flows. The suitability of an intermittent facility for such studies has been established. The reattachment of a straight separating shear layer was studied and certain properties have been correlated with the external Reynolds number in both the laminar and transitional flow regimes. The effects of conicity on the separated length are shown to be severe and the need for small side plates is established. An equivalent axisymmetric model was used to check side plate effectiveness. The reattachment pressure rise parameter was measured and found to be strongly affected by the state of the shear layer. For the fully laminar flows, the pressure distribution through reattachment was smooth and the reattachment point of the dividing streamline was at the top of the pressure rise as assumed by Chapman. If, however, the shear layer was transitional, then the pressure distribution displayed a kink and the reattachment pressure was below the peak value. In this case, the reattachment parameter was found to be a function of flap angle and Reynolds number and was correlated in terms of these parameters. The variation of the separated length with Reynolds number exhibited opposite trends in the laminar and

transitional flow régimes and a criterion is suggested to define the state of the flow. The measured and calculated laminar pressure distributions and peak heat transfer rates are compared. The variation of the separated length with flap angle and the growth rate of the shear layer have been predicted by Cooke's theory. Taking the pressure rise parameter as unity and assuming the 'dead air' temperature to be equal to the wall value, good agreement between theory and experiment was obtained for cavity depths greater than five times the boundary layer thickness at separation.

Acknowledgements

The author would like to thank his supervisor, Mr. J.L. Stollery, most sincerely for his constant interest and the many helpful suggestions which he has made in the course of the present study.

Thanks are also due to Drs. D.A. Needham and B.E. Richards who have helped the author, particularly in discussions on the experimental problems encountered.

The author expresses his gratitude for the services of the library staff and also the staff of the Aeronautics Department workshop, particularly Mr. F. Fone, for the extreme care taken in constructing the models.

The author wishes to express his sincere gratitude to his wife, Lesley, for typing the thesis and for the care and patience which she has employed during the course of this work, and finally, to record his appreciation of the help given by Dr. T. Opatowski in the printing of the thesis.

LIST OF CONTENTS

		Page
Abstract		2
Acknowledgements		4
List of Illustrations		7
Notation		9
1.	INTRODUCTION	12
2.	REVIEW OF THE LITERATURE	14
3.	THEORETICAL STUDIES	18
3.1.	Characteristics of the Separated Flow	18
3.1.1.	Separated length	19
3.1.2.	Rate of growth of the shear layer	25
3.2.	Reattachment Pressure Distribution	26
3.3.	Heat Transfer Characteristics	31
3.3.1.	Heat transfer rate distribution	31
3.3.2.	Peak heat transfer rate	34
3.3.3.	Effect of reattachment angle	37
4.	EXPERIMENTAL WORK	41
4.1.	The Hypersonic Gun Tunnel	41
4.1.1.	Description	41
4.1.2.	Tables of test conditions	43
4.2.	Description of Models	45
4.3.	Instrumentation	47
4.4.	Flow Visualisation Techniques	48
4.4.1.	Schlieren photography	48
4.4.2.	High speed ciné photography	49
4.4.3.	Surface visualisation	49

Page

5. RESULTS AND DISCUSSION 52

5.1. Cylinder and Wedge Studies in Uniform Flow 52

5.1.1. Separated length 54

5.1.2. Influence of transition 56

5.1.2.1 Location of transition 57

5.1.2.2 Flow establishment time 58

5.1.2.3 Shear layer stability 58

5.1.3. Heat transfer rate distributions 59

5.2. Straight Separations in Conical Flow 61

5.2.1. Upstream influence - step height effect 62

5.2.2. Separated length 65

5.2.3. Influence of Reynolds number 67

5.2.4. Effect of side plates 70

5.3. Straight Separations in Uniform Flow 71

5.3.1. Effect of side plates 71

5.3.2. Separated length - correlation with Cooke's theory 74

5.3.3. Pitot pressure profiles of the attached and separated layers 78

5.3.4. Influence of shear layer transition 82

5.3.5. The reattachment parameter 89

5.3.6. Pressure and heat transfer rate distributions 94

5.3.6.1 Reattachment pressure distribution 95

5.3.6.2 Reattachment heat transfer rate distribution 98

5.3.7. Comparison between conical and uniform flows 104

6. CONCLUSIONS 106

List of References 110

Appendix A 117

List of Illustrations

		Page
1	Sketch of separated supersonic flow field.	118
2	Dividing streamline velocity ratio.	119
3	Influencing parameters of the separated laminar flow.	120
4	Growth of the mixing layer.	123
5	Mixing layer velocity and density profiles.	124
6	Variation of peak heat transfer rate with flap angle.	126
7	Free stream unit Reynolds number at $M_\infty = 8{\cdot}2$.	127
8	Wedge and rearward-facing step models.	128
9	Axisymmetric and half-scale rearward-facing step models.	129
10	Flow visualisation techniques.	130
11	Pitot pressure traverses behind a cylinder at $M_\infty = 8{\cdot}2$ and $Re/in. = 0{\cdot}24 \times 10^6$.	131
12	Schlieren photograph of wedge-separated flow at $M = 8{\cdot}2$.	133
13	Correlation of the wedge separated length in terms of Reynolds number.	134
14	Variation of transition with unit Reynolds number for an attached boundary layer.	135
15	Pitot profiles of the wedge boundary layer at $M = 5{\cdot}7$ and $Re_{x1} = 1{\cdot}45 \times 10^6$.	136
16	Centre-line heat transfer distributions down a step and wedge base for laminar and transitional separations.	137
17	Effect of step height on the straight-separated flow at $M = 9{\cdot}7$ and $Re/in. = 0{\cdot}24 \times 10^6$.	139
18	Schlieren photographs demonstrating step height effect on straight separations at $M = 9{\cdot}7$.	141
19	Correlation of straight-separated length and reattachment angle for conical flow at $M = 9{\cdot}7$.	143
20	Schlieren photographs illustrating the variation of separated length with flap angle at $M = 9{\cdot}7$.	144
21	The independence of the separated length on attached flow length in a $M = 9{\cdot}7$ conical flow.	147
22	Reynolds number effect on the length of straight separations at $M = 8{\cdot}2$ and $9{\cdot}7$.	148
23	Side plate similarity in conical flow at $M = 9{\cdot}7$.	149

		Page
24	Oscilloscope traces of the pressure transducer outputs.	150
25	Transverse and streamwise pressure distributions in separated flow at M = 8·2 - side plate effects.	151
26	Photographs of a straight laminar separation from the axisymmetric rearward-facing step model at M = 8·2.	153
27	Correlation of straight-separated length and reattachment angle in uniform flow at M = 8·2.	154
28	Relation between reattachment peak pressure ratio and flap angle at M = 8·2.	155
29	Variation of laminar separated length with reattachment pressure rise for M = 8·2.	156
30	Correlation of laminar separated length in terms of reattachment angle and comparison with theory.	157
31	Pitot pressure and Mach number profiles in the attached and separated regions of laminar flow.	158
32	Variation of base properties in relation to transition location.	163
33	Reattachment pressure rise parameter as a function of flap angle and Reynolds number.	165
34	Correlation of the reattachment parameter in the laminar, transitional and turbulent régimes at M = 8·2.	166
35	Pressure distributions in the separated region and location of the reattachment point at M = 8·2.	167
36	Laminar and transitional pressure distributions for various values of Reynolds number at M = 8·2.	171
37	The effect of flap angle on the pressure distributions in the step-separated flow at M = 8·2.	172
38	Laminar pressure distribution of the straight-separating flow - comparison of experiment with theory at M = 8·2.	173
39	Flat plate heat transfer distributions in laminar flow and comparison with theory.	175
40	Reattachment heat transfer distributions for various unit Reynolds number and comparison with theory.	176
41	Comparison of pressure and heat transfer distributions for laminar and transitonal reattachments at $\alpha_w = 10{\cdot}4^{\circ}$.	179
42	Effect of flap angle on the reattachment heat transfer distribution at M = 8·2.	180
43	Correlation of the reattachment peak heat transfer rate with the boundary layer thickness at separation.	182

Notation

Symbols

a	speed of sound.
C	constant in the temperature - viscosity relation, defined by equation 3.1(i).
C_f	skin friction coefficient.
C_p	pressure coefficient.
c_p	specific heat at constant pressure.
D	cylinder diameter.
h	step height or half the wedge base height.
L	streamwise distance measured downstream of the step.
L_{sep}	length of the separated layer.
$L_{s.h}$	step to hinge height.
L_t	distance of transition point from the leading edge.
L_r	distance of reattachment point from the leading edge.
M	Mach number.
N	reattachment parameter $\left[= \frac{p_r - p_2}{p_3 - p_2}\right]$
n	θ_2/θ_1
Pr	Prandtl number.
p	pressure.
p_o	pitot pressure.
$\dot{q}$	heat transfer rate.
R	reattachment point.
Re	Reynolds number.
St	Stanton number.
T	absolute temperature.
u	velocity in the x - direction.
v	velocity in the y - direction.
w	total temperature ratio $T_t(y)/T_{t_2}$
x	distance along the surface from the leading edge.
x_1	distance between the step and leading edge.
y	distance measured normal to the surface.

α_w reattachment flap angle.

γ ratio of specific heats.

δ boundary layer thickness.

δ^* boundary layer displacement thickness.

η normal distance parameter (= y/δ)

θ boundary layer momentum thickness.

μ viscosity.

ν kinematic viscosity.

τ shear stress (= $\mu \partial u/\partial y$)

Subscripts

A attached value.

av average of quantity.

1 undisturbed conditions upstream of step.

2 external to the shear layer.

3 downstream of reattachment zone.

4 initial driver conditions.

b initial conditions in the barrel.

∞ free stream.

* ratio of quantity to value at edge of shear layer.

aw adiabatic wall.

d 'dead air' region.

e outer edge of boundary layer or shear layer.

f.p flat plate.

l shear layer thickness below the dividing streamline.

r reattachment point.

s separation point.

st stagnation point.

T total shear layer thickness.

t total (or reservoir) conditions.

u shear layer thickness above the dividing streamline.

w wall.

Superscripts

–	conditions along the dividing streamline of the shear layer.
*	conditions evaluated at a 'reference temperature', defined by equation 3.15.

1. INTRODUCTION

In the field of aerodynamics, one of the most significant problems at present is that of flow separation. This complex mechanism is of fundamental importance to the aeronautical engineer as its occurrence can seriously affect the design performance of an aerodynamic surface. For this reason, a concerted effort is being made to understand, in detail, the characteristics and effects of flow separation.

Flow separation is induced by the action of an adverse pressure gradient and when this condition is present it is essential to know whether or not boundary layer separation will occur, and to what extent. A discontinuity in body geometry, which occurs in wedge compression corner and step flows, can induce pressure gradients severe enough to cause boundary layer separation. Many problems arise from flow separation including loss of control surface effectiveness, aerodynamic instability, base pressure drag and, particularly at hypersonic speeds, the occurrence of extremely high reattachment heat transfer rates.

Until now, the bulk of the theoretical studies have been made at subsonic and low supersonic Mach numbers. In order to test the reliability of the theoretical work thoroughly the need was felt for detailed experimental data at hypersonic Mach numbers where it is easier to achieve fully laminar flow.

Theoretical studies have been directed towards the solution

of fully laminar and turbulent separations, the former having received most attention as it may be treated analytically without requiring empirical information. Transition, which might be provoked by boundary layer separation, is known to have a substantial effect on the flow and, at present, defies a comprehensive theoretical solution.

One method of solution of laminar separations is the dividing streamline concept in which the flow is divided into separate regions, each of which is analysed separately. This approach, which requires a detailed understanding of the reattachment pressure rise of the shear layer, was originally proposed by Chapman et al. in 1957. Cooke (1963) employed momentum integral techniques to evaluate the velocity distribution along the dividing streamline and used the reattachment relation suggested by Chapman et al.

The aim of this study was to investigate, in detail, the reattachment of a laminar shear layer at hypersonic speeds, particularly the conditions at the reattachment point. It was hoped that this information would provide a check on the validity of the assumptions made by Cooke in developing his theory and allow the prediction of the scale of the separated flow. The scale of the flow geometry was measured in both conical and uniform flow and the effect of such influencing parameters as free stream Reynolds number were determined. The effect of shear layer transition on the separated length was investigated in the hope of defining the state of reattachment.

2. REVIEW OF THE LITERATURE

The original similarity solution of the laminar mixing of a compressible fluid was proposed by Chapman in 1951. Since then, this idea has been developed for supersonic laminar and turbulent separated flows by a number of authors. Notable amongst these contributions is the work of Cooke (1963) in which he extended Chapman's analysis to include the effects of a finite initial thickness shear layer, and enabled estimates to be made of the scale of separation. The dividing streamline approach requires a specific understanding of the conditions at reattachment and relatively little data concerning this region is available, particularly at hypersonic speeds.

Foremost among the parameters requiring study is the reattachment parameter N, originally proposed by Nash (1962) for turbulent flows. Recent experimental results, such as those of White (1965) have indicated this parameter to be less than unity, thus contradicting Chapman's original assumption.

More recently, other methods of solution of the separated flow problem have been proposed which regard the interaction as a whole and do not require a definition of N. The moment of momentum solution of Lees et al. (1964) is a notable example and Childs et al. (1966) have also avoided the use of N by proposing a control volume analysis of the separation "bubble". The various theoretical models considered in this study are discussed in Section 3.

Various authors have studied the effect of transition on the base flow mechanism (see Section 5.3.4.), and although definite trends have been established, a certain controversy exists concerning their interpretation.

The most relevant reports of experimental studies are listed in the following table.

Experimental studies concerning step and base separations.

Reference	Model	M_∞	Re_{x_1}	$\frac{x_1}{h}$	Location of transition	Remarks
Bogdonoff (1952)	cone - cylinder	2.95	0.7×10^6 - 10 "	6.72	boundary layer, shear layer and fully turbulent	no fully lam. reattmts., transition at separation for $Re_{x_1} = 1.6 \times 10^6$
Carrière (1965)	flapped cavity	2.2 - 3.5	——	——	turbulent	two critical points at reattachment. length of reattachment vs. shear layer thickness
Carrière et al. (1961)	"	"	——	——	"	$T_t(y)$ variable thro' mixing region. boundary layer thickness effects

CONTINUED OVER

Reference	Model	M_∞	Re_{x_1}	$\frac{x_1}{h}$	Location of transition	Remarks
Carrière et al. (1964)	cone - sting - cone	3·04	unit Re = $0{\cdot}04\times10^6$/in - 5·1 " "	=7·0	turbulent, boundary layer and shear layer	straight separations. critical points at reattachment
Chapman (1951)	cone - cylinder	2·0	$0{\cdot}5\times10^6$ - 10·0 "	10·0	"	no laminar reattachments. transition for $Re_{x_1} = 4{\cdot}1\times10^6$
Charwat et al. (1958)	wedge	1·98, 2·78	$0{\cdot}2\times10^5$ - 7·0 "	8·0	shear layer and downstream of reattachment	transition data correlates with $x_1/h.Re_{x_1}^{1/2}$. transition at R for $Re_{x_1} = 6{\cdot}0\times10^4$
Crocco et al. (1952)	blunt body	2·0	$0{\cdot}1\times10^6$ - 19·0 "	10·0	all régimes	base pressure variation as for present study. transition at R for $Re_{x_1} = 2{\cdot}5\times10^5$
Gadd et al. (1956)	wedge	2·0, 3·0	$1{\cdot}0\times10^5$ - $4{\cdot}0\times10^6$	8·0	boundary layer and shear layer	extends data of Charwat et al. into the turbulent régime

CONTINUED OVER

Reference	Model	M_∞	Re_{x_1}	$\frac{x_1}{h}$	Location of transition	Remarks
Hurlburt (1966)	flapped cavity	2·85	$1·77\times10^5$ - 7·1 "	10·0	shear layer	R found from visualisation. $0·6 < N < 0·7$. L_{sep} decreases with unit Re., α_w = constant
Kavanau (1954)	cone - cylinder	2·84	$0·5\times10^5$ - 4·0 "	16·0	shear layer and downstream of reattachment	transition at R for Re_{x_1} = $1·5\times10^5$
Rom et al. (1964)	rear-facing step (2-D)	1·5, 2·5	$2·0\times10^3$ - $2·0\times10^5$	9·0	"	effect of transition on $\dot{q}$(maximum) $\dot{q}_{max}\ x_1/h.Re_{x_1}^{1/2}$
Roshko et al. (1966)	axisymm. rear-facing step	2·0 - 4·0	$1·05\times10^6$ - 1·57 "	6·6	fully turbulent	no end effects. measured N = 0·5
Van Hise (1959)	ogive	2·62	$0·5\times10^5$ - $6·0\times10^6$	16·0	shear layer and downstream of reattachment	transition at R for Re_{x_1} = $4·0\times10^5$
White (1965)	rear-facing step (2-D)	7·0	$9·0\times10^5$	up to 16·6	downstream of reattachment	empirically N=0·5 . base pressure for small steps
Present study	flapped cavity	8·2	$1·70\times10^5$ - $1·28\times10^6$	8·0, 14·0	shear layer and downstream of reattachment	N= 1 for laminar reattachment. $N = f(Re_\infty, \alpha_w)$ - shear layer transition.

3. THEORETICAL STUDIES

3.1. Characteristics of the Separated Flow

Separated flows may be split into various types depending upon the state of the separation and reattachment points. Two basic types exist; cavity flows in which both the separation and reattachment points are fixed by the body geometry, and compression corner flows in which both these points are free to move. The two other types of separated flow are base flows, where the separation point is fixed and the reattachment point free, and forward-facing step flows where the reverse is true. In the present study two types of base flows are considered; that behind a wedge where the reattachment point is at the confluence of the two separated shear layers and that behind a rearward-facing step in which the reattachment occurs onto a solid surface. The aim of the study is to investigate the reattachment process and the flow geometry of the above flows. In order to simplify the separation mechanism of the rearward-facing step flows, straight separations, affected by adjusting the adverse pressure gradient with a downstream compression surface are considered.

Fig.1 illustrates the main features of the separated flow and the surface pressure distribution. The separated region may be divided into two distinct parts, namely a constant pressure mixing region followed by a reattachment zone through which the pressure and heat transfer rate rise rapidly. Normally, the separating boundary

layer undergoes a strong expansion at the step and the pressure falls abruptly to the base value. The shear layer thickness grows with distance from the step and then thins as it is compressed in the reattachment zone. This essentially isentropic compression forces the layer to return to the free stream direction with an associated pressure rise to the free stream value. The high momentum streamtubes in the separated layer are able to withstand this adverse pressure gradient and thus escape downstream, however, lower energy streamtubes are reversed to form a low momentum recirculating cone downstream of the step. A dividing streamline exists which stagnates at the reattachment point. The essential difference between the flow mechanism of the normal rearward-facing step and the flapped cavity used in the present study is that the expansion at the step is removed in the latter case, thus forcing a base pressure which is constant and equal to the free stream value. The peak pressure downstream of the reattachment zone is close to the inviscid wedge value.

3.1.1. Separated length

Chapman (1950) and Lock (1951) investigated the velocity profiles for constant pressure, laminar mixing of a viscous, compressible, high-velocity stream with a fluid at rest assuming a Prandtl number of unity. By solving the boundary layer differential equations with the appropriate boundary conditions Chapman looked for a similarity solution for the shear layer velocity profiles. He assumed a linear temperature - viscosity relationship of the form,

$$C\,\frac{T}{T_\infty} = \frac{\mu}{\mu_\infty} \qquad \ldots(3.1.i)$$

where $$C = \left[\frac{T}{T_\infty}\right]^{\frac{1}{2}} \frac{T_\infty + 110^\circ K}{T + 110^\circ K} \qquad \ldots(3.1.ii)$$

from Sutherland's viscosity law

and showed that the dividing streamline velocity ratio, $\bar{u}_*$, was a constant and equal to 0·587 for all conditions.

Chapman et al. (1957) and Chapman and Korst (1957) proposed a theoretical analysis of leading-edge separated flows in which they considered the essential mechanism to be the balance between mass flow scavenged from the 'dead air' region by the mixing layer and mass flow reversed back into the 'dead air' region by the pressure rise through the reattachment zone. For steady flow, without bleed, the dividing streamline at separation was also the dividing streamline at reattachment. The solution depended upon the assumption that $\bar{p}_t$, the total pressure on the dividing streamline as it approached the reattachment zone was equal to the terminal static pressure p_3 $(=p_r)$ and that the compression was isentropic. The Mach number $\bar{M}$ along the dividing streamline was related to the corresponding velocity $\bar{u}$, by the Busemann integral of the energy equation assuming that the 'dead air' temperature T_d , was equal to the recovery temperature T_{aw} $(=T_{t_2}$ for $P_r = 1)$. This resulted in an expression for the base pressure p_b (assumed to be equal to the external pressure p_2) ,

$$\frac{p_r}{p_2} = \left[\frac{1 + \frac{\gamma-1}{2} M_2^2}{1 + (1 - \bar{u}_*^2) \frac{\gamma-1}{2} M_2^2} \right]^{\frac{\gamma}{\gamma-1}} \qquad \ldots(3.2)$$

where subscript r represents the reattachment point and subscript 2 represents conditions outside the shear layer.

For T_d not equal to T_{t2} , $\bar{M}$ and $\bar{u}$ were related by the Crocco Integral for $P_r = 1$,

$$w = (1 - w_d)\, u_* + w_d \qquad \ldots(3.3)$$

where w is the stagnation temperature ratio ($= T_t(y)/T_{t2}$) , and $w_d = (T_d/T_{t2})$ i.e. the ratio evaluated for the 'dead air' region. This leads to the expression given by Wood (1961),

$$\frac{p_r}{p_2} = \left[\frac{w_d (1 - \bar{u}_*) \left(1 + \frac{\gamma-1}{2} M_2^2\right) + \left(1 + \frac{\gamma-1}{2} M_2^2\right) \bar{u}_*}{w_d (1 - \bar{u}_*) \left(1 + \frac{\gamma-1}{2} M_2^2\right) + \frac{\gamma-1}{2} M_2^2 \bar{u}_* (1-\bar{u}_*) + \bar{u}_*} \right]^{\frac{\gamma}{\gamma-1}} \qquad \ldots(3.4)$$

Cooke (1963) replaced equation 3.3 with the following expression from Carrière and Sirieix (1961), who assumed that the total temperature T_{t2} , varied with u_*^2 across the mixing layer,

$$w = (1 - w_d)\, u_*^2 + w_d \qquad \ldots(3.5.i)$$

which reduces to a relation in terms of the static temperatures namely,

$$\frac{T}{T_2} = \frac{T_d}{T_2} - \frac{(\gamma-1)}{2} M_2^2 u_*^2 + \frac{T_{t2} - T_d}{T_2} u_*^2 \qquad \ldots(3.5.ii)$$

He used equation (3.5.i) to give

$$\frac{p_r}{p_2} = \left[\frac{w_d \, (1 - \bar{u}_*^2) \left(1 + \frac{\gamma-1}{2} M_2^2\right) + \left(1 + \frac{\gamma-1}{2} M_2^2\right) \bar{u}_*^2}{w_d \, (1 - \bar{u}_*^2) \left(1 + \frac{\gamma-1}{2} M_2^2\right) + \bar{u}_*^2} \right]^{\frac{\gamma}{\gamma-1}} \qquad \ldots(3.6)$$

The original assumption of Chapman's that the dividing streamline stagnates at the terminal static pressure has received a lot of attention. Holder and Gadd (1955) pointed out that experimental work did not support this and work of Sirieix (1960) pointed to the same conclusion. The latter experiments suggested that the reattachment occurred halfway up the pressure rise. Noting these experimental results, Nash (1962) introduced a parameter N, termed the reattachment pressure rise parameter and defined by ,

$$N = \frac{p_r - p_2}{p_3 - p_2} \qquad \ldots(3.7)$$

Nash was concerned with turbulent reattachment and chose a mean value of 0·35 for this parameter. Experiments such as those of White (1965) at $M_\infty = 7$, indicated that a value of $N = 0{\cdot}5$ was more realistic for laminar flow and Cooke used this value though other workers, including Kirk (1954) and Beheim (1961), have taken $N = 1$ for both laminar and turbulent reattachments.

Knowing the conditions downstream of the reattachment zone (and hence M_2) and using the empirical expression (3.7), the base pressure can be determined by substituting the Chapman value of $\bar{u}_*$ (= 0·587) into equation (3.6). However, the assumption that $\bar{u}_*$

is a constant is only true for a leading-edge separation in which the shear layer grows from zero thickness and the velocity profiles are thus similar. This assumption holds for very long separated lengths where the velocity profiles become similar and the effects of the boundary thickness at separation, δ_s, become negligible. In realistic separated flows with finite δ_s, the length scale is small and $\bar{u}_*$ is not constant, rising from zero at separation to an asymptotic value of 0·587. A study of equation (3.6) indicates that an increase in $\bar{u}_*$ with the length of separation, L_{sep}, will cause a rise in the reattachment pressure ratio p_r/p_2 and hence a larger reattachment angle, α_w.

Kirk (1954) considered the problem of an initial boundary layer thickness for turbulent separating flows and regarded the shear layer as growing from a virtual origin upstream of the step. Cooke also analysed this problem of the separation of a finite thickness boundary layer and his solution can be used to predict the lengths of the straight separations considered in this study and their variation with α_w.

In his analysis he retained many of the assumptions made by Chapman, notably that in the 'dead air' region the velocity is zero and the pressure there is constant. He used sinusoidal velocity profiles to define the shear layer flow and applied momentum integral techniques to relate the velocity on the dividing streamline with the separated length. The results are shown in Fig.2 in which $\bar{u}_*$ is plotted against $\log_{10}\left[\dfrac{L_{sep}\, u_1 \nu_2}{x_1\, u_2 \nu_1\, n^2}\right]$

As the flow properties are continuous across the separation point for a straight separation the last term reduces to the ratio of the length of the shear layer to the length of the attached boundary layer upstream of separation. Fig. 2 includes the results of Denison and Baum (1962) who gave an exact solution to the same problem starting with a Blasius profile and it is seen that their results give considerably different values for $\bar{u}_*$. Cooke compared his results with experimental data obtained by Ginoux (1960) for laminar flow over a rearward-facing step and found good agreement between the predicted and measured separated lengths. The results of Denison et al. did not compare so well with the experimental data suggesting that Cooke's value for $\bar{u}_*$ is the more accurate.

The procedure for determining the length of the straight separation is as follows: knowing the free stream conditions and the reattachment angle, α_w, the pressure ratio p_r/p_2 can be determined from isentropic flow tables and equation (3.7). Hence $\bar{u}_*$ is determined from equation (3.6) using an assumed value for T_d. Fig. 2 gives the relationship between $\bar{u}_*$ and L_{sep}, the separated length. It is worth noting that the separated length and the dividing streamline velocity do not depend on the unit Reynolds number of the flow or the boundary layer thickness at separation. Indeed L_{sep} is only a function of the Mach number, M_2, and the length before separation, x_1. The Chapman method, in which a zero initial thickness shear layer is assumed, gives $x_1 = 0$ and $\bar{u}_* = 0.587$ and L_{sep} is a function of M_2 alone.

It must be stressed that Cooke's method assumes a "free-

interaction" separated flow which is free from direct downstream influence. If the shear layer is thick enough to be influenced by the presence of the wall then the interaction cannot be regarded to be "free". However, the boundary layer thickness at separation, δ_s , and hence the shear layer thickness, δ_T , do depend upon Reynolds number. This suggests that as long as the step is large compared to the thickness of the shear layer then Reynolds number independence should hold for laminar flow. When the shear layer is thick it probably cannot be uncoupled from the internal recirculating region, in which case Cooke's assumption that the shear layer behaves like a free jet with zero velocity on one side will be violated. To summarise, for a "free-interaction" separation, the ratio of the shear layer length to the length before separation may be expressed as follows,

$$\frac{L_{sep}}{x_1} = f(\tilde{u}_*) = g(\alpha_w, M_2, w_d, N) \qquad \ldots(3.8)$$

where $w_d = T_d/T_{t2}$

Fig. 3 illustrates the dependence of the flow geometry on each of these four parameters and the experimental data is discussed in Section 5.3.2.

3.1.2. Rate of growth of the shear layer

The growth rate of the mixing layer can be determined from Cooke's momentum integral analysis. He assumed that the mixing layer thickness, δ_T , could be divided into upper and lower regions, separated by the dividing streamline, and of thickness δ_u and δ_l

respectively. The analysis led to the following expressions,

$$\delta_u = \delta_T(1 - \bar{u}_*) \quad , \qquad \delta_1 = \delta_T \cdot \bar{u}_* \qquad \ldots(3.9)$$

and $$\frac{\delta_T}{\delta_s} = \frac{1}{1 + b\bar{u}_* + c\bar{u}_*^2} \qquad \ldots(3.10)$$

where $1 = 0{\cdot}1366$, $b = -0{\cdot}0465$, $c = 0{\cdot}3169$

The relation between $\bar{u}_*$ and L_{sep}/x_1 is known (see Fig. 2) and hence it is possible to determine the growth of the layer with distance with the aid of equations (3.9) and (3.10). The results are plotted in Fig. 4.

3.2. Reattachment Pressure Distribution

(a) Newtonian solution

A modified Newtonian method was used to determine the pressure distribution on the reattachment surface at a Mach number of 8.2. The mixing layer is regarded as an inviscid jet comprised of separate particles, each of which, on impact with the surface, loses its normal momentum. Considering that the ratio of directed to random K.E. is equal to $\frac{\gamma-1}{2} M^2$ it was thought that the model might prove relatively successful at the high Mach numbers considered in the present study.

Using the modified form of the Newtonian pressure coefficient,

$$C_p = (\gamma+1) \sin^2 \alpha_w \qquad \ldots(3.11.i)$$

the following expression was obtained for the pressure distribution on the flap,

$$\frac{p}{p_2} = \left(\frac{\rho}{\rho_2}\right)\left(\frac{u}{u_2}\right)^2 \frac{\gamma(\gamma+1)}{2} M_2^2 \, \mathrm{Sin}^2 \alpha_w + 1 \qquad \ldots(3.11.ii)$$

(where γ is taken to be 1.4)

ρ and u are 'local' values in the constant pressure shear layer and subscript 2 denotes external conditions.

The dividing streamline velocity at reattachment and the extent of the reattachment zone were determined as indicated in the previous sections. Two density and velocity profiles were considered, namely the Chapman compressible, asymptotic profiles ($\bar{u}_* = 0.587$) and Cooke's compressible sinusoidal profiles determined at the same value of $\bar{u}_*$. The former were evaluated for Pr = 0.72 and 1.0 and found to be almost identical. These profiles are illustrated in Fig. 5 which shows a good comparison between them for that part of the shear layer above the dividing streamline.

The comparison of the resulting pressure distributions with experiment was poor and is discussed in Section 5.3.6.1. and illustrated in Fig. 38(a).

(b) Momentum integral methods

Lees and Reeves (1964) calculated the pressure distribution of a shock wave / boundary layer interaction by the simultaneous solution of the momentum and moment of momentum ordinary differential

equations together with the Crocco - Lees boundary layer mass balance equation which couples the viscous and inviscid flows. An iterative procedure was necessary to match the regions upstream and downstream of shock impingement. The method incorporated the use of exact - similar - reversed velocity profiles in the separated region and required the numerical integration of simultaneous differential equations. Hankey and Cross (1967) succeeded in obtaining an approximate closed-form solution of the same governing equations to obtain solutions for various laminar separated flows at supersonic speeds. This method has been slightly modified here to predict the pressure distribution for a straight separating mixing layer.

Adopting the procedure of Lees and Reeves, Hankey and Cross considered the transformed equations for momentum and first moment of momentum, which were obtained by integrating across the boundary layer and making use of Stewartson's co-ordinates and the continuity equation. By noting that the ratio of the transformed energy and momentum thickness was nearly constant over a large range of the velocity profile parameter, which specifies the velocity profiles, and is proportional to the shape at the surface, they were able to combine the two equations.

Lees and Reeves correlated the transformed boundary layer shape factor, $\mathcal{H}^{-1}$, with the pressure gradient parameter, K , for various values of wall to free stream temperature ratios and showed that there existed a double valued relationship. For the same

adverse pressure gradient, two types of flow are possible i.e. separated and attached.

By transforming back to the physical plane and applying an approximate coupling equation between the inviscid and viscous flows a simple second order differential equation was obtained,

$$L^2 (d^2 M_e/dx^2) - (M_e - M_\infty) = 0 \qquad \ldots(3.12)$$

where L is a length scale.

A closed form solution was possible provided that L did not vary appreciably over the interval of integration. Two types of solution are possible depending upon the sign of $d\mathcal{H}^{-1}/dK$, namely,

Attached Flow:

$$M_e - M_\infty = A_1 . e^{x/L} + A_2 . e^{-x/L} , \qquad d\mathcal{H}^{-1}/dK < 0 \qquad \ldots(3.13)$$

Separated Flow:

$$M_e - M_\infty = B_1 \cos x/iL + B_2 \sin x/iL , \qquad d\mathcal{H}^{-1}/dK > 0 \qquad \ldots(3.14)$$

To summarise, Hankey et al. obtained this simple closed form solution by assuming that,

(i) The ratio of the transformed energy and momentum thicknesses is constant.

(ii) Variation in $\mathcal{H}$ (or δ^*) is considered much greater than the variation of θ or M_e.

To obtain a complete solution to the straight separation problem two boundary conditions must be applied i.e. $M_e(-\infty)$ and $M_e(+\infty)$, the external Mach numbers for upstream and downstream of the

interaction. In addition matching is required at the hinge and re-attachment points where the values of M_e and M_e' (hence K) are considered to be continuous. The co-ordinates are given in Fig. A and summarises the appropriate matching and boundary conditions. Three flow régimes exist for which the coefficients A_i and B_i must be determined. The co-ordinate system is established with the hinge at $x = 0$.

Fig. A

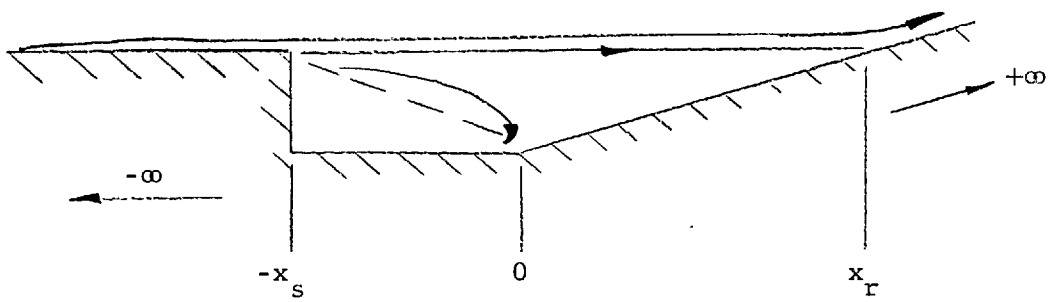

Table I:

Condition	x	M_e	M_e'	M_e''	K
Undisturbed upstream	$-\infty$	$M\infty -$	0	0	0
Step	$-x_s$	"	"	"	"
Hinge	0	"	"	"	"
Reattachment point	x_r	Continuous	Continuous	Discontinuous	K_s
Undisturbed downstream	$+\infty$	$M\infty +$	0	0	0

Application of these tabulated conditions leads to the values of the undetermined coefficients and we obtain equations for Mach number

in the three flow régimes. The pressure distributions are obtained from the Mach number calculations using the isentropic relationships.

The comparisons between theory and experiment for different values of α_w and free stream unit Reynolds number are shown in Fig. 38 and discussed in Section 5.3.6.1.

3.3. Heat Transfer Characteristics

At hypersonic speeds, the heat transfer to an aerodynamic surface can be extremely high, particularly in regions of flow stagnation such as the reattachment zone of a separated shear layer. Holden (1964) measured the total heat transfer to axisymmetric spiked bodies and found the most important influencing parameter to be the position of the shear layer reattachment point. In some critical cases he found the total heat transfer to the face of a cone to be more than doubled by the presence of a spike. There is clearly a need to predict such reattachment heat transfer rates and the effect of such parameters as reattachment angle in all the flow régimes.

3.3.1. Heat transfer rate distribution

Van Driest's (1952) paper gave the solution for the laminar heat transfer to a flat plate as a function of Reynolds number, Mach number and wall to free stream temperature ratio. He solved the simultaneous, differential equations of mass, momentum and energy, using the Crocco method, for arbitrary Prandtl number and assumed

the Sutherland law of viscosity - temperature variation for a constant specific heat gas. The Stanton number, St , was shown to be a function of Pr and $g^*(0)$, the shear function evaluated at the wall.

Rubesin and Johnson (1949) and Young and Janssen (1952) established that if the values of the density and viscosity in a boundary layer were calculated with relationships which hold for constant property fluids at an intermediate 'reference temperature', defined by empirical expression, then they accurately describe the actual conditions in a supersonic boundary layer.

Eckert, in 1955, used this 'reference temperature' technique to determine heat transfer rates in a zero pressure gradient flow. He used the empirical expression for 'reference temperature' which was proposed by Young and Janssen,

$$\text{i.e.} \quad T^* = T_\infty + 0{\cdot}5(T_w - T_\infty) + 0{\cdot}22(T_{aw} - T_\infty) \qquad \ldots(3.15)$$

where the reference viscosity was evaluated using Sutherland's viscosity law, namely,

$$\mu^* = 2{\cdot}27 \frac{T^{*3/2}}{T^* + 110} \times 10^{-8} \quad \frac{lb_f \cdot sec}{ft^2} \qquad \ldots(3.16.i)$$

where T is measured in ^oK ;

$$\text{alternatively} \quad \frac{\mu^*}{\mu_\infty} = \left(\frac{T^*}{T_\infty}\right)^{3/2} \times \frac{T_\infty + 110}{T^* + 110} \qquad \ldots(3.16.ii)$$

Applying the following Blasius relation for the skin friction

factor, C_f , and evaluating the Stanton number, St , at the reference conditions,

$$C_f = 0{\cdot}664 \,/\sqrt{Re_x^*} \quad ,$$
$$St = h_c/\rho^* c_p u_e = (C_f/2)Pr^{*-2/3} \qquad \ldots(3.17)$$

Eckert expressed the heat transfer rate as,

$$\dot{q}_w = h_c (T_{aw} - T_w)$$
$$= \frac{0{\cdot}332 \rho^* c_p u_e (Pr^*)^{-2/3} (T_{aw} - T_w)}{\sqrt{Re_x^*}} \qquad \ldots(3.18)$$

where h_c is the heat transfer coefficient and subscript e refers to conditions at the outer edge of the boundary layer.

The two theoretical models are compared with the measured 'flat plate' values in Fig. 39.

Various authors have extended the 'flat plate' solutions in an attempt to predict the distribution of surface properties in finite pressure gradient flows.

Cheng et al. (1961) considered the problem of blunt leading-edge effects in high temperature, hypersonic flow. Following ideas proposed by Lees (1956) for blunt-nosed bodies they assumed local 'flat plate' similarity in determining heat transfer rates. The solution depended on the observation of Lees that the thermal boundary layer is rather insensitive to pressure gradient, particularly if the

boundary layer is cooled and p_w/p_e is large. Consequently, the pressure gradient term in the momentum equation was ignored, reducing the problem to that of a 'flat plate' . For plane flows, again evaluating the density and viscosity at the 'reference temperature' they proposed,

$$\dot{q}_w = \frac{0{\cdot}332\,\rho^*\,c_p\,u_e\,(Pr^*)^{-2/3}(T_{aw} - T_w)}{\sqrt{Re_x^*}}\left(\frac{p}{p_\infty}\right)\left\{\int_0^x \frac{p}{p_\infty}\,\frac{dx}{L}\right\}^{-1/2} \qquad \ldots(3.19)$$

where L is a reference length.

Hence, knowing the surface pressure distribution equation (3.19) may be used to determine the surface heat transfer. The comparison of the theoretical model with experiment is illustrated in Fig. 40 and discussed in Section 5.3.6.2.

3.3.2. Peak heat transfer rates

Cooke's analysis of a mixing layer may be used in conjunction with Eckert's 'flat plate' heat transfer theory to determine the peak heat transfer rate at reattachment and the subsequent distribution downstream of the interaction. It has been shown in Section 3.1.2. that the thickness of the mixing layer above the dividing streamline (which will pass downstream through the reattachment zone) can be estimated in terms of the boundary layer thickness at separation and the appropriate dividing streamline velocity. By applying the condition of continuity across the reattachment zone, the thickness of the

reattaching layer may be represented in terms of the thickness at separation, δ_s ,

$$\delta_3 = \frac{\pi \rho_2 u_2}{2 \rho_3 u_3} \left[\bar{u}_* + \frac{2}{\pi} (1-\bar{u}_*) \right] 1 \left[\frac{1 - \bar{u}_*}{1+b\bar{u}_*-c\bar{u}_*^2} \right] \delta_s \qquad \ldots(3.20)$$

subscript 3 denotes conditions downstream of reattachment.

It is assumed that the reattachment thickness is reached by a boundary layer advancing from an origin upstream and growing in the external free-stream conditions existing downstream of the reattachment zone. The length is obtained from Cooke's expression for displacement thickness,

$$\delta_3 = 4.795 \left[\frac{\nu_3 C_3 x_3}{u_3} \right]^{1/2} \qquad \ldots(3.21)$$

where C is the constant in the temperature - viscosity relation (equation (3.1.i)).

Knowing δ_3 , from equation (3.20), the length of growth of the boundary layer, x_3 , is determined from equation (3.21). This value is substituted into equation (3.18) together with the flow properties downstream of the reattachment zone to give an estimation of the peak heat transfer rate, which is assumed to occur where the boundary layer is thinnest. The comparison between the theoretical and measured peak heat transfer rates are shown in Fig. 40.

Chung and Viegas (1961) derived an approximate expression

for the average heat transfer rate in the reattachment region of a two-dimensional, laminar shear layer flow normal to a wall. In their incompressible analysis, the reattaching flow was considered inviscid but rotational and the viscous effects were assumed to be confined to the boundary layer growing along the wall. They developed a closed-form solution of the flow field from which the pressure and velocity distributions along the wall were obtained. The length of the reattachment zone was defined as the length required for the wall velocity to reach the dividing streamline value and was empirically related to the length of the separated shear layer. The heat transfer analysis was based on the theory developed by Lees (1956) using the pressure and velocity distributions mentioned above. Due to the drastic reduction of the local heat transfer within the small length, L , (which was of the order of the mixing layer thickness), a semi-empirical expression for the average heat transfer in this zone was developed for $0{\cdot}1 \leqslant p/p_t \leqslant 0{\cdot}5$, i.e.

$$\dot{q}_{w_{av}} = 0{\cdot}103\ \bar{u}_*^{3/2}\ Pr^{-2/3} c_p\ Re_{L_{sep}}^{3/4} \left(\frac{p_e}{p_{t_e}}\right)^{-\frac{1}{2}} \left[0{\cdot}76+1{\cdot}411\ \frac{p_e}{p_{t_e}}\right] \frac{\mu_e (T_{aw}-T_w)}{L_{sep}}$$

$$= G \text{ , say} \qquad \ldots(3.22)$$

where L_{sep} is the length of the mixing layer.

Chung and Viegas assumed the asymptotic value for $\bar{u}_*$. Equation (3.22) has been modified to include a variable $\bar{u}_*$.

In order to provide a rough check on this approximate theory, the stagnation point heat transfer to a cylinder is derived by

applying the blunt body formula of Lees. Substitution of the approximate Newtonian value for the stagnation velocity gradient from Cohen and Reshotko (1955) gives,

$$\dot{q}_{w,st} = 0{\cdot}47\ Pr^{-2/3}\sqrt{(\rho_e\ \mu_e)_{st}}\ \ (h_{e_{st}} - h_w)\left[\frac{\sqrt{2}}{6}\frac{u_\infty}{R}\right] \qquad \ldots(3.23)$$

where R is the radius, h the static enthalpy and u_∞ denotes the velocity ahead of the bow shockwave.

By considering the stagnation point heat transfer to a cylinder whose radius is equal to the step height considered in the present study, it is hoped that it will be possible to establish the order of magnitude of the measured peak heat transfer rates. The results are shown in Fig. 40.

3.3.3. Effect of reattachment angle

The expressions developed in the previous section offer a solution to the problem of a normal reattaching flow whereas the angles of reattachment considered in this study are small. Consequently, an analysis is proposed that will include the effect of angle on the stagnation velocity gradient and hence peak heat transfer.

Lees proposed that the heat transfer to a two-dimensional stagnation point could be expressed as,

$$\dot{q}_{w,st} = 0{\cdot}5\ Pr^{-2/3}\sqrt{(\rho_e\ \mu_e)_{st}}\ \ (h_{e_{st}} - h_w)\sqrt{\frac{\bar{u}}{L}}\ .\ F(x) \qquad \ldots(3.24)$$

where L is the length of the reattachment zone, $\bar{u}$ is the velocity

of the stagnating streamline and,

$$F(x) \quad \frac{1/\sqrt{2}\ (p/p_{t_e})\ (u_e/\bar{u})}{\left[\int_0^{x/L} (p/p_{t_e})(u_e/\bar{u})\ d(x/L)\right]^{1/2}}$$

At a stagnation point, p/p_{t_e} is unity and, assuming a linear velocity - distance relation, $F(x)$ reduces to,

$$\frac{1}{\sqrt{2}} \left[\frac{1}{\bar{u}} \left(\frac{du_e}{d^x/_L}\right)_{x=0}\right]^{1/2}$$

which can be substituted back into equation (3.24). Hence,

$$\dot{q}_{w,st} \propto \left[\frac{1}{\bar{u}} \left(\frac{du_e}{d^x/_L}\right)_{x=0}\right]^{1/2} \qquad \ldots(3.25)$$

and the average reattachment heat transfer for a general reattachment angle, α_w, is obtained from equation (3.22) to give,

$$(\dot{q}_{w,\alpha_w})_{av} = G. \left[\frac{(du_e/d^x/_L)_{x=0,\alpha_w}}{(du_e/d^x/_L)_{x=0,st}}\right]^{1/2} \qquad \ldots(3.26)$$

where subscript st denotes orthogonal reattachment.

To get some idea of the stagnation point velocity gradients in equation (3.26), a method is used which was proposed by Milne - Thomson in 1949. This involves the potential flow solution of the direct impact of two equal, incompressible jets (which are illustrated in Fig. B)

Two streams A_1 and A_2, each of thickness k and travelling

at a speed U_∞, impinge symmetrically at an included angle of $2\alpha_w$ and branch off into two other streams B_1 and B_2 of thickness h_1 and h_2 respectively. The streamline $y = 0$ may be regarded as a solid surface. The ratio h_1/h_2 is determined in terms of α_w from the continuity equation, i.e.

$$H_b = \frac{h_1}{h_2} = \frac{1 + \cos \alpha_w}{1 - \cos \alpha_w} \qquad \ldots(3.27)$$

FIG. B:

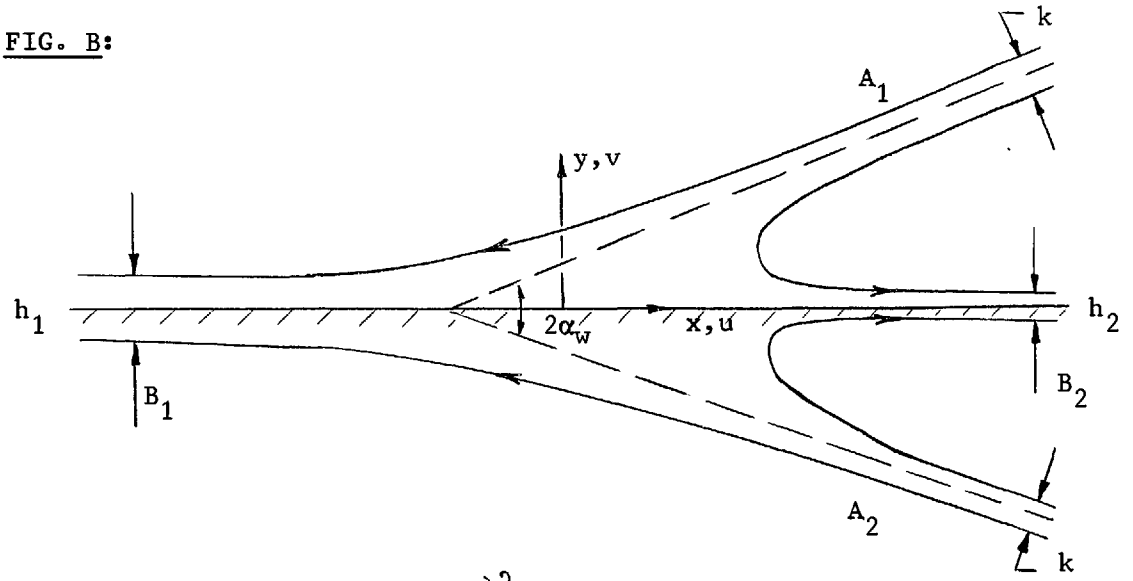

The complex velocity, $\mathcal{V}$, and the complex distance parameter, z, are related by the expression,

$$z = \frac{U_\infty}{\pi}\left[\frac{h_1}{b_1}\log\left(1 - \frac{\mathcal{V}}{b_1}\right) + \frac{h_2}{b_2}\left(1 - \frac{\mathcal{V}}{b_2}\right) - \frac{k}{a_1}\log\left(1 - \frac{\mathcal{V}}{a_1}\right) - \frac{k}{a_2}\left(1 - \frac{\mathcal{V}}{a_2}\right)\right] \qquad \ldots(3.28)$$

where $b_1 = U_\infty$, $b_2 = U_\infty e^{i\pi}$, $a_1 = U_\infty e^{i\alpha_w}$, $a_2 = U_\infty e^{-i\alpha_w}$

and $z = x + i\,y$, $\mathcal{V} = u - i\,v$

On the surface, $y = 0$, $z = x$ boundary

$v = 0$, $\mathcal{V} = u$ conditions

Substituting for a_1, a_2, b_1, b_2 and the boundary conditions and considering only the real part we obtain,

$$\frac{\pi x}{h_2} = H_b \log\left[1 - \frac{u}{U_\infty}\right] - \log\left[1 + \frac{u}{U_\infty}\right]$$

$$- \frac{(H_b+1)}{2}\left[\cos\alpha_w \log\left\{1 - 2\frac{u}{U_\infty} + \frac{u}{U_\infty}^2\right\} + \sin\alpha_w \tan^{-1}\left\{\quad\right\}\right]$$

where $\left\{\quad\right\} = \dfrac{2\frac{u}{U_\infty}\sin\alpha_w\left(1 - \frac{u}{U_\infty}\cos\alpha_w\right)}{\left(1 - \frac{u}{U_\infty}\cos\alpha_w\right)^2 - \left(\frac{u}{U_\infty}\right)^2\sin^2\alpha_w}$ ...(3.29)

Differentiating equation (3.29) and putting $x = 0$, $u = 0$ at the stagnation point we obtain a relationship for the stagnation velocity gradient in terms of α_w i.e.

$$\left.\frac{d(u/U_\infty)}{d(\pi x/h_2)}\right|_{x=0,\ u=0} = \frac{\cos\alpha_w - 1}{4\sin^2\alpha_w} \qquad ...(3.30)$$

Hence the stagnation point velocity gradient ratio, appearing in equation (3.26), can be determined and is plotted in Fig. 6.

The success with which heat transfer rate properties can be predicted by the solutions mentioned above is limited and is discussed in Section 5.3.6.2.

4. EXPERIMENTAL WORK

4.1. The Hypersonic Gun Tunnel

4.1.1. Description

The experimental study was performed in the Imperial College gun tunnel. This is an intermittent, blowdown facility incorporating a free, light, aluminium piston. The original tunnel has been described by Stollery et al. (1960) whilst the subsequent modifications and recalibration appear in a report by Needham (1963).

In brief, the tunnel consists of a high pressure drive vessel of 4 cu.ft. capacity designed to operate with a drive pressure of 3000 p.s.i.a. Immediately downstream of the pressure vessel, and separated from it by a double diaphragm assembly, is the barrel which is 20 ft. long and has an I.D. of 3 inches. The barrel contains a volume of test gas at a pressure of up to 100 p.s.i.a. The nozzle, located at the downstream end of the barrel, enters a square cross-section, open-jet type working section, downstream of which is a 10 inch diameter diffuser leading to a dump tank. The diaphragms at the upsteam and downstream ends of the barrel are made of unscribed aluminium and 'Sellotape' respectively. The tunnel is operated at Mach numbers of 7·5, 10 and 15, using a 10° semi-angle conical nozzle with various throat diameters and at 8·2 with the use of a contoured nozzle. Both nozzles have exit diameters of 8 inches and the diameter of the inviscid cone of test gas which is expanded into the working

section is approximately 5 inches.

The light piston, which weighs 100 grms., is located at the upstream end of the barrel and when the diaphragms fracture, it accelerates down the barrel compressing the test gas ahead of it. The shock wave preceeding the piston heats the gas to temperatures as high as $1300^{\circ}K$ and the high temperature and pressure gas is then expanded through the nozzle into the working section.

The free stream flow parameters may be varied by operating the tunnel at different drive (reservoir) and driven (barrel) pressures. The free stream total pressure is a fraction (approx. 80%) of the drive pressure, p_4, whereas the free stream total temperature is a function of the drive pressure ratio, p_{41}. Free stream Reynolds number is calculated from the reservoir conditions by assuming that the gas is perfect and that the expansion through the nozzle is isentropic. Fig. 7 shows the calculated Reynolds number range of the tunnel at a Mach number of 8.2. One important factor which limits the Reynolds number range is the occurrence of condensation in the test gas at low values of p_{41} (i.e. low free stream total temperature) and the figure includes the condensation limit established experimentally by Daum (1963).

The total running time of the tunnel, which is estimated as the time taken for the pocket of compressed gas to discharge through the nozzle, is a function of the drive pressure ratio, p_{41}, and the throat diameter. For relatively low Mach numbers, and hence large throat sizes, the running times are short, conversely when Mach numbers

are high the running times are long. For example, to obtain a useful duration of run at Mach 7 the tunnel must be operated under relatively low drive pressure ratios, a value of p_{41} of 40 being necessary for a running time of 30 m.secs. whereas at Mach 10 the same value of p_{41} allows a running time of 140 m.secs. However, care must be exercised when recording measurements during the total running time due to the drop in reservoir pressure which is caused by the arrival of the reflected expansion head at the nozzle location approximately 50 m.secs. after the start of the run. This curtails the period of steady pressure to about 30 m.secs. duration in each acoustic wave, commencing at about 8 m.secs after the initial shock in the starting process.

4.1.2. Tables of test conditions

I Cylinder and wedge studies

Group No.	M_∞	p_4 p.s.i.a.	p_{ib} p.s.i.a.	$p_{t\infty}$ p.s.i.a.	$T_{t\infty}$ ^oK	Re_∞ per inch
1 - 8	8.2	2000	14.7	1580	1290	2.37×10^5
	"	"	100	1640	680	6.99×10^5
9 - 11	8.2	1000	50	820	670	3.50×10^5
	"	1500	75	1230	"	5.25×10^5
	"	2000	100	1640	"	6.99×10^5
	"	"	90	1650	695	6.75×10^5
	"	600	24	490	724	1.87×10^5 *-
	"	1000	40	816	"	3.12×10^5 *-
	"	1500	60	1225	"	4.68×10^5 *

CONTINUED OVER

Group No.	M_∞	p_4 p.s.i.a.	p_{ib} p.s.i.a.	$p_{t\infty}$ p.s.i.a.	$T_{t\infty}$ °K	Re_∞ per inch
9 - 11	8·2	2000	80	1632	724	$6·24 \times 10^5$ *
	"	2500	100	2042	"	$7·80 \times 10^5$ *
	"	2000	65	1640	775	$5·62 \times 10^5$
	"	2500	81·1	2050	"	$7·02 \times 10^5$
	"	2000	50	1620	854	$4·73 \times 10^5$
	"	1000	14·7	800	1038	$1·69 \times 10^5$
	"	1500	22·1	1200	"	$2·54 \times 10^5$
	"	2000	29·4	1600	"	$3·38 \times 10^5$
	"	2500	36·8	2000	"	$4·23 \times 10^5$
	"	2000	14·7	1580	1290	$2·37 \times 10^5$

* Flow geometry study (Group 11)

\- Boundary layer profile study (Group 10)

II Rearward-facing step studies

Group No.	M_∞	p_4 p.s.i.a.	p_{ib} p.s.i.a.	$p_{t\infty}$ p.s.i.a.	$T_{t\infty}$ °K	Re_∞ per inch
13 - 15	9·7	1000	24·5	800	866	$1·59 \times 10^5$
	"	1500	18	1200	1110	"
	"	2000	14·7	1600	1290	"
	"	2500	44·1	2000	975	$3·36 \times 10^5$
	"	1000	14·7	800	1030	$1·18 \times 10^5$
	"	1500	21·7	1200	"	$1·78 \times 10^5$
	"	2000	29·4	1600	"	$2·37 \times 10^5$
	"	2500	36·7	2000	"	$2·96 \times 10^5$
12	8·2	500	16·3	400	780	$1·40 \times 10^5$
	"	1000	32·5	800	"	$2·80 \times 10^5$

CONTINUED OVER

Group No.	M_∞	p_4 p.s.i.a.	p_{ib} p.s.i.a.	$p_{t\infty}$ p.s.i.a.	$T_{t\infty}$ ^oK	Re_∞ per inch
15 - 17	8.2	500	14.7	400	820	1.30×10^5
	"	1000	25	800	860	2.37×10^5
	"	1500	37.5	1200	"	3.56×10^5
	"	2000	50	1600	"	4.74×10^5

4.2. Description of Models

Three distinct types of model were used in the experimental study. Cylinder and wedge models were used in the preliminary work whereas, for the later detailed studies, a flapped cavity model, consisting of a rearward-facing step with a downstream flap, was considered.

The cylinder model was of 1" diameter and had a span of 5". It was supported from the sides by $\frac{3}{8}$" diameter rods, the ends of which were connected to a rigid side support mounting. The 10^o half-angle wedge models were of 5 " span and 2" base height and were also side mounted, the side supports in this case being wedge cross-section bars of 10^o half-angle and $\frac{3}{8}$" base. The preparatory model was made of wood as it was required solely for flow visualisation studies.

The instrumented wedge model was constructed of mild steel and had a measured leading edge thickness of approximately 0.001" . Separate base plates were used for the measurement of pressure and heat transfer rate. Rows of pressure tappings of $\frac{1}{16}$" diameter were located down the base at certain spanwise positions, including the

centre span. Tappings were also spaced along the base centre line in order that side effects might be detected. The model was hollow to accommodate four pressure transducers, the leads of which were led out behind the side supports without disturbing the flow. Heat transfer rates were measured with thin film gauges, which were painted onto the 2 mm. thick pyrex glass base plate. The gauges, which measured approximately $\frac{1}{2}$" long and $\frac{1}{20}$" wide, were spaced at intervals of 0·1" down the mid-span of the base and also at larger intervals across the span to measure possible side effects. The pyrex was drilled in order that the electrical leads could be led out of the model without disturbing the base flow. Fig. 8 shows the wedge model with its base instrumented for heat transfer measurements.

The flapped cavity model, which is also shown in Fig. 8, was of 5" span and sting mounted from its underside. The leading edge thickness was maintained at approximately 0·001" and the bevel angle was 10°. The leading edge to step length was 2" or 3·5" and step heights ranging from $\frac{1}{16}$" to $\frac{1}{2}$" were considered. The flap downstream of the step was made of $\frac{1}{4}$" thick gauge plate and had a 4" chord length, it could be rotated through about 30° and its position relative to the step was variable. Downward-facing side curtains were attached to the model between the leading edge and the hinge to prevent high pressure disturbances, generated at the underside of the model, affecting the separated flow. The flap was instrumented for the measurement of pressure and heat transfer rate along its centre line (as shown in Fig. 8). The pressure tappings and heat transfer gauges were spaced

at 0·1" and 0·2" intervals respectively. Provision was made for the spanwise distributions of pressure and heat transfer rate to be measured. To facilitate the measurement of the low pressures encountered in the separated flow region the transducers were mounted in the support sting. Care was needed to thoroughly seal the hinge and the step junction and so prevent base bleed occurring from the underside of the model into the separated region.

The basic model was supplemented with axisymmetric and half-scale models which are shown in Figs. 9(a) and 9(b). The axisymmetric model consisted of a mild steel, 2·5" diameter cylinder around which was wrapped a $\frac{1}{4}$" step, 2" downstream of the leading edge. The two-dimensional flap was simulated by cone frustums of 10·5° and 13° half-angle which could be positioned at the required step to hinge length. The model was supported in a collar held by wedge cross-section side supports positioned behind the compression surface. The model was not instrumented but used only for flow visualisation studies.

4.3. Instrumentation

The pressures and heat transfer rates were displayed on two-beam Tektronix 502 oscilloscopes and recorded by Land polaroid cameras.

Solartron NT4 - 313, 0-15 psia. and 0-30 psia. and C.E.C. 4-326, 0-10psia. strain gauge diaphragm transducers were used to measure pressure. The former were operated with an excitation voltage of 5 volts with a peak output voltage of 20 mV. whereas the latter operated with a 10 volt excitation voltage with a corresponding maximum

output of 40 mV. The transducers record the out-of-balance voltage produced across a Wheatstone bridge when an applied pressure causes a displacement of the diaphragm. The transducers have a nominal linear calibration over their full range, however, as the test pressures encountered were of the order 0·01 - 1·00 psia. the gauges were carefully recalibrated in this range.

The transducers were calibrated statically. The output voltages were measured on a Solartron digital voltmeter. A McLeod gauge was used to record pressures in the 0-10 mm. of mercury range and higher values were measured with an oil manometer. Though the low range calibrations were not linear, they were found to be repeatable to within $\pm 1\%$.

Heat transfer rate was measured with the thin film platinum gauges mentioned in the previous section. Each gauge was situated in one arm of a Wheatstone bridge and its change of resistance with temperature during a run caused an out-of-balance voltage, proportional to the surface temperature. This output was amplified approximately 25 times and integrated in a five channel electronic analogue unit to give the surface heat transfer rate distribution which was recorded on an oscilloscope. The construction of the gauges, the analogue equipment and the calibration technique has been fully described by Holden (1964).

4.4. Flow Visualisation Techniques

4.4.1. Schlieren photography

One of the main requirements of the experimental study was the need to establish certain details of the separated flow geometry, including the boundary layer growth, the length of the separated layer, the angles of separation and reattachment. Another requirement was to detect transition of the boundary layer or the separated shear layer. Spark schlieren photography, which detects density gradients in the flow, was a valuable technique with which the above data could be established.

The spark was generated by the discharge of a 0.1μF capacitor at a potential of 15 KV. Coaxial with the spark gap was a constant light source used to aligne the system. A delay circuit was used to generate the spark at a pre-set time which was typically 22 m.secs., commencing at about 8 m.secs. after the initial shock in the starting process.

4.4.2. High speed ciné photography

A Fastax 16 mm. camera, operating at 5000 frames per second, was used to study details of the flow establishment time and the stability of the separated flow field. The results are discussed in Section 5.1.2.1.

4.4.3. Surface visualisation

Surface visualisation techniques were employed with the flapped cavity model in an attempt to establish the location of the reattachment line of the separated shear layer and also the extent of the two-

dimensional flow and the effectiveness, or otherwise, of side plates bounding the separated flow region.

The first medium tried was low viscosity silicon oil which was spotted onto the reattachment surface. The spot size was 0.05" diameter which was regarded as the optimum value from a study performed by Meyer (1966). This surface shear measuring technique proved to be quite valuable and the reattachment line, where there is no shear, could be located within a band of 0.1". It was just possible to detect the reversed flow upstream of the reattachment line and also the side wash effects occurring in the reattachment region. When this region was bounded by side plates the oil spots indicated that the side wash had been cancelled without the generation of any disturbance to the flow. Close to the step, where the surface shear is very small, the oil spot technique proved to be insensitive. Fig. 10(b) shows a typical oil spot pattern.

Light talcum powder was used as an alternative method of determining the extent of the separated region. The results were disappointing, though the residual deposit of powder indicated the general extent of the separated flow, only a rough qualitative estimate of the reattachment line was possible. However, the powder technique was useful in other ways. Fig. 10(a) shows a schlieren picture which indicates the flow recirculation downstream of the step, which is made visible by the powder. The application of powder at the step and hinge positions provided a check that there was no bleed into the

'dead air' region due to poor sealing.

It was necessary to define the reattachment point more precisely than was possible using oil spots. This was achieved using a forward-facing, surface pitot probe technique. At the reattachment point, the velocity is zero and thus the static and pitot pressures are equal. Upstream of reattachment where the flow is reversed, the pitot pressure (which is, in effect, the base pressure behind the probe) is less than the static pressure. The converse is true downstream of reattachment. Hence, the reattachment point occurs at the intersection of the measured static and pitot pressure distributions. This technique proved to be both precise and repeatable.

The probe was inserted through the static pressure tappings (as shown in Fig. 1) and great care was exercised in insuring an air-tight seal. Consistent with not incurring excessive response times, the orifice, which was rectangular in cross-section, was made as small as possible, 0.010" deep and 0.045" wide.

5. RESULTS AND DISCUSSION.

5.1. Cylinder and Wedge Studies in Uniform Flow

(a) Cylinder in uniform flow

The aims of the preliminary cylinder studies were twofold, namely to test the sensitivity of the schlieren apparatus in detecting a separated mixing layer and to measure pitot pressure profiles through the wake in order to establish the existence and extent of side effects. Interest was centred on the near wake flow, i.e. the region as far as the recompression zone at the wake neck where the mixing layers converged. The flow conditions for this series of tests (Groups 1-3) are defined in the table of Section 4.1.2. on page 43.

Both the separated mixing layers and the wake neck, which occurs approximately one diameter downstream of the cylinder, are discernable from schlieren photographs. The lip shocks, occurring at the separation points and the trailing shocks, generated at the neck recompression zone, are also clearly visible. Further details of the wake flow are not detectable, particularly the wake growing downstream of the neck. A study of the photographs indicated that transition was occurring in the mixing layers before their confluence at the wake neck.

The schlieren system measures $d\rho/dy$ and for a hypersonic, laminar boundary layer, where the maximum density gradient is very

pronounced, the layer appears as a thin line. However, as the layer becomes transitional, the increased mixing causes a reduction in density gradient and the line weakens and vanishes.

It was hoped that the flow would be fully laminar but, unfortunately, it was not possible to reduce the Reynolds number or increase the Mach number to provide conditions more likely to maintain a fully laminar separated flow.

Pitot pressure distributions were measured both across the shear layers and in a spanwise direction at a location just upstream of the wake neck i.e. one diameter downstream of the cylinder. The results are shown in Figs. 11(a) and 11(b). Spanwise measurements were made at various vertical distances, Z/D, from the wake centre-line and Fig. 11(a) shows that strong end effects were clearly evident. The flow was sensibly two-dimensional for some 60% of the cylinder centre-span along the axis of symmetry, however, this extent of two-dimensional flow decreased as Z/D increased and vanished at $Z/D = 1.5$.

The profiles across the shear layer were measured at various spanwise positions, y/D . Within the centre 60% of the span the profiles were sensibly similar and indicated a pronounced trough at the centre line, within the 'dead air' region. However, as Fig. 11(b) shows, side effects were evident at 80% of the centre span, the profile indicating a sharp rise of the base pressure.

Due to the onset of transition discussed above, it was decided to study its effect upon the separated flow geometry. A wedge model

was used for these tests as the geometry forced fixed separation points.

(b) Wedge in uniform flow

Spanwise pitot pressures were measured downstream of the wedge, without side plates, to establish the presence of side effects. The free stream conditions were the same as those used in the previous cylinder studies. The results indicated that the side effects present were similar in extent to those determined behind the cylinder model, i.e. the region of uniform flow on the axis of symmetry was found to occupy 60% of the centre span at a distance of one base width downstream of the wedge.

A schlieren photograph of the base flow is presented in Fig. 12. A study of the photographs indicated two main points, firstly, transition was occurring, either in the attached boundary layer or in the separated mixing layer, depending upon the flow conditions, and secondly, unsteadiness was present in the separated flow.

5.1.1. Separated length

Characteristic properties of the mixing layer geometry, notably the average value of L_{sep}, the separated length, were measured over a considerable range of Reynolds number (which is tabulated in Section 4.1.2., page 43). In some tests the boundary layer was tripped into turbulence by a strip of three-dimensional roughness placed across the wedge $\frac{3}{4}$" downstream of the leading edge. The strip consisted of closely spaced glass spheres of 40 thou. diameter

(which is of the order of the boundary layer thickness).

In order to relate the flow geometry for both free and solid surface reattachments, some tests were performed with a 'splitter plate' fixed to the wedge base to form a rearward-facing step with a height equal to half the wedge base width. The results are shown in Fig. 13 in which the ratio L_{sep}/x_1 is plotted against Re_{x_1}, the Reynolds number based on the wedge chord, at a local Mach number of 5.7. The results are compared with the previous experiments of Rom and Seginer (1964) who measured L_{sep} for a fully laminar flow for a Mach number range of 1.5 - 2.5.

Within the accuracy of measurement, the mixing layer lengths for the free and solid surface reattaching flows were equal and exhibited the same variation with Reynolds number. This indicated that the presence of a solid reattachment surface, which imposes the condition of zero streamwise velocity along it, does not seriously affect the base flow mechanism.

The photographs indicated that when the boundary layer was 'untripped', transition occurred on the wedge surface. Consequently, the corresponding increase of L_{sep} with Re_{x_1} shown in Fig. 13 was expected. Crocco and Lees (1952) predicted this phenomenon in their approximate mixing theory. They argued that as the Reynolds number increases, the base pressure (and hence the separated length) increases because of the growth in the boundary layer thickness at the trailing

edge as the transition point moves forward. For fully turbulent flow, in which the transition point is practically fixed i.e. close to the leading edge, they predicted that the base pressure drops slowly with increasing Reynolds number because of the normal decrease in the boundary layer thickness at the trailing edge. The 'tripped' boundary layer data agreed with this argument and the photographs also indicated that the flow on the wedge surface was fully turbulent. The data of Rom and Seginer, at a lower Reynolds number and Mach number range, show that, for fully laminar flows, L_{sep} increases with Re_{x_1}. This result is confirmed by the laminar step separations of the present study (which are given in Section 5.2. and 5.3.) Clearly there is a strong variation of base properties in relation to the transition location, This behaviour is discussed fully in Section 5.3.4.

Unfortunately, the variation of L_{sep} with Re_{x_1} for separations of transitional shear layers could not be studied with the wedge model due to the limitation of the Reynolds number range available. However, subsequent step studies do include this important intermediate régime.

5.1.2. Influence of transition

As the phenomenon of transition is clearly of importance to the separated flow it was thought necessary to study it in some depth, particularly the way in which its location on the wedge surface is affected by the free stream unit Reynolds number. The movement was thought to be a likely cause of the instability detected in the mixing

layer and this hypothesis was investigated.

5.1.2.1. Location of transition

The onset of transition within a laminar boundary layer is a function of the free stream Mach number M_∞, unit Reynolds number Re_∞, and wall-to- recovery temperature ratio T_w/T_{aw}. In the present tests (Group 9 in the table of Section 4.1.2., page 43) transition of the 'untripped' boundary layer was measured from the schlieren photographs over a range of Re_∞ and T_w/T_{aw} at a 'local' M = 5.7. The results are illustrated in Fig. 14, where comparison is made with data from previous studies.

For a constant T_w/T_{aw} there is a linear correlation between Re_∞ and Re_{L_t}, the Reynolds number based on the length to transition. The slope of the line is less than 45^o and thus indicates that the transition point moves forward in the boundary layer as Re_∞ increases.

In order to provide a conclusive check on the state of both the 'tripped' and 'untripped' boundary layer, pitot pressure profiles were measured at the wedge trailing edge for T_w/T_{aw} = constant. The profiles are illustrated in Figs. 15(a) and 15(b) in which they are compared with both laminar and turbulent theoretical profiles determined from the analyses of Van Driest (1951 and 1952).

The character of the wedge boundary layer determined from the schlieren pictures is clearly substantiated by these results.

5.1.2.2. Flow establishment time

A possible criticism of separated flow studies performed in an intermittent facility such as a gun tunnel is that the complicated separated flow mechanism might not establish a steady state within the available running time.

Needham (1965) investigated the establishment time for the flow over a wedge compression corner at $M_\infty = 9.7$. He took a high speed ciné film of the separated flow covering the whole of one run and measured the length of the separated region at intervals of $\frac{1}{2}$m.sec. Comparing the plot of L_{sep} against time with a typical free stream pitot pressure trace, he found that the initial response of the separated flow was faster than that of the probe itself and that L_{sep} followed the fluctuations in pitot pressure very closely.

Exactly the same technique was employed in this study at $M_\infty = 8.2$. High speed ciné films were taken of the wedge separated flows (with and without the 'splitter' plate attached) which have been described, and also of a rearward-facing step which had an attached flow length of 3". The response of the separated flow for all three models was extremely rapid leading to the conclusion that the gun tunnel is quite suitable for this type of study, the only limitation being the response time of the instrumentation.

5.1.2.3. Shear layer stability

The ciné film studies indicated a fundamental difference in the

behaviour of the transitional wedge separated flows and the fully laminar flow generated by the smaller step model.

For the latter model, the length of the separated region followed the fluctuations in the pitot pressure very closely suggesting that the mechanism is quite stable. However, a distinct and regular oscillation of the length of the separated region of the wedge models was observed which was quite independent of any variation in the tunnel conditions. This suggests that the motion of the transition point on the wedge surface and the associated variation of the boundary layer thickness, caused by fluctuations in the free stream pressure, generate an instability of the pressure in the separated flow region which does not exist when the flow is fully laminar.

5.1.3. Heat transfer rate distributions

Prior to considering the heat transfer rate distribution to the wedge base, this property was measured on a rearward-facing step model, which had a $\frac{3}{4}$" step located $4\frac{3}{4}$" downstream of the leading edge. It was felt that it would be useful to compare the surface distribution of this property for the cases of both free and solid surface re-attaching flows. The centre-line heat transfer rate distributions were measured both up to and down the step at $M_\infty = 8.2$, $Re_\infty = 2.37 \times 10^5/\text{in.}$ and $T_t = 1290\ ^\circ K$, for which conditions the boundary layer was entirely laminar. These distributions are shown in Fig. 16(a).

It can be seen that the flat plate distribution compared well

with the theoretical distribution of Eckert and the distribution of heat transfer down the step exhibited two points of interest; firstly, the rate of heat transfer to the step was approximately one order of magnitude lower than the equivalent flat plate value and secondly, the distribution had a distinct peak at a location about 40% up the step height. The peak is thought to be generated by the shearing action of the low-speed recirculating flow where it comes closest to the step surface and the boundary layer is thinnest.

The heat transfer rate distribution along the centre line of the wedge base was measured, both with and without side plates spanning the near wake region, for $M_\infty = 8.2$ and $Re_\infty = 2.37 \times 10^5$/in. and 6.99×10^5/in. Due to the transitional state of the separating boundary layer and its associated unsteadiness the measurements of heat transfer rate were also unsteady and difficult to define, particularly at the lower Reynolds number. However, the higher Reynolds number data shown in Fig. 16(b), established certain points; the order of magnitude of the distribution was the same as that measured on the rearward-facing step and two heat transfer peaks were detected, located symmetrically about the base mid-height, indicating that the mechanism is similar to that behind the rearward-facing step. This is contrary to the conjecture that the maximum heat transfer rate occurs at the mid-point of the base. The presence of side plates had little effect on the character of the heat transfer rate distributions, this was expected due to the unsteadiness of the separated flow.

5.2. Straight Separations in Conical Flow

Flapped cavity model

Weiss et al. (1966) studied turbulent wedge separation at $M_\infty = 2.95$ and $Re_{x_1} = 7.0 \times 10^6$ and observed a profound effect of the shoulder expansion on the base flow region. The strong normal pressure gradient generated by this expansion and the following compression wave at the separation point were shown to cause a large curvature of the dividing streamline.

Due to this problem and those encountered in the previous studies, attention was centred on the problem of straight separating flow over a flapped cavity. Schlieren techniques were used to establish the presence of straight separations, the priciple being that, for such a condition, the waves generated at the separation point are weakest.

In order to establish fully laminar flow, the model length was reduced and the free-stream Mach number was increased to $M_\infty = 9.7$ with the use of a conical nozzle. This model provided an ideal flow for testing Cooke's mixing layer analysis, and the high pressures in the reattachment zone made it possible to measure N, the reattachment pressure rise parameter. It was also hoped that problems of boundary layer transition and mixing layer unsteadiness would be removed, and that the base pressure, being equal to the free-stream static pressure, would be measurable. Rather than establishing a relationship between the separation angle and the flow parameters, the important characteristic

with the straight-separating flow was the mixing length and its variation with α_w, the reattachment angle.

The flow conditions used for this series of tests (Groups 13 - 15) are presented in Table II of Section 4.1.2. on page 44.

5.2.1. Upstream influence - Step height effect

Flapped cavity model - straight separations

One of the basic assumptions contained in Cooke's mixing layer analysis is that the mixing layer is free from any influence which might be generated downstream of the separation point. In practice, this assumption can be easily violated. When the ratio of the step height to the boundary layer thickness, L/δ_s, is small enough, the interaction between the mixing layer and downstream surfaces can severely affect the flow mechanism and thus prevent a "free-interaction" separation.

In the ideal case, where the bottom of the cavity is well away from the lower boundary of the separated layer, the velocity is zero inside the 'dead air' region and the flow over it is like that of a free jet with zero velocity one side and free stream velocity the other side. The presence of a wall, with its associated shear can invalidate this simple picture. Consequently, before a study of the mixing layer length can be started it is necessary to investigate the effect of step height, h , upon the flow and to establish, if possible, a critical step height, h_{crit}, above which upstream influence has no effect.

Straight separations were established for a range of step heights (between $\frac{1}{16}$" and $\frac{1}{2}$") and flap angles for $Re_{\infty} = 2.37 \times 10^5/in.$, with no side plates attached to the model. The length of the straight shear layer was taken to be that of a horizontal line drawn parallel to the free stream flow direction from the separation point to a point on the reattachment flap, (which will be called the geometric reattachment point). For a fixed value of α_w, the length was measured for each value of h, the procedure being repeated for four other values of α_w. It was hoped that, for α_w constant, the mixing length, L_{sep}, would asymptote to a fixed value as the step height was increased, thus indicating that a free-interaction separation was established. In such circumstances the theoretical assumption is valid.

Results plotted in Figs. 17(a) and 17(b) show that a critical step height does exist and that its value is a function of the reattachment pressure rise, h_{crit} becoming larger as α_w increases. For the reattachment angles considered in subsequent studies a typical value for $(h/\delta_s)_{crit}$ is $\simeq 5$.

For step heights smaller than the critical value, where δ_s is thick, the shear layer is compressed at the step corner for a fixed α_w and the separation is no longer straight. L_{sep} increases, indicating a higher value of the base pressure, p_2. This rise of p_2 with δ_s was observed by White (1965) who performed experiments on a conventional rearward-facing step flow at Mach 7.

The observed violation of the straight separation over the

flapped cavity is explained in physical terms by considerations of the influence of the surface below the step on the dividing streamline velocity, $\bar{u}_*$. For $h > h_{crit}$, where δ_s is relatively thin, Cooke's assumption of 'free-interaction' is valid, i.e. $\bar{u}_*$ (and hence L_{sep}) are constant for a particular value of α_w. However, when $h < h_{crit}$ and δ_s is relatively thick, then the shear layer is thick enough to be influenced by the presence of the wall. In this case, the interaction is no longer 'free' and, as δ_s depends upon Reynolds number, the Reynolds number independence predicted by Cooke no longer applies. The viscous shear imposed by the wall reduces the value of $\bar{u}_*$ and the dividing streamline requires a longer separated length to enable $\bar{u}_*$ to reach its original value corresponding to the constant α_w . In order to achieve this increase in L_{sep} , the shear layer must compress at the step corner, thus causing p_2 to rise. The dependence of p_2 on $\bar{u}_*$ is clearly shown by equation (3.2.) from which it can be seen that, as $\bar{u}_*$ decreases the reattachment pressure rise ratio p_r/p_2 of the dividing streamline decreases. However, assuming the pressure rise paramater N , to be constant, p_r is fixed for a constant α_w and thus p_2 must rise.

If the shear layer is to remain horizontal, with p_2 constant for a fixed α_w , then L_{sep} must be increased by moving the flap further away from the step (as shown by the results of Fig. 17). This allows the dividing streamline to attain the value of $\bar{u}_*$ which enables it to reach the pressure rise ratio p_r/p_2 . Alternatively, if L_{sep} is

considered constant, then to maintain the shear layer horizontal α_w and hence p_r/p_2 would have to be reduced.

Typical schlieren photographs of the flapped cavity flow are shown in Fig. 18 which illustrates the effect of step height on the shear layer length.

5.2.2. Separated length

As a mixing layer with finite initial thickness grows, the velocity on the dividing streamline, $\bar{u}_*$, increases from zero at the step and asymptotes to the Chapman value of 0.587 which corresponds to the case of zero initial shear layer thickness. In physical terms, $\bar{u}_*$ increases with L_{sep}, as predicted in Fig. 2, and the dividing streamline is able to withstand a higher pressure rise p_r/p_2 (as shown by equations (3.6) and (3.7)). However, for a horizontal separation, p_2 is fixed and equal to the upstream pressure and thus the downstream pressure and hence α_w must increase. The limiting value of α_w , will be reached as $\bar{u}_*$ approaches the Chapman value.

If a horizontal separation is established and the flap is then moved towards the step, keeping α_w constant, then the balance between $\bar{u}_*$ and α_w is violated. The shear layer attempts to maintain L_{sep} constant and does this by compressing at the step causing p_2 to rise, and thus reattaching further down the flap. Cooke's analysis has been described in Section 3.1.1. and the relation between L_{sep}/x_1 and $\bar{u}_*$ is shown in Fig. 2. The fact that L_{sep}/x_1 is the controlling length

scale indicates the importance of the body length x_1 in determining the length of the separated region.

Initial tests were performed at $Re_\infty = 2.37 \times 10^5/in.$ with flapped cavity models which did not have side plates attached. Three values of x_1 were considered i.e. 1.75" , 2.0" and 3.5" and the step height was varied from $\frac{1}{4}$" to $\frac{1}{2}$". δ_s was kept small to ensure that any upstream influence effects generated downstream of the step would be prevented. Care was taken to position the model surface accurately at a fixed distance from the nozzle centre line in order to ensure that the effective incidence of the leading edge in the conical flow was constant.

As expected, α_w increased with L_{sep} and was observed to tend towards a constant limiting value. Unfortunately, this value could not be established due to the onset of cavity flow closure. This limitation occurs when the ratio of cavity length to depth, L_{sep}/h , becomes sufficiently large for the flap to lose its effectiveness, i.e. a small step height h can only support a relatively small straight separated length. Under such conditions, the adverse pressure gradient imposed by the flap ceases to control the separation mechanism and the mixing layer expands at the step to reattach on the cavity floor. Merritt (1964) established an empirical expression for the critical value of L_{sep}/h at which the laminar cavity flow closes,

i.e. $$\frac{L_{sep}}{h} \geq \frac{2Re_{x_1}^{1/2}}{M_\infty^2} \qquad \ldots(5.1)$$

Charwat et al. (1961) also found a critical cavity length for supersonic, turbulent separations and established that the pressure distribution along the cavity floor depended on this length rather than the geometry of the reattachment surface. Subsequent pressure distributions in which the pressure is uniform upstream of the flap indicate that the cavity lengths considered here are relatively short.

The variation of L_{sep} with α_w is shown in Fig. 19 for three values of x_1. A comparison between the results led to the surprising result that the correlating length scale was the absolute separated length and not L_{sep}/x_1 i.e. for a fixed α_w the separated length was constant regardless of the value of x_1. This conclusion contradicts the theoretical argument of Cooke and is impossible on dimensional grounds. It would suggest that the mixing layer behaves as a free jet, emerging from the step location, which is independent of the body shape.

The schlieren photographs in Figs. 20 and 21 illustrate the variation of L_{sep} with α_w and the effect of x_1 on L_{sep} respectively. Subsequent tests in uniform flow (presented in Section 5.3.) showed the correlating length scale to be L_{sep}/x_1 for all values of x_1 and suggested that the conical data was open to criticism.

5.2.3. Influence of Reynolds number

The effect of boundary layer thickness on the separated flow geometry, with regard to upstream influence effects, has been described

in Section 5.2.1. for flows in which $h < h_{crit}$. However, contrary to the analysis of Section 3.1.1. in which the base properties are shown to be unit Reynolds number independent, it was expected that this thickness would also affect the separated flow mechanism when $h > h_{crit}$. In other words, it is thought doubtful that the interaction will ever be entirely 'free' or that the shear layer can be uncoupled from the internal re-circulating region as assumed by Cooke. For a constant Mach number, the flow parameter which controls the separation thickness, δ_s, and also the mixing coefficient in the separated layer, is the free stream unit Reynolds number Re_∞.

Crocco and Lees (1952) regarded mixing, or the transport of momentum from the outer stream to the dissipative flow, to be the fundamental physical process determining the base flow properties. Following their argument, the base pressure (and hence the length of the separated layer) is a function of both the thickness δ_s and the mixing coefficient of the layer, k, the effect of each being in the opposite sense for a variation of Re_∞. This explains the large differences in behaviour of a separated flow with Reynolds number in the various flow régimes. They predicted that, for fully laminar flow, the mixing coefficient, k_{lam}, of the separated layer is the dominant controlling parameter, whereas, in the turbulent régime, the boundary layer thickness is the important term. Transition confuses the picture somewhat and its effect is described in detail in Section 5.2.2.

Considering the case of fully laminar flow, they showed than an increase in the Reynolds number causes a decrease in the mixing coefficient, the effect of which is to cause less mass to be scavenged from the 'dead air' region. Due to this reduction of the mixing rate and the less efficient mixing, the rate of increase of $\bar{u}_*$ with distance is diminished. In the case of a straight-separating shear layer on the flapped cavity model the dividing streamline is no longer able to accomplish the reattachment pressure rise ratio p_r/p_2 associated with a fixed α_w and p_2 rises. In order for p_r/p_2 of the dividing streamline to be reached by a horizontal shear layer, L_{sep}, and hence $\bar{u}_*$, must increase with the Reynolds number. This trend was expected in the present study as schlieren photographs indicate that the flow is laminar over the full extent of the separation.

The length of the separation was measured for a range of Re_∞ between 1.18×10^5 and 3.96×10^5/in. using a flapped cavity model with a leading-edge to step length of 3.5", without side plates. The flow total temperature was approximately constant.

The results are shown in Fig. 22(a) where L_{sep}/x_1 is plotted against Re_{x_1}, the Reynolds number based on the attached flow length. It can be seen that the expected laminar trend is evident, L_{sep} being a weak function of Re_{x_1}. The result of varying Re_{x_1} by changing x_1 for constant unit Reynolds number is the same which suggests that the unit Reynolds number is not, in itself, the influencing parameter, but Re_{x_1}.

5.2.4. Effect of side plates

Though the variation of L_{sep} with α_w illustrated in Fig. 19 showed the expected trend, the reattachment angle for a given separated length was far in excess of that predicted using Cooke's mixing theory. This phenomenon was assumed to be caused by the presence of side-wash effects in the reattachment zone which caused a loss of the flap effectiveness.

Two basic types of side plate were employed to test this assumption, namely those extending parallel from the separation point to include the base region and the reattachment pressure rise, and those extending from the beginning of the reattachment pressure rise to a point downstream of the peak. Both types generated precisely similar flows in which the variation of L_{sep} with α_w (shown in Fig. 19) was much closer to the predicted distribution. A typical photograph of the two types of side plates and the associated flow pattern is shown in Fig. 23. Repeatable results were obtained using smaller side plates which enclosed the reattachment pressure rise only. The conclusions, which were supported by oil spot visualisation tests, substantiated the assumption that side flow occurred only in the region of the reattachment point where the streamwise momentum was small and the pressure higher than the free stream static value.

Many doubts have arisen about the validity of tests performed in conical flow in which models without side plates have been used, the main cause for concern being the lack of comparison between the measured and

predicted correlating length scales of the separated region. The independence of L_{sep} on x_1 is thought to be due to the effects of conicity where models of different length scales were used in a source flow stream which expanded in a downstream direction. However, conclusions concerning the effect of step height and Reynolds number, discussed in Sections 5.2.1. and 5.2.3. respectively, are suggested to be qualitatively correct. In these particular studies great care was taken to maintain x_1 constant and the model was always tested in exactly the same position in the working section. Subsequent tests, which are presented in Section 5.3. confirm this view.

To avoid doubts over conicity and side effects all further studies were made using models with side plates in a Mach 8·2, uniform flow provided by a contoured nozzle.

The conical and uniform flow studies are compared and contrasted in the discussion in Section 5.3.7.

5.3. Straight Separations in Uniform Flow

Flapped cavity model

5.3.1. Effect of side plates

The flow visualisation techniques mentioned in the previous section suggested the merit of side plates in this study of step flows, in which three-dimensional side flows are severe for the small span models considered. However, before detailed studies of the separated

flow were commenced, the validity of the assumption that the use of such devices provided a truly two-dimensional flow, free of side effects, without generating disturbances, was thoroughly checked in the uniform flow. Two techniques were used.

The first method entailed the measurement of transverse pressure distributions on models with and without the addition of side plates. The distributions were measured at two locations downstream of the step, denoted by x_s/h , namely the constant pressure 'dead air' region (where $x_s/h = 1{\cdot}2$) and the reattachment zone, close to the reattachment point ($x_s/h = 4{\cdot}8$). Spanwise pressures could be measured at tappings spaced $\frac{3}{4}$" and $1\frac{1}{2}$" to each side of the model centre-line. The streamwise pressure distributions were also measured, with and without the addition of side plates, and the two compared. The measurements were made for $x_1 = 3{\cdot}5$" , $h = \frac{1}{4}$" and $\alpha_w = 9{\cdot}2^{\circ}$ at $Re_{\infty} = 2{\cdot}37 \times 10^5$/in. and the transverse and streamwise distributions are shown in Figs. 25(a) and 25(b) respectively.

Fig. 25(a), as expected, showed that the 'dead air' pressure was constant across the span whether or not side plates were used, whereas the transverse distribution in the reattachment region, which exhibited a symmetrical parabolic shape with a peak at the centre-line when side plates were not present, was forced to a constant value by their addition. It was noted that the centre-line pressure was not affected by the side plates, thus indicating that side effects diminished to zero on this line. The equivalent streamwise distributions

were identical showing that side plate disturbance effects were non-existent.

As straight separations were required for a constant value of α_w, the step to hinge distance $L_{s.h}$, had to be less for the case of the model without side plates than that in which they were present due to the loss in flap effectiveness caused by flow escaping over its side.

To check a possible loss of flap effectiveness due to an inadequate length of reattachment surface, the streamwise pressure distribution was measured with the 4" flap replaced by one measuring 8". No variation was observed and it was concluded that the reattachment surface length was adequate, provided that it extended downstream of the peak pressure at the end of the reattachment zone.

The axisymmetric model, described in Section 4.2., was used to provide the second method for checking side plate effectiveness. The procedure was to generate straight separated flows on both the axisymmetric model and the two-dimensional model with side plates for similar free stream conditions and model geometries. The effectiveness of the side plates would be established if both types of model generated the same separated length.

For $Re_\infty = 2.37 \times 10^5/in.$, $x_1 = 2.0"$, $h = \frac{1}{4}"$ and a flap angle of 10.4^o, straight separations were established and identified from schlieren photographs, such as the one shown in Fig. 26 for the axisymmetric model. The lengths obtained with the two models were in

very good agreement (see Fig. 27).

This thorough investigation proved the validity of the side plates and they were used in all the subsequent investigations in which the aspect ratio of the separated region (defined as the ratio of the model span to the separated length) was relatively small i.e. between 1.7 and 3.

5.3.2. Separated length - Correlation with Cooke's theory

At M = 8.2 it was expected that transition would occur within the mixing layer at the higher values of Reynolds number and indeed, the 'kink' in the pressure distribution shown in Fig. 25 indicated its presence in that particular case.

In order to compare Cooke's mixing theory with the experimental data, it was vital that fully laminar reattachments could be established and identified. Three techniques were used to establish the flow régime, namely, schlieren methods, the measurement of pitot profiles in the attached boundary layer and the separated shear layer and finally, the study of the pressure and heat transfer distributions.

A series of straight separations were generated on the flapped cavity model at the free-stream conditions shown in Table II (page 44) using the side-plated models. Three values of x_1 were considered i.e. 1.75" , 2.0" and 3.5" and the step height h was varied from $\frac{1}{4}$" to $\frac{3}{8}$". The relationship between the separated length and the reattachment angle is shown in Fig. 27. As was shown in the tests performed in the

conical flow, the addition of side plates to the model clearly increased the effectiveness of the reattachment surface.

For a constant unit Reynolds number the expected trend was evident. As predicted by Cooke, the correlating length scale was shown to be L_{sep}/x_1 for all values of x_1 which indicated the importance of the body length x_1 in determining the length of the mixing layer. The reattachment angle α_w, increased with L_{sep}/x_1 and was observed to asymptote to a constant maximum value. Hurlburt (1966) established the same trend of L_{sep}/x_1 with α_w for similar straight separations from a flapped cavity model at $M_\infty = 2.85$ (see Fig. 32(a)). In physical terms, this variation meant that as the mixing layer length increased (and with it the dividing streamline velocity, $\bar{u}_*$), the shear layer was able to withstand a larger pressure rise, and hence reattachment angle, due to its higher energy content. The fact that α_w tended to a constant value showed that the shear layer had reached a limiting (or asymptotic) state in which $\bar{u}_*$, and hence the energy level, had risen to a maximum value. Chapman's similarity solution of a mixing layer growing from zero thickness with a constant $\bar{u}_*$ (= .587) can be used to predict this limiting condition only.

The reattachment pressure rise ratio p_3/p_2, was measured and its variation with α_w is shown in Fig. 28 which shows that, though p_3/p_2 is relatively independent of Reynolds number, its variation with α_w exhibits a similar asymptotic behaviour to that of L_{sep}/x_1. The corresponding relation between L_{sep}/x_1 and p_3/p_2 for laminar reattachment

shown in Fig. 29, exhibits a limited range of linearity i.e.

$$L_{sep}/x_1 \sim (p_3/p_2) \qquad \ldots(5.2)$$

for $0.6 < L_{sep}/x_1 < 1.3$

This indicates the larger pressure rise that the increased separated lengths can withstand before the asymptotic limit is reached.

The limiting condition of the flow mechanism considered in this study is that of an attached, flat plate boundary layer namely, as α_w and hence L_{sep}/x_1 tend to zero, the step height must also reduce identically to zero. This condition is quite different to that which occurs for a compression corner separated flow i.e. that of incipient separation, the condition at which the attached boundary layer just separates due to the induced adverse pressure gradient generated by a finite flap angle. For comparison, Fig. 27 includes the value of α_w for incipient separation determined for the same flow conditions by Needham. This value of 7.8^o compares with the asymptotic value of 10.4^o measured in the present study.

A severe Reynolds number effect of the flow geometry was clearly evident (see Fig. 27) and was thought to be due to the onset of transition in the shear layer at the higher values of Re_{x_1}, the separation Reynolds number. The effect of the transition was to cause the separated length to fall sharply with increasing Re_{x_1}, for a constant α_w. This phenomenon, which is of fundamental importance to the base flow problem, is discussed fully in Section 5.3.4.

At the lower values of Re_{x_1} the flow appeared to be entirely

laminar and these results were compared with Cooke's theoretical analysis. The comparison which is shown in Fig. 30, is seen to be very good for the separated lengths considered, the main error of the theory being an over-estimation of the limiting angle of reattachment. This value, which was evaluated using the assumption that $\bar{u}_* \rightarrow .587$ as $L_{sep}/x_1 \rightarrow \infty$, was found to be a factor of two greater than the measured value. The results clearly show that the shear layer profile approaches the Chapman distribution, corresponding to the case of zero initial thickness, more rapidly than predicted by the asymptotic, theoretical model. However, it must be stressed that this divergence occurs at large values of separated length which would be impossible to achieve experimentally with the flapped cavity models considered due to the occurrence of flow closure.

As discussed in Section 3.1.1., two basic assumptions about the flow mechanism have to be made when applying Cooke's theory. They concern the estimation of N, the reattachment parameter, and the value of T_d, the 'dead air' temperature. The best correlation with the measured L_{sep}/x_1 vs. α_w relationship was obtained by assuming that $N = 1$ and $T_d = T_w$, the wall temperature.

N was measured for both the laminar and transitional reattaching flows and was found to be unity in the former case, since the peak pressure was measured at the reattachment point. The onset of transition was found to severely affect N, causing the dividing streamline to stagnate at a lower pressure. A discussion of N and its measurement

is presented in Section 5.3.5. The low heat transfer rates measured in the separated region suggest that the assumption $T_d = T_w$ is realistic, even though other investigators, including Chapman, assumed $T_d = T_{t2}$. A subsequent comparison between the measured and Van Driest's theoretical separated layer profiles confirmed the validity of the present assumption.

The validity of using the Carrière and Sirieix expression for the variation of total temperature with u_* across the mixing layer, rather than that of Crocco, has been justified by the good agreement obtained between theory and experiment. Cooke also established a good comparison between his results and some experimental data of Ginoux (1960) for laminar rearward-facing step flows using this relation.

The experimental results presented in Fig. 22(a) showed that L_{sep}/x_1 increased with Re_{x_1} in the laminar régime. However, this trend was very slow indicating that the contrasting effects on the base flow of variations in the boundary layer thickness and the shear layer mixing rate were almost compensating each other for a change of Reynolds number (as was suggested by Crocco and Lees). Consequently, the unit Reynolds number independence shown by Cooke's laminar theory was regarded as being reasonable.

5.3.3. Pitot profiles of the attached and separated layers

A probe with a rectangular cross-section orifice measuring 0.16" deep and 0.70" wide was used to measure pitot profiles at three locations

in the flapped cavity flow, namely, just ahead of the step, approximately half-way along the shear layer and downstream of the reattachment zone. The relevant test conditions were $M = 8.2$, $Re_{\omega} = 0.13 \times 10^5/in.$, $x_1 = 2.0"$ and $\alpha_w = 10.3^{\circ}$.

Fig. 31(a) shows the pitot pressure profile of the attached boundary layer. The well known laminar form is evident, the majority of the mass flux being situated at the outer edge of the layer. The figure also shows a comparison between the measured Mach number profile, plotted against the normal distance parameter $y/x\sqrt{Re_x}$, and that determined from the laminar theory of Van Driest for the same free stream conditions. It can be seen that the two compare extremely well and the Van Driest thickness (defined as extending to the streamline along which $u_* = 0.99$) is within 3% of the measured value.

In order to convert the pitot pressure to Mach number it is assumed that the normal static pressure gradient in the boundary layer is zero, which is quite valid in the case of a zero stream-wise pressure gradient. It is extremely difficult to check this assumption with a static pressure probe due to interference effects and the long response times incurred in trying to measure a small pressure with a limited orifice size.

The pitot pressure profile of the shear layer shown in Fig. 31(b) also exhibits a laminar shape. The step height was $\frac{1}{4}"$, and if the layer is considered to be divided into upper and lower thicknesses, δ_u and δ_l, extending above and below this height, it can be seen that the

upper part exhibits the form of an attached layer, carrying the bulk of the mass flux, the pressure at the step height being approximately the ambient static value. The cavity is full of low-velocity, recirculating flow and an attempt was made to measure the reversed flow profile. The reversed flow could be detected with a forward-facing probe which measured pressures below the ambient static value in this region. By reversing the probe it was just possible to detect pressures above this value thus indicating the recirculation. The results indicated an extremely low momentum content, the reversed flow pitot pressure being of the same order as the static value. The zero velocity streamline was identified by extrapolation of the pitot pressure profile to the ambient static value, however this technique was crude considering the extent of low momentum flow described above.

The measured values of δ_u and δ_l were within 12% and 30% respectively of the values 0·086" and 0·055" predicted from the momentum integral technique of Section 3.1.2.

Once again, the Mach number profile was determined using the assumption of constant static pressure, which is certainly valid when there is no expansion or compression at the step. In order to compare the profile with the Van Driest attached layer profile, the total shear layer thickness, δ_T, was taken to extend from the measured zero velocity streamline. The comparison between the profile shapes, shown in the figure, is seen to be very good if the Van Driest profile is determined assuming $T_d = T_w$ whereas the comparison is poor if it is assumed that

$T_d = T_{t2}$. However, the measured δ_T ($\simeq 0{\cdot}14''$) was much larger than that predicted by Van Driest for an attached layer. This result was expected and illustrates the increased rate of growth of the separated mixing layer.

The assumption in Section 3.1.2. that the dividing streamline separated straight from the step was checked by measuring the Mach number ratio along it, $\bar{M}_*$, and comparing it with the value obtained from the calculated $\bar{u}_*$ at the traverse position L/x_1 (obtained from Fig. 2). Assuming (as in Section 5.3.2.) that T_d is equal to the wall temperature T_w, the dividing streamline temperature ratio, $\bar{T}_*$ was determined from equation (3.5.(ii)) and, using the relation

$$\bar{M}_* = \bar{u}_*/\bar{a}_* \qquad \ldots(5.3.)$$

$\bar{M}_*$ was found to be 0·19, which compared well with the measured value of 0·20. This result supported the assumption that $T_w = T_d$ and contrasted with the value of $\bar{M}_* = 0{\cdot}11$ obtained by using Chapman's assumption that $T_d = T_{t2}$.

The pitot pressure and Mach number profiles of the reattached boundary layer for $M_\infty = 5{\cdot}78$ and $T_w/T_\infty = 2{\cdot}7$ are illustrated in Fig. 31.(c). They show a laminar form in the outer region of the layer which is closely related to the Van Driest profile. However, the high values of the pressure close to the wall suggested the existence of a relatively high mass flow. This was explained by the fact that the traverse was made relatively close to the reattachment point, where, due to the high rate of centrifugal compression,

the layer was thin (see Figs. 19, 20 and 21) and had not yet re-established an attached flat plate character. One would expect the profiles to revert to this character downstream of the reattachment zone, where both the normal and streamwise pressure gradients are zero. Under these conditions the mass flow, forced close to the wall at reattachment, would be able to move towards the edge of the boundary layer.

These conclusions confirmed the assumption that the entire separated flow mechanism was fully laminar.

5.3.4. Influence of shear layer transition

- Straight separations

The transition studies and the subsequent measurement of N and the pressure and heat transfer distributions were performed for flapped cavity separations selected from those discussed in Section 5.3.2. and displayed in Fig. 27. The step height was constant ($h = \frac{1}{4}$") and two values of attached flow length (x_1 = 2·0" and 3·5") were used. The salient flow parameters are listed in the table shown in Appendix A.

The non-dimensional length L_{sep}/x_1 is correlated in terms of Re_{L_r}, the Reynolds number based on the total length of the mixing layer from the leading edge to the reattachment point, and the results are shown in Fig. 32. The effect of Reynolds number on the separated length in the laminar and transitional flow régimes is demonstrated,

L_{sep}/x_1 exhibiting a distinct peak at $Re_{L_r} \simeq 0{\cdot}9 \times 10^6$ for all values of α_w and x_1 considered. For $Re_{L_r} < 0{\cdot}9 \times 10^6$ the variation of L_{sep}/x_1 was small whereas, for $Re_{L_r} > 0{\cdot}9 \times 10^6$, the separated length decreased rapidly with increasing Re_{L_r} and using the techniques described before it was established that the former trend was exhibited by the fully laminar reattaching flow whereas the latter was caused by transition moving upstream of the reattachment point. The peak value of L_{sep}/x_1 occurred when transition was located at the reattachment point.

Additional laminar data could not be obtained due to the limited Reynolds number range of the facility.

The fact that the maximum L_{sep}/x_1 occurred at a constant value of Re_{L_r} for all values of x_1 suggests that the location of transition within the straight mixing layer is independent of the length of the flow which is attached to that which is separated, but is only a function of unit Reynolds number. This further suggests that the mechanism of transition in the shear layer is analogous to that in a fully attached boundary layer. Results obtained for the model without side plates exhibited a transitional behaviour and are shown in Fig. 22(b) where L_{sep}/x_1 is plotted against Re_{x_1} for $x_1 = 3{\cdot}5"$.

The existence of the high base pressure (and hence L_{sep}/x_1) which was evident for the laminar flows and the variation with Reynolds number had already been explained in terms of the shear layer mixing rate and this argument can be extended to consider the effect of

transition. As the Reynolds number is increased and transition eventually begins to move upstream into the mixing layer, the local mixing rate k_{turb} ($\simeq 5 - 10\ k_{lam}$) counteracts the controlling effects present in the laminar régime. The precipitous drop of L_{sep}/x_1, which is observed for straight separations with fixed α_w when the separation Reynolds number is increased, is due to the large increase in the mixing rate. This increase is much more important than the associated increase in the mixing layer thickness which, by itself, would have an opposite effect on the straight separated length. The relatively high values of L_{sep}/x_1 observed for the straight separations in laminar flow are established due to the low laminar mixing rate. The precipitous drop of L_{sep}/x_1 (for constant α_w) would be expected to become less rapid as the transition point moves close to the step as the decrease of the boundary layer thickness at the step is now the controlling effect. Eventually, as the transition point moves upstream of the step, L_{sep}/x_1 of the separation (straight or otherwise) would begin to rise due to the increased thickness of the step boundary layer caused by the upstream movement of the transition point as the Reynolds number increases. This behaviour was demonstrated by the transitional wedge flows (shown in Fig. 13). The variation of the base properties in relation to the transition located is shown in Fig. 32 for all the flow régimes.

The present results are compared with the straight separation data of Hurlburt which are presented in Fig. 32(c) where L_{sep}/x_1 is plotted against Re_{x_1} for $x_1 = 1.0"$. The latter results, obtained

at $M_\infty = 2{\cdot}85$, clearly exhibit a transitional trend and the levelling-out of L_{sep}/x_1 at the higher values of Reynolds number indicated that the transition point was close to the step. This surmise was substantiated by schlieren photographs of the flow.

The dividing streamline velocity $\bar{u}_*$ is strongly affected by the viscous mixing in the shear layer and its variation, due to the onset of transition determines the length of the separation. Due to the low mixing rate in the laminar shear layer the rate of increase of $\bar{u}_*$ is low and relatively long separated lengths are required to enable the dividing streamline to accomplish the reattachment pressure rise. However, when transition enters the layer, it causes a rapid increase in the mixing action; the shear layer is re-energised and $\bar{u}_*$ increases thus enabling the dividing streamline to satisfy the reattachment criterion within a shorter separated length. If one considered a horizontal shear layer where L_{sep} is maintained constant then, as the mixing rate increases with the onset of transition, the flap angle and hence p_r/p_2 would have to be increased due to the increase in $\bar{u}_*$. These trends are shown by the experimental results of Fig. 32(a).

Contrary to the previous discussion, Hurlburt suggests that his experimental results demonstrate laminar characteristics, basing his argument on the variation of a laminar mixing rate with Reynolds number. The present laminar data indicate that this effect is too weak and indeed in an opposite direction to cause the variation exhibited by his results. He calculated the dividing streamline velocity for a range of Reynolds numbers by determining the reattachment

pressure p_r , and incorporating Chapman's limiting solution of a layer with zero initial thickness. Regarding the reattachment point to be located at a point on the flap, level with the step corner, he found that the reattachment parameter N, was between 0·6 and 0·7 . Substituting p_r into equation (3.2.) he calculated that $\bar{u}_*$ asymptoted to 0·665. Indeed, if it is assumed that N = 1 , then Hurlburt's data gives $\bar{u}_* = 0{\cdot}73$. These very high values of reattachment pressure, and hence $\bar{u}_*$, suggest the presence of a high mixing rate in the shear layer. It has been argued earlier that this increase is explained by the onset of transition upstream of the reattachment point which also explains his observed variation of L_{sep}/x_1 with Reynolds number shown in Fig. 32(c).

The limitations of Chapman's laminar analysis have been described and it is thought doubtful that the separated lengths considered by Hurlburt were long enough for the mixing layer to establish a limiting velocity profile. The assumption that the reattachment point is fixed geometrically is contradicted by the results of Section 5.3.5. which indicated that its location is above the horizontal line and that it is a function of both pressure gradient and Reynolds number.

Many investigators have measured base pressures, using models with laminar separating boundary layers. However, a certain controversey exists concerning the variation of this pressure (which is analagous to the variation of the separated length) in the fully laminar régime.

Chapman (1951) and Chapman et al. (1952) considered a laminar separating flow at $M_\infty = 1.25 - 3.1$ and correlated the variation of base pressure with the parameter $x_1/hRe_{x_1}^{1/2}$ which expresses the ratio δ_s/h for a laminar layer at the step. They established that the base pressure dropped linearly with this term and, extrapolating the experimental data to zero boundary layer thickness i.e. $x_1/hRe_{x_1}^{1/2} = 0$, they found that the minimum base pressure agreed with that determined by the Chapman - Korst inviscid theory. Nash (1962) who showed that this extrapolation overestimated the limiting pressure due to the rapid decay of pressure at small values of δ_s, established that the minimum pressure occurred when transition was close to the separation point and the boundary layer was thin. This conclusion agrees with the argument presented here, namely that when transition is located just downstream of separation, the boundary layer thickness, and not the mixing rate, is the controlling effect and the governing parameter is $x_1/hRe_{x_1}^{1/2}$ since the flow up to the step is still laminar. As the Reynolds number increases, the boundary layer thins and the pressure reaches a minimum value before the transition 'jumps' upstream of separation. This condition which is shown in Fig. 32.(b) corresponds to the limiting value obtained by Chapman - Korst in their analysis of a zero initial thickness mixing layer.

This argument is corroberated by the results of Charwat et al. (1958) who studied the separation of laminar and transitional shear layers from a wedge at $M_\infty = 1.98$ and 2.78 and $1 \times 10^4 <$

$Re_{x_1} < 7 \times 10^5$ and established the same trends of base pressure as shown in the present flapped cavity study. The base pressure in the transitional régime correlated with the parameter $x_1/hRe_{x_1}^{1/2}$ and they extended the results into the régime of fully turbulent separation by incorporating the results of Gadd et al. (1956) who considered an identical wedge geometry at $M_\infty = 3.0$.

Some authors, including Bogdonoff (1952), Reller and Hamaker (1955) and Carrière and Sirieix (1964) have regarded this behaviour to be due to a fully laminar mechanism and not one in which transition is occurring in the mixing layer. However, Kavanau (1954) and Van Hise (1957) have obtained data which exhibits the Reynolds number variation shown by the present laminar data.

Miller et al. (1964) studied wedge compression corner separations at Mach numbers between 8 and 22 and observed the variation of L_{sep} with Re_∞. They found that, at low supersonic speeds, an increase of Re_∞ decreased the separated length whereas the reverse occurred at $M_\infty = 16$. These results suggest that transition was occurring in the separated layer at the lower Mach numbers which they considered.

Hama (1967) has illustrated the variation of base pressure with Reynolds number and the characteristics are shown in Fig. 32(b). The four flow régimes are clearly evident and the laminar and shear layer transition variations compare with the present data. The variations of base pressure shown in Fig. 32(b) for the cases of

boundary layer transition and fully turbulent flow also compare with those established in the previous wedge studies of Section 5.1.1. which are shown in Fig. 13.

5.3.5. The reattachment parameter

The extreme importance of defining a correct value of the reattachment pressure rise parameter N, when applying the dividing streamline analysis to a separated flow problem has already been described and the theoretical predictions illustrated in Fig. 3(b) show the profound effect which this parameter can have on the flow geometry. However, up to the present time, a precise knowledge of N and its dependence on the influencing flow parameters in the various flow régimes is not available even though some authors have used experimental evidence to suggest particular values for fully laminar and turbulent flows. The effect of transition on the reattachment mechanism has not been studied to the author's knowledge. For these reasons, the measurement of N was considered to be essential and results were obtained using the techniques already described. Both surface static and pitot pressures were measured successfully and typical oscilloscope traces of the transducer outputs are shown in Fig. 24.

The variations of the reattachment parameter with the angle of reattachment and Re_{L_r} for the flapped cavity model are shown in Figs. 33(a) and 33(b) respectively. For a fully laminar shear layer it was observed that the dividing streamline reattached at the peak of the

reattachment pressure rise, i.e. $N = 1$, and the mechanism was independent of both the pressure gradient and the external Reynolds number. However, when transition entered the layer, the reattachment mechanism was severely affected, N decreasing for an increase of both the angle of reattachment and the Reynolds number.

It is suggested that the difference in behaviour of N in the laminar and transitional flows is due to the change of the shear layer mixing rate and the fact that the pressure recovery which takes place downstream of the reattachment point is associated with the rehabilitating velocity profile. In the case of a laminar reattachment, where the mixing rate is low and the reattaching layer thin, it is assumed that the shear layer profiles are independent of Reynolds number, as was suggested by Cooke's theory. The compensating effects of the boundary layer thickness at separation and the laminar mixing rate (which have already been described) also explain the observed independence of the base flow properties on this parameter.

When the Reynolds number is further increased and transition moves upstream into the shear layer it is suggested that the rapid increase of mixing rate and shear layer thickness distort the laminar velocity profile. The corresponding change of the pressure recovery of the dividing streamline at reattachment then causes the observed variation of N with the Reynolds number.

It was noted that in all the reattachments considered the reattachment point, though variable, was always located downstream of

the geometrical position, being furthest downstream for laminar flow. As transition entered the layer with increasing Reynolds number the point moved closer to the geometrical position. This observation contradicts Hurlburt's assumption that the reattachment point is fixed. Due to the large pressure gradients present, a small error in the estimation of the reattachment point would lead to a large error in the value of p_r , the reattachment pressure.

For the transitional flows considered it was thought useful to try and relate N with a parameter including both α_w and Re_{L_r} . If one considers the case of a turbulent flow in which the boundary layer profile is approximated with a 1/7th. power law, the thickness of the layer is inversely proportional to the 1/5th. power of the Reynolds number. It has already been suggested that, when transition is located upstream of the reattachment point, then the shear layer thickness has an effect on N and thus it was thought possible that N would be correlated by some parameter including Re_{L_r} . Indeed, a single line correlation of this type was found using the parameter $(\alpha_w . Re_{L_r}^{1/5})$ and it is shown in Fig. 34.

It is seen that N varies linearly with $(\alpha_w . Re_{L_r}^{1/5})$ for the transitional data and that its value decreases from 1·0 to 0·35 in the range $2·2 < (\alpha_w . Re_{L_r}^{1/5}) < 3·1$. This range is regarded to cover the entire régime of shear layer transition. For $(\alpha_w . Re_{L_r}^{1/5}) < 2·2$, the reattachment is laminar and N is constant and also equal to unity which confirms Chapman's original assumption. The layer is assumed to be

fully turbulent for $(\alpha_w \cdot Re_{L_r}^{1/5}) > 3 \cdot 1$ due to the fact that the lowest value of the reattachment parameter ($N = 0 \cdot 35$ at $(\alpha_w \cdot Re_{L_r}^{1/5}) = 3 \cdot 1$) was identical to the value proposed by Nash for fully turbulent separations.

It is suggested that this value of N is constant (as in the laminar régime) due to the relative independence of Reynolds number exhibited by turbulent flows and that large variations are caused by the onset of transition. The figure shows the range of $(\alpha_w \cdot Re_{L_r}^{1/5})$ covered by Hurlburt's investigation and again suggests that his results display transitional behaviour.

Carrière and Sirieix (1964) and Carrière (1965) studied the reattachment mechanism of a turbulent shear layer for $M_\infty = 3$ to 6. Rather than establishing a reattachment point and a value for N, they determined the existence of two critical points, K_1 and K_2, on the reattachment pressure rise. They used a rearward-facing step, downstream of which was a corner P. The adjustment of a flap allowed them to impose an arbitrary, constant pressure, p_3, downstream of P and they studied the effect of p_3 on the induced pressure distribution p(x), comparing it with the reference or unperturbed distribution $p^*(x)$. The upstream critical point, K_1 was found to be very close to the reattachment point, R whereas K_2 occurred further downstream. The two points displayed the following properties:

For all positions of P behind K_1, the distribution p(x) was unchanged provided that p_3 was adjusted to equal the unperturbed $p^*(x=P)$ after K_1. If $p_3 < p_{K_1}$ then the base pressure and $p^*(x)$ were affected.

For positions of P behind K_2, the curve p(x) remained unaltered up

to K_1 provided that p_3 was between the limits $p_3(max)$ and $p_3(min)$. $p(x)$ became different to $p^*(x)$ if p_3 occurred outside these limits and the base pressure was affected.

Following these results, Carrière et al. thought it logical to replace N with the parameter $\bar{w}$. Due to the significance of the point K_1 they defined $\bar{w} = \frac{p - p_2}{p_{K_1} - p_2}$ where $\bar{w} = 0$ at the start of the pressure rise and $\bar{w} = 1$ at the point K_1.

From their experimental results, they found that the extent of the two-dimensional reattachment zone from $\bar{w} = 0$ to $\bar{w} = 1$ was $7{\cdot}5\lambda$, where λ was the thickness of the shear layer at the end of the constant pressure mixing region. Indeed the transitional reattachment pressure distributions of Fig. 35 for α_w constant show that the length of the pressure rise up to R , and the associated value of N , increase with the mixing layer length, and hence λ, as the Reynolds number is reduced.

As extraneous disturbances to the pressure distribution downstream of the dividing streamline stagnation point would have no effect on the recirculating flow behind the step, the fact that the reattachment point is closely analogous to the upstream critical point K_1 (as shown by Carrière and Sirieix) would seem to be reasonable. Following the results of the present study, it is suggested that the critical point occurs at the peak of the pressure rise for a laminar reattachment whereas, for turbulent flows, where N is low, then the

critical pressure is also low and K_1 occurs on the pressure rise. This is shown by the conclusions of Carrière and Sirieix.

It must be stressed that these conclusions are confined to supersonic speeds. Nash (1962) collected experimental data on the reattachment parameter and its variation with Mach number for both subsonic and supersonic turbulent flows. Though N was constant and equal to 0·35 in the latter case, the subsonic flow exhibited values of $N > 1$. At low speeds, the flow mechanism is not amenable to the dividing streamline analysis of Chapman - Korst. Values of N exceeding unity occur at these speeds because the reattachment pressure rise exhibits a distinct peak and p_r, although less than the pressure maximum, is larger than the downstream pressure p_3. At supersonic speeds the pressure rises continuously from p_2 to p_3 without a distinct maximum (as shown by the results in Section 5.3.6.1.) and thus N cannot exceed unity.

5.3.6. Pressure and heat transfer rate distributions

The pressure and heat transfer rates in the reattachment zone were well within the measuring capability of the instrumentation, and checks on both the repeatability and spanwise variation of both these properties established the steadiness and two-dimensionality of the flow during the period of steady tunnel conditions. The onset of transition in the reattaching layer was clearly illustrated by both the pressure and heat transfer distributions.

5.3.6.1. Reattachment pressure distributions

The schlieren photographs in Figs. 18, 20 and 21 illustrate the main characteristics of the flow pattern and the model geometry. The reattaching shear layer is seen to thin rapidly as it encounters the large adverse pressure gradient induced by the flap and a strong oblique shock wave is visible at its outer edge. The associated reattachment pressure distributions are shown in Fig. 35 in which the ratio of the local pressure on the flap to the upstream value p/p_2 is plotted against x_h/h, the non-dimensional streamwise distance measured from the flap hinge, which is located at a variable distance $L_{s.h}$ downstream of the step. The figures includes the surface pitot pressure distributions and the locations of the reattachment point.

For all the step-hinge lengths considered, the surface static pressure was constant and equal to the upstream value in the 'dead air' region downstream of the step and began to rise at the flap hinge. When the reattachment was fully laminar the pressure rose continuously to a maximum value which asymptoted to the inviscid value of the downstream pressure determined from oblique shock tables. However, the onset of transition had a distinct effect upon this laminar behaviour, the pressure rise ceased to be continuous and exhibited a definite peak value which was approximately equal to the calculated inviscid pressure. A 'kink' was observed in the pressure rise, where the pressure levelled-off and then increased, which became more severe as the reattachment angle and Reynolds number increased

and indeed, at the largest flap angle considered ($\alpha_w = 10{\cdot}4^o$) the distribution exhibited a distinct unsteadiness of the flow. Ginoux (1958) observed spanwise perturbations in the reattachment region of a $M_\infty = 2{\cdot}05$ laminar separating flow which are thought to be attributable to the onset of transition. The reattachment point, R , given by the intersection of the surface static and pitot pressure distributions, is seen to move down the pressure rise as the reattachment angle and Reynolds number increase.

The influence of transition on the pressure distribution is clearly exhibited in Fig. 36 where the distributions for various Reynolds numbers are compared for each reattachment angle considered. The effect of α_w is shown in Fig. 37 which indicates the increase of the pressure gradient and the decrease of the length of the reattachment zone as α_w increases.

The measured distributions and those calculated using the simplified moment of momentum solution of Hankey and Cross (see Section 3.2.) are shown in Fig. 38. One point of difference between the two is the location of the reattachment point, R , whereas R was determined experimentally to be at the peak of the pressure rise, the theory required that R was located at the inflection point of the distribution. However, the comparison is seen to be good considering that the analysis is meant to apply to low supersonic speeds and also embodied several sweeping assumptions. Certain of these assumptions, particularly that of a small variation of the momentum thickness through

the interaction, were considered to be valid for the case of the flapped cavity where there were no discontinuities at the separation point.

It is thought that the main error involved in the method is the poorly defined technique for evaluating the interaction length L (which was discussed in Section 3.2.) The assumption that L is constant and has an average value over the interval of integration is considered to be too limiting in regions of advanced separation where the pressure gradient is large.

As the theory requires the values of the upstream and downstream Mach numbers as boundary conditions and uses matching at the hinge and reattachment points, where M_e and M_e' are assumed to be continuous, the resulting distribution is forced to a certain extent to match with that measured in the experiment. The critical parameter with which to test the theory is the length scale of the interaction. The results illustrated in Fig. 38 show that the predicted length scale exceeds the measured value and thus indicated a more gradual recompression than that which was observed experimentally.

Pitot profiles of the separated mixing layer have shown that the growth rate determined from the momentum integral analysis of Section 3.1.2. compares well with the measured value. This predicted growth rate was incorporated in the Newtonian solution of Section 3.2. to determine the reattachment pressure distribution. Fig. 38(a) compares the predicted and measured pressures and shows that the calculated growth rate gives a reattachment length which underestimates

the measured value by 40% and that Newtonian techniques are clearly inadequate for predicting the reattachment pressure distribution. An inviscid, corpuscular flow model in which the dominant mechanism is the directed kinetic energy is too simple in the reattachment region where severe viscous and pressure gradient forces exist.

5.3.6.2. Reattachment heat transfer rate distribution

The comparison between the measured flat plate heat transfer distributions and those predicted using the methods of Eckert and Van Driest (see Section 3.3.1.) is shown in Fig. 39. It is thought that the rather poor comparison is due to the effect of leading edge bluntness. The curvature of the leading edge shock wave associated with model bluntness causes a non-uniform flow external to the boundary layer which influences its growth and hence the surface heat transfer. It was decided, therefore, to reference all the subsequent reattachment heat transfer rates with the flat plate distribution as given by Eckert's method.

The heat transfer rate, $\dot{q}$, was non-dimensionalised with respect to the local flat plate value. The reattachment distributions along the cavity for constant angle of reattachment and various Reynolds numbers, are shown in Fig. 40 where $\dot{q}/\dot{q}_{fp}$ is plotted against x_s/h, a non-dimensional streamwise distance measured from the step. This co-ordinate correlates the measurements better than x_h/h because the heat transfer rate, which is a minimum in the 'dead air' region,

rises from the step and not the hinge (as in the case of the pressure), regardless of the step-hinge length.

The laminar distributions are continuous. For the reattachment angles considered the heat transfer rate rises from the base of the step (where it is an order of magnitude below the local flat plate value), to a maximum at the end of the interaction which is 6 to 8 times the local flat plate value (evaluated for upstream conditions). Downstream of the interaction the reattached layer rehabilitates in the downstream flow conditions and the heat transfer rate is observed to adopt a flat plate character i.e. $\dot{q}/\dot{q}_{fp}$ = constant. The figure includes the geometric and measured reattachment points (R_g and R_m) and indicates that the maximum heat transfer rate (which is expected to occur where the attached layer is thinnest) occurs close to, but just downstream of, the measured reattachment point which coincides with the peak of the pressure rise.

One conclusion is that the reduction of the attached heat transfer rate values in the 'dead air' region is entirely nullified by the high rates in the reattachment zone and suggest that the use of flow separation to reduce average surface heating is limited at high speeds. This behaviour at hypersonic speeds was observed by Nicoll (1964) and Holloway et al. (1965) for cavity and step separated flows.

The onset of transition in the mixing layer is clearly exhibited in the figure; as the Reynolds number increases the gradient

of $\dot{q}/\dot{q}_{fp}$ is observed to increase sharply and a distinct peak is evident downstream of the measured reattachment point. The peak values of $\dot{q}/\dot{q}_{fp}$ are very high, reaching as much as seventeen times the local flat plate values. For the highest Reynolds number considered the heat transfer rates close to and downstream of the peak exhibit an unsteadiness which was also observed in the equivalent pressure distributions. The increase in the gradient of $\dot{q}/\dot{q}_{fp}$ as transition occurred was expected and is due to the associated increase of the mixing rate in the layer. This leads to a 'fuller' velocity profile and increased shear. The distinct peak of the pressure distribution for transitional reattachment indicates an over-compression of the mixing layer. Also the heat transfer rate distributions suggest the existence of extremely thin attached layers with a minimum thickness occurring at the heat transfer peak and not at the reattachment point. The schlieren photographs shown in Fig. 18 lend supporting evidence to this conclusion.

The remarked behaviour of the reattachment point and the location of the thinnest attached boundary layer is clearly exhibited in Fig. 41 in which the heat transfer rate and pressure distributions are compared for laminar and transitional reattachments at $\alpha_w = 10{\cdot}4^{\circ}$ and three values of Re_∞. The figure shows that, regardless of the state of the mixing layer, both the distributions reach a maximum value at approximately the same streamwise location thus suggesting that the reattaching layer has a minimum thickness at the peak of the pressure

rise.

The merit of using x_s/h as a correlating length scale is clearly shown by Fig. 42 which shows constant Reynolds number distributions of $\dot{q}/\dot{q}_{fp}$ for various values of α_w. It is seen that the effect of α_w on $\dot{q}/\dot{q}_{fp}$ is relatively small compared to that of Reynolds number for the limited range of $8.1^{\circ} \leqslant \alpha_w \leqslant 10.4^{\circ}$.

It has already been noted that, provided the boundary layer at separation is laminar, a suitable correlating parameter for the base flow is h/δ_s, the ratio of step height to boundary layer thickness which is expressed by the term $hRe_{x_1}^{1/2}/x_1$ for a laminar flow. The separated length data illustrated in Fig. 32(a) showed that as the Reynolds number increases and δ_s decreases transition moves upstream in the mixing layer and the base pressure falls causing an associated increase in the abruptness of the pressure rise at reattachment (see Fig. 36), thus resulting in high velocity gradients. The corresponding increase in $\dot{q}_{max}/\dot{q}_{fp}$ is clearly shown in Fig. 40 for low Reynolds number, and hence low $hRe_{x_1}^{1/2}/x_1$, the heat transfer distribution is smooth and the reattachment gradual, $\dot{q}_{max}/\dot{q}_{fp}$ reaching the local flat plate value (evaluated for downstream external conditions on the flap). However, for higher Reynolds numbers, where δ_s is thin, $\dot{q}_{max}/\dot{q}_{fp}$ peaks severely.

Rom and Seginer (1964) noted the same 'peaking' behaviour of $\dot{q}_{max}/\dot{q}_{fp}$ with a rearward-facing step model for $hRe_{x_1}^{1/2}/x_1 > 15$. They determined the variation of $\dot{q}_{max}/\dot{q}_{fp}$ with $hRe_{x_1}^{1/2}/x_1$ for $1.5 < M_\infty < 2.5$

and $2 \times 10^4 < Re_{x_1} < 2 \times 10^5$ and established the following relation,

$$\dot{q}_{max}/\dot{q}_{fp} = 0.0465 \, (hRe_{x_1}^{1/2}/x_1)^{1.3} \qquad \ldots(5.4.)$$

which is shown in Fig. 43.

The present results for $48 < (hRe_{x_1}^{1/2}/x_1) < 105$ are included in the figure and fall about the same line. The importance of the boundary layer thickness at separation on the flow mechanism is clearly established.

Fig. 40 shows the disappointing comparison between the experimental heat transfer rate distributions and those predicted using the laminar theory of Cheng et al. which incorporated the empirical pressure distribution (see Section 3.3.1.). These results contrast with those of Miller et al. (1964), who studied a wedge compression corner separation at $M_\infty = 16$ and $\alpha_w = 7.5^o$ and obtained a good comparison with Cheng's theory for lower reattachment pressure gradients. Consequently the results show, not surprisingly, that the assumption that the thermal boundary layer is insensitive to pressure gradient and that local flat plate similarity exists is clearly inadequate for a reattaching flow in which the pressure gradient is high.

As the flat plate distribution downstream of the reattachment point, predicted from equation (3.18.), requires that the heat transfer rate is infinite at the origin or the re-established boundary layer (taken as the measured reattachment point), the momentum integral method of Section 3.3.2. is used to establish the minimum boundary layer thick-

ness and its distance downstream of the geometric reattachment point. Equation (3.18.) can then be applied to determine the peak heat transfer rate at this point and the subsequent downstream distribution. The figure shows that this predicted location coincides with the measured reattachment point, however, the resulting heat transfer rates are well below the measured values.

The comparison between the peak heat transfer rates predicted from equation (3.22.) (containing the appropriate value of $\bar{u}_*$) and the measured values is fair considering the low reattachment angles studied and remembering that the predicted values were for a normal reattachment. The stagnation heat transfer to a cylinder of radius equal to the step height is included in the figure and provides a rough check on the order of magnitude of the present results. The correlation for α_w shown in Fig. 6 exhibits a much smaller effect than that suggested by the cylinder results and the corresponding values of the predicted $\dot{q}_{max}$ do not compare with the measured values.

It is seen that none of these simple but crude models offer a good prediction of the heat transfer rate distribution of a laminar, reattaching shear layer, which is not surprising if one considers the assumptions which have been made. Whereas the theoretical treatment for the heat transfer to flat plates and blunt-nosed bodies is well advanced, there is a clear need for methods of predicting this quantity in flows where the pressure gradient is large and the surface has some

arbitrary slope.

5.3.7. Comparison between conical and uniform flow

The contrasting effects of the conical and uniform flows on the length of the shear layer have been described in Section 5.2.2. and 5.3.2.

The experimental studies at $M_\infty = 9.7$ were made using two-dimensional models of various lengths and the conicity of the flow presented two main problems i.e. the presence of a streamwise pressure gradient and an effective incidence of the free stream relative to the model surface. As a range of step heights was considered, great care was taken to ensure that the surface of the model was located at a fixed distance from the nozzle centre-line (=0.75") in order that the effective incidence of the leading edge was a constant value.

Due to these effects, all the resulting reattachment pressure distributions were scaled by the equivalent measured flat plate values. However, the length scale of the separated flow cannot be scaled and it is felt that its behaviour as a free jet, independent of the upstream attached length, is caused by the presence of the streamwise pressure gradient.

The variations of L_{sep}/x_1 with α_w for the laminar, $M_\infty = 8.2$ and $T_t = 860^oK$, uniform flow and the $M_\infty = 9.7$ and $T_t = 1030^oK$, conical flow were compared for the models with side plates. x_1 was kept constant to allow for the different correlating length scales and the variation of

the separated length for the two types of flow was shown to exhibit the same form.

L_{sep} was observed to decrease for M_∞ increasing and α_w constant. This variation is shown by the theoretical conclusions of Section 3.1.1. which are shown in Fig. 3(a) for a constant pressure rise p_r/p_2 and $N = 1$. This laminar behaviour would be seriously affected if transition was located upstream of the reattachment point, as discussed in Section 5.3.4.

It is stressed that these results can only be regarded in a crude qualitative manner due to the conicity effects present.

6. CONCLUSIONS

A detailed experimental study of separated flows has been performed in the hypersonic gun tunnel and properties of both the separated shear layer and the reattachment region have been measured and correlated with the main influencing parameters. The suitability of an intermittent facility for such a study has been demonstrated by the ability to measure these properties and the established steadiness of the separated flow in the running time available.

For the case of a straight-separating shear layer in uniform flow where the cavity depth was greater than five times the boundary layer thickness the theoretical model of Cooke, incorporating $N = 1$ and $T_d = T_w$, was found to predict the observed laminar variation of the separated length with reattachment angle, though it over-estimated the limiting (or asymptotic) reattachment angle by a factor of two. The correlating length scale, predicted by the theory, was confirmed experimentally and the results indicated the importance of the body length as an influencing parameter on the length of the shear layer.

The effect of Reynolds number on L_{sep}/x_1 was found to be very small and the results suggested that the contrasting effects of boundary layer thickness and the shear layer mixing rate on the base flow were almost compensating. Consequently, the independence of

L_{sep}/x_1 on Reynolds number, predicted by the theory, was thought to be reasonable.

Successful pitot probe surveys of the shear layer demonstrated the laminar nature of the flow and a comparison of the measured and calculated Mach number profiles corroberated the assumption that $T_d = T_w$, although the predicted effect of wall cooling was larger than that observed experimentally. The rate of growth of the shear layer, exhibited by the pitot pressure profiles, compared satisfactorily with that predicted by Cooke's method.

The experimental results obtained using models with side plates in uniform flow have established the validity of Cooke's supersonic theory as a solution for the problem of hypersonic laminar step separated flows provided the cavities were deep enough for the separation to be free from direct influence from downstream.

It has been shown that the onset of transition in the shear layer as the Reynolds number increases has a profound effect on the base flow mechanism. In the laminar régime L_{sep}/x_1 was relatively high and ovserved to increase slowly with Reynolds number for a constant reattachment angle, whereas the occurrence of transition caused L_{sep}/x_1 to fall precipitously, due to the associated large increase of the local mixing rate. The difference in the behaviour of the base flow mechanism in the two régimes explains the anomalous results of some authors who, it is thought, have been unaware of the presence of transition upstream of the reattachment region.

The peak value of L_{sep}/x_1 was found to occur at a constant Re_{L_r}, the Reynolds number based on the total length of the layer to the reattachment point, for all the values of α_w, x_1 and Re_∞ considered, and a criterion was established to define the location of the transition point and the state of the reattaching shear layer.

The flow régime in the reattachment region has been shown to have a critical effect on the reattachment parameter N. In the case of laminar reattachment the dividing streamline was found to stagnate at the peak of the pressure rise and was independent of both the pressure gradient and the external Reynolds number. This indicated the validity of Chapman's original assumption that N = 1 and the dividing streamline recompresses isentropically, and justified its substitution in the analysis of Cooke.

When transition occurred the reattachment mechanism was severely affected, and N was found to be a function of both α_w and unit Reynolds number, decreasing for an increase of both these parameters. The variation of N with the unit Reynolds number was analogous to that of L_{sep}/x_1 and is explained by the presence of the large local mixing rates in the shear layer. It has been shown that N varied linearly with the term $(\alpha_w . Re_{L_r}^{1/5})$ in the transitional régime and that it decreased from unity to 0·35, the turbulent value proposed by Nash.

The onset of transition has been found to have a distinct effect on the reattachment pressure and heat transfer distributions

which indicated an unsteadiness of the flow at the higher values of α_w and Re_∞. The laminar pressure distributions have been predicted quite successfully using a simplified moment of momentum analysis although the predicted length scale of the interaction exceeded the measured value. However, whereas the results justified the extrapolation of this particular supersonic solution to hypersonic Mach numbers, a simple Newtonian solution has been found inadequate.

Theoretical predictions of the laminar heat transfer distributions were not confirmed by experiment, although the maximum value, which was observed to occur at the peak of the pressure rise, has been predicted satisfactorily and correlated in terms of $h.Re_{x_1}^{1/2}/x_1$ for laminar separating flows.

The need for side plates, to prevent a loss of flap effectiveness, and uniform free stream conditions has been shown to be essential in the step separated flow studies, and the severe effects of conicity on the length of separation have been established.

List of References

Beheim M.A.

"Flow in the base region of axisymmetric and two-dimensional configurations."

NASA TR R-77 , (1961)

Bogdonoff S.M.

"A preliminary study of Reynolds number effects on base pressure at M = 2.95."

J.Aeronaut. Sci. 19 , No. 3 , (1952)

Carrière P.

"Recherches récentes effectuées a l'ONERA sur les problèmes de recollement."

O.N.E.R.A. publication no. 275 , (1965)

Carrière P. and Sirieix M.

"Facteurs d'influence du recollement d'un écoulement supersonique."

O.N.E.R.A. publication MT 20 , (1961)

Carrière P. and Sirieix M.

"Résultats récants dans l'etude des problèmes de mélange et de recollement."

O.N.E.R.A. publication no. 165 , (1964)

Chapman D.R.

"Laminar mixing of a compressible fluid."

NACA TR 958 , (1950)

Chapman D.R.

"An analysis of base pressure at supersonic velocities and comparison with experiment."

NACA Rep. 1051 , (1951)

Chapman D.R. and Korst H.H.

"Theory for base pressures in transonic and supersonic flow."

J. App. Mechanics 24 , pp. 484 - 485 , (1957)

Chapman D.R., Kuehn D.M. and Larson K.H.

"Investigation of separated flows in supersonic and subsonic streams with emphasis on the effect of transition."

NACA Rep. 1356 , (1958)

Chapman D.R., Wimbrow W.R. and Kester R.H.

"Experimental investigation of base pressure in blunt-trailing-edge wings at supersonic velocities."

NACA Rep. 1109 , (1952)

Charwat A.F., Roos J.N., Dewey F.C. and Hitz J.A.

"An investigation of separated flow. Part I: the pressure field."

J. Aerospace Sci. 28 , No. 6 , (1961)

Charwat A.F. and Yakura J.K.

"An investigation of two-dimensional base pressure."

J. Aeronaut. Sci. 25 , No. 2 , (1958)

Cheng H.K., Hall J.G., Golian T.C. and Hertzberg A.

"Boundary layer displacement and leading edge bluntness effects in high temperature hypersonic flow."

J. Aerospace Sci. 28 , No. 5 , (1961)

Childs M.E., Paynter G.C. and Redeker E.

"The prediction of separation and reattachment flow characterisitics for two-dimensional supersonic and hypersonic boundary layers."

AGARD CP No. 4 , Part 1 , (1966)

Chung P.M. and Viegas J.R.

"Heat transfer at the reattachment zone of separated laminar boundary layers."

NASA TN D-1072 , (1961)

Cohen C.B. and Reshotko E.

"Heat transfer at the forward stagnation point of blunt bodies."

NACA TN 3513 , (1955)

Cooke J.C.

"Separated supersonic flow."

British A.R.C. 24,935 , (1963)

Crocco L and Lees L.

"A mixing theory for the interaction between dissipative flows and nearly isentropic flows."

J. Aerospace Sci. 19 , No. 10 , (1952)

Daum F.L.

"Air condensation in a hypersonic wind tunnel."

AIAA J.1 , No. 5 , (1963)

Denison M.R. and Baum E.

"Compressible free shear layer with finite initial thickness."

AIAA J.1 , No. 6 , (1963)

Eckert E.R.G.

"Engineering relations for skin friction and heat transfer to surfaces in high velocity flows."

J. Aeronaut. Sci. 22 , No. 8 , (1955)

Gadd G.E., Holder D.W., Regan J.D.

"Base pressure in supersonic flow."

British A.R.C. 17,490 , (1956)

Ginoux J.J.

"The existence of three-dimensional perturbations in the reattachment of a two-dimensional supersonic boundary layer after separation."

AGARD Rep. 272 , (1960)

Hama F.R.

"Experimental studies on the lip shock."

AIAA preprint 67-29 , (1967)

Hankey W.L. and Cross E.J.

"Approximate closed-form solutions for supersonic laminar separated flows."

AIAA J.5 , No. 4 , (1967)

Holden M.S.

"Heat transfer in separated flow."

Univ. of London Ph.D. Thesis , (1964)

Holloway P.F., Sterrett J.R. and Creekmore H.S.

"An investigation of heat transfer within regions of separated flow at a Mach no. of 6.0 ."

NASA TN D-3074 , (1965)

Hurlburt R.L.

"Experimental investigation of the reattachment of a laminar separated shear layer at M = 3 ."

Princeton Univ. M.S. Thesis , (1966)

Kavanau L.L.

"Results of some base pressure experiments at intermediate Reynolds numbers with M = 2.84 ."

J. Aerospace Sci. 21 , p 257 , (1954)

Kirk F.N.

"An approximate theory of base pressure in two-dimensional flow at supersonic speeds."

R.A.E. TN Aero. 2377 , (1954)

Lees L.

"Laminar heat transfer over blunt-nosed bodies at hypersonic speeds."

Jet Prop. 26 , No. 4 , (1956)

Lees L and Reeves B.L.

"Supersonic separated and reattaching laminar flows : I General theory and application to adiabatic boundary layer - shock wave interactions."

AIAA J.2 , No. 11 , (1964)

Lock R.C.

"The velocity distribution in the laminar boundary layer between parallel streams."

Quart. J. Mech. and App. Maths., Vol. 4 , p 42 , (1951)

Nicholl K.M.

"A study of laminar hypersonic cavity flows."

AIAA J.2 , No. 9 , (1964)

Meritt G.E.

"Hypersonic laminar flow over cavities and steps."

Univ. of Southampton Ph.D Thesis , (1964)

Meyer R.F.

"A note on a technique of surface flow visualisation."

N.R.C. (Canada) Aero. Rep. LR-457 , (1966)

Miller D.S., Hyman R. and Childs M.E.

"Mach 8 to 22 studies of flow separations due to deflected control surfaces."

AIAA J.2 , No. 2 , (1964)

Milne-Thomson L.M.

"Theoretical Hydrodynamics." 2nd Edition.

Published Macmillan , 1949

Nash J.F.

"An analysis of two-dimensional turbulent base flow including the effect of the approaching boundary layer."

British A.R.C. 24,000 , (1962)

Needham D.A.

"Progress report on the Imperial College hypersonic gun tunnel."

Imperial College Dept. of Aeronautics Rep. 118 , (1963)

Needham D.A.

"Laminar separation in hypersonic flow."

Univ. of London Ph.D Thesis , (1965)

Reller J.O. Jr. and Hamaker F.M.

"An experimental investigation of the base pressure characteristics of non lifting bodies of revolution at Mach numbers from 2.73 to 4.98 ."

NACA TN 3393 , (1955)

Rom J. and Seginer A.

"Laminar heat transfer rates to a two-dimensional backward facing step from the high enthalphy supersonic flow in the shock tube."

AIAA J.2 , No. 2 , (1964)

Rubesin M.W. and Johnson H.A.

"A critical review of skin friction and heat transfer solutions of the laminar boundary layer of a flat plate."

Trans. A.S.M.E. Vol. 71 , p 385 , (1949)

Sirieix M.

"Pression de culot et processus de melange turbulent en ecoulement supersonique."

La Recherche Aeronautique No. 78 , (1960)

Stollery J.L., Maull D.J. and Belcher B.J.

"The Imperial College gun tunnel : August 1958 - July 1959."

J. Royal Aero. Soc. Vol. 64 , No. 589 , (1960)

Van Driest E.R.

"Turbulent boundary layer in compressible fluids."

J. Aerospace Sci. 18 , p 145 , (1951)

Van Driest E.R.

"Investigation of laminar boundary layer in compressible fluids using the Crocco method."

NACA TN 2597 , (1952)

Van Hise V.

"Investigation of variation in base pressure over Reynolds number range in which wake transition occurs for two-dimensional bodies at M = 1·95 to 2·92 ."

NASA TN D-167 , (1959)

Weiss R.F. and Weinbaum S.

"Hypersonic boundary layer separation and the base flow problem."

Avco-Everett Res. Lab. Rep. 221 , (1965)
also AIAA J.4 , No. 8 , (1966)

White R.A.

"Laminar separation and reattachment behind a downstream facing step at hypersonic Mach no., including the effects of the approaching boundary layer."

Aero. Res. Inst. of Sweden. FFA Rep. 103 , (1965)

Wood C.J.

"Hypersonic separated flows."

Univ. of London Ph.D. Thesis , (1961)

Young A.B.W. and Janssen E.

"The compressible boundary layer."

J. Aerospace Sci. 19 , pp 229-236 , (1952)

State of shear Layer	α_w^o	$(U/\nu)_\infty$ per in.	Re_{x_1}	$L_{s.h}$ ins.	$\frac{L_{sep}}{x_1}$	Re_{L_r}	$T_{t\infty}$ °K	$\frac{T_w}{T_\infty}$	$\frac{\delta_s}{h}$	$\frac{P_3}{P_2}$	N
Laminar	8·1	$1·30 \times 10^5$	$4·55 \times 10^5$	0·40	0·62	$0·74 \times 10^6$	820	5·10	0·39	3·92	1·0
Transitional	"	2·37 "	8·30 "	0·13	0·54	1·28 "	860	4·84	0·29	4·00	0·87
Transitional	9·2	1·30 "	4·55 "	1·40	0·84	0·84 "	820	5·10	0·39	4·34	0·85
Transitional	"	2·37 "	8·30 "	1·05	0·74	1·44 "	860	4·84	0·29	4·57	0·55
Transitional	"	3·56 "	12·46 "	0·13	0·48	1·84 "	"	"	0·236	4·34	0·48
Laminar	10·3	1·30 "	2·60 "	0·90	1·14	0·56 "	820	5·10	0·296	5·10	1·0
Transitional	"	2·37 "	4·74 "	0·90	1·14	1·02 "	860	4·84	0·22	5·21	0·47
Laminar	10·4	1·30 "	2·60 "	1·20	1·31	0·59 "	820	5·10	0·296	5·26	1·0
Transitional	"	2·37 "	4·74 "	1·30	1·36	1·12 "	860	4·84	0·22	5·35	0·46
Transitional	"	3·56 "	7·12 "	0·70	1·03	1·45 "	"	"	0·18	5·17	0·36

Conditions concerning the straight separated flows.

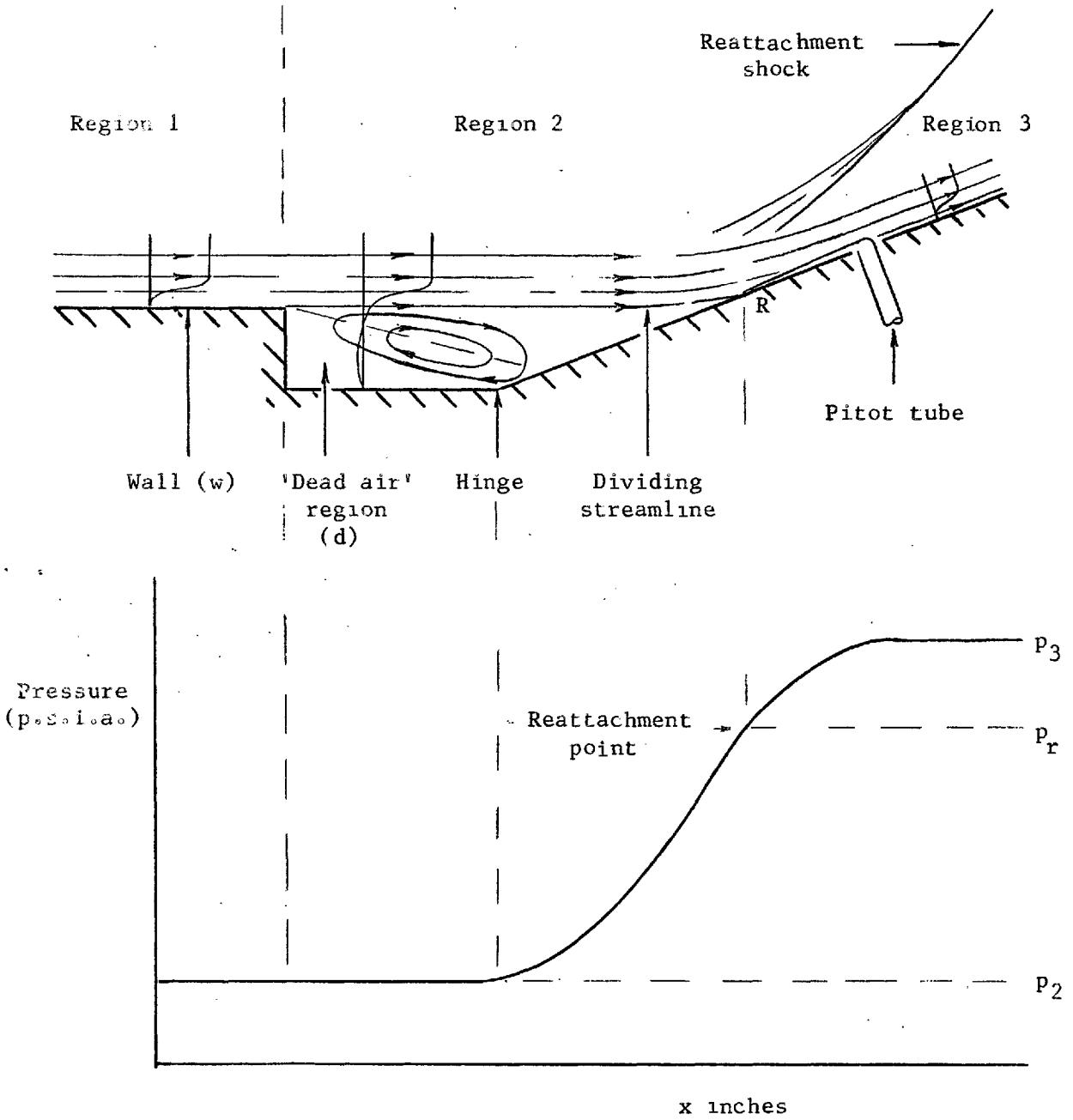

FIG.1. Sketch of separated supersonic flow field.

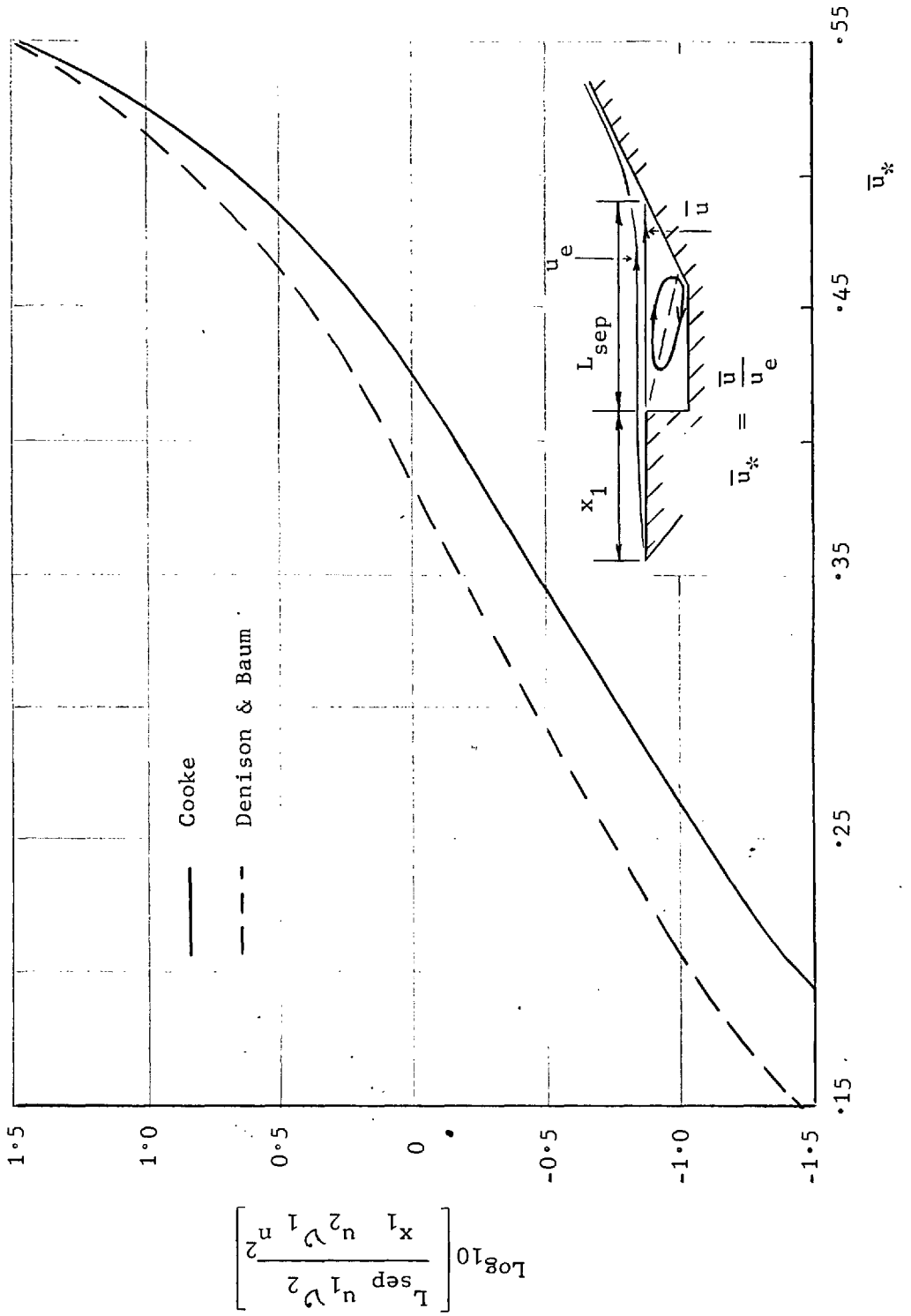

FIG. 2. The dividing streamline velocity ratio.

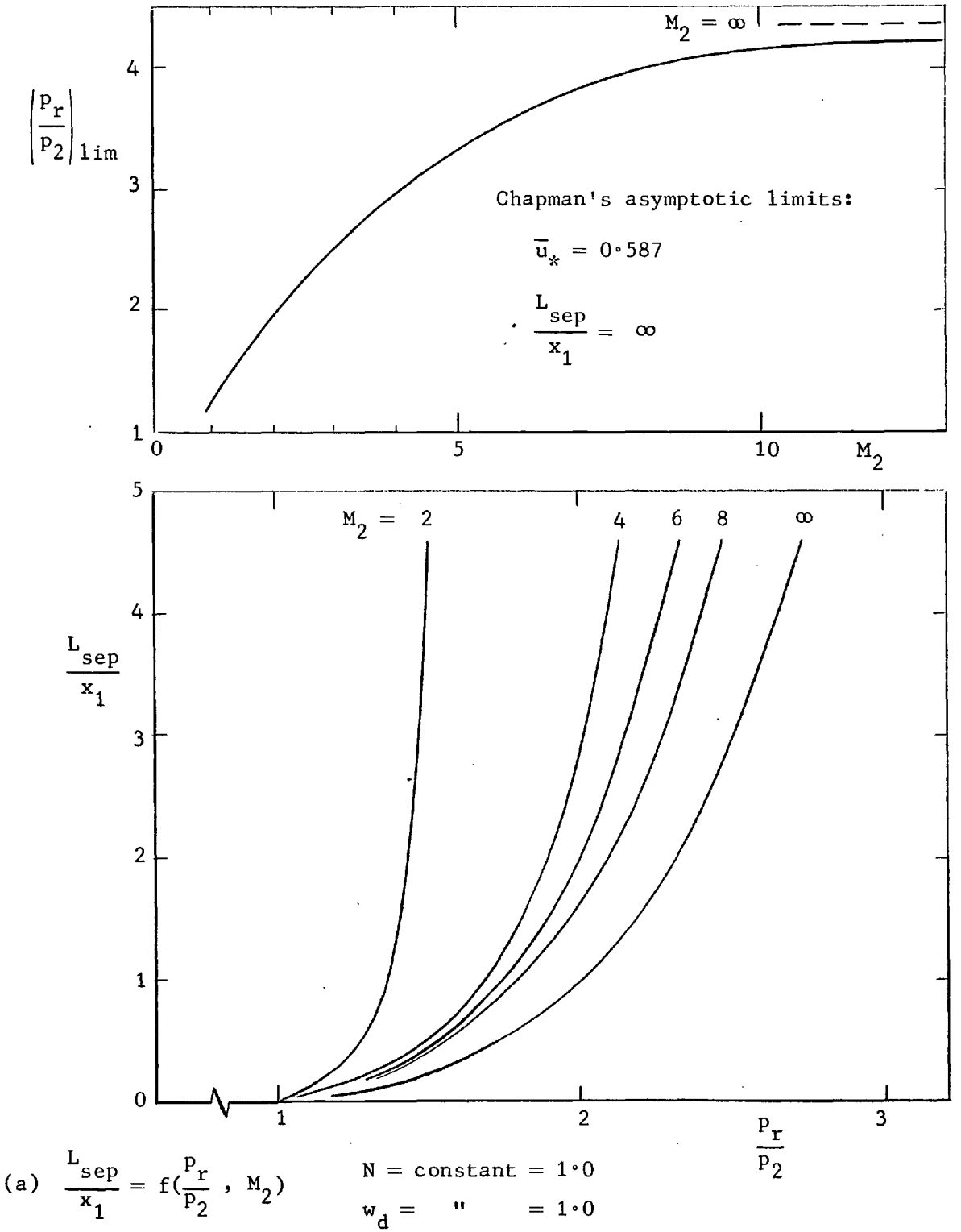

FIG. 3. Influencing parameters of the separated laminar flow.

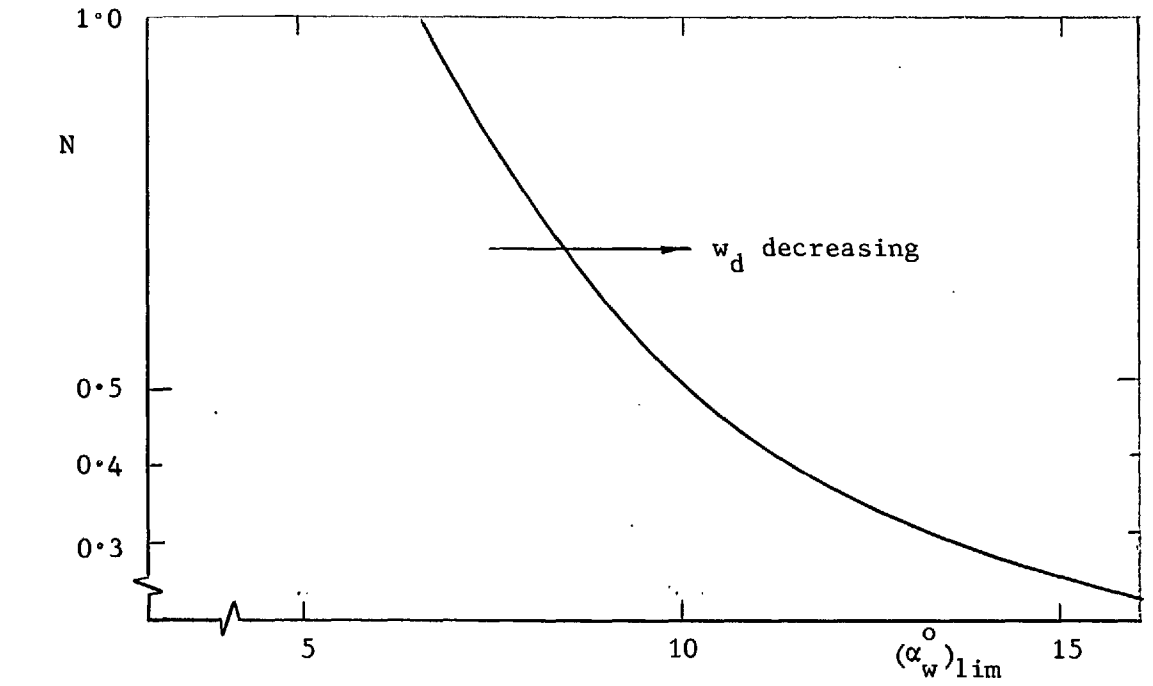

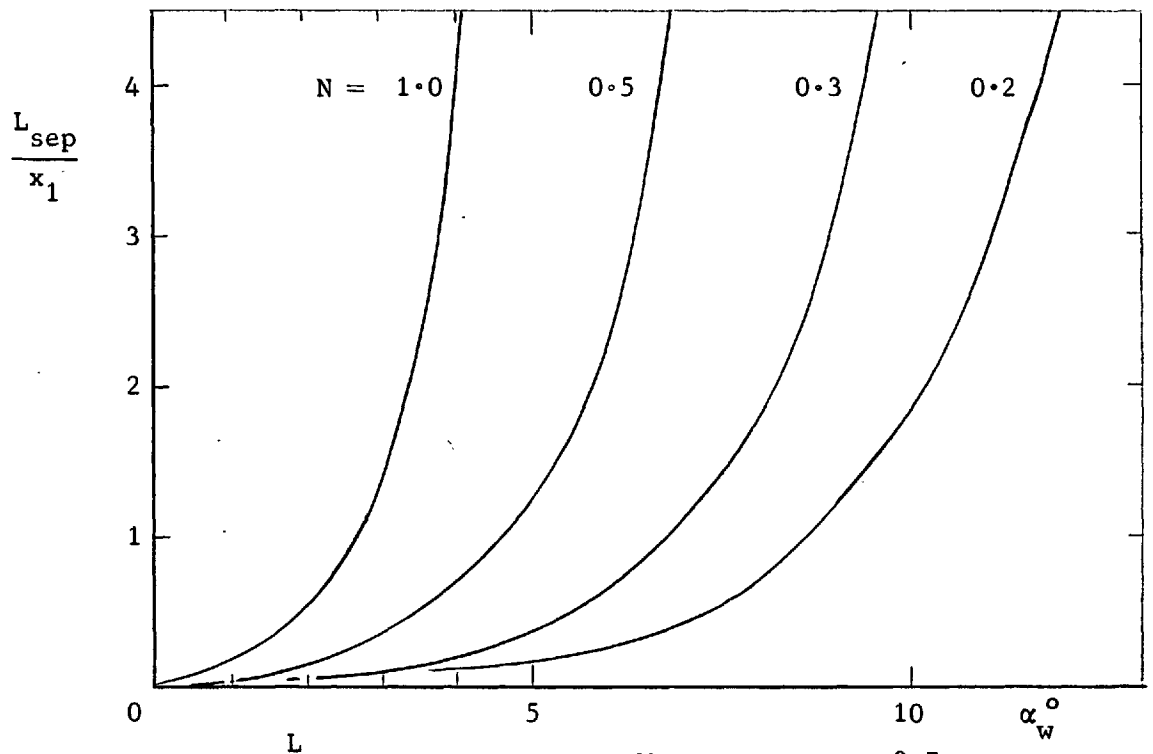

(b) $\frac{L_{sep}}{x_1} = f(\alpha_w, N)$ M_2 = constant = 9·7
w_d = " = 1·0

FIG. 3. continued.

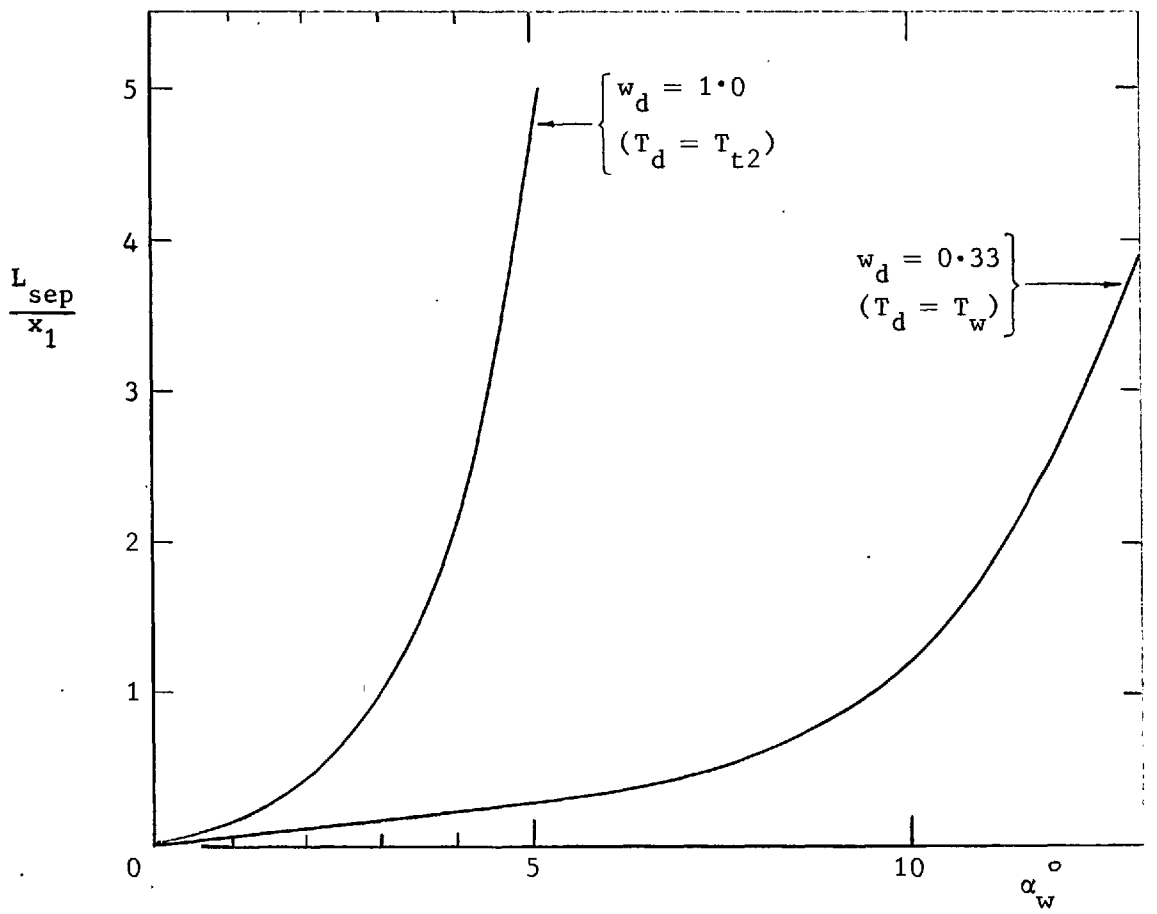

(c) $\frac{L_{sep}}{x_1} = f(\alpha_w , w_d)$ N = constant = 1·0
M_2 = " = 8·2

FIG. 3. concluded.

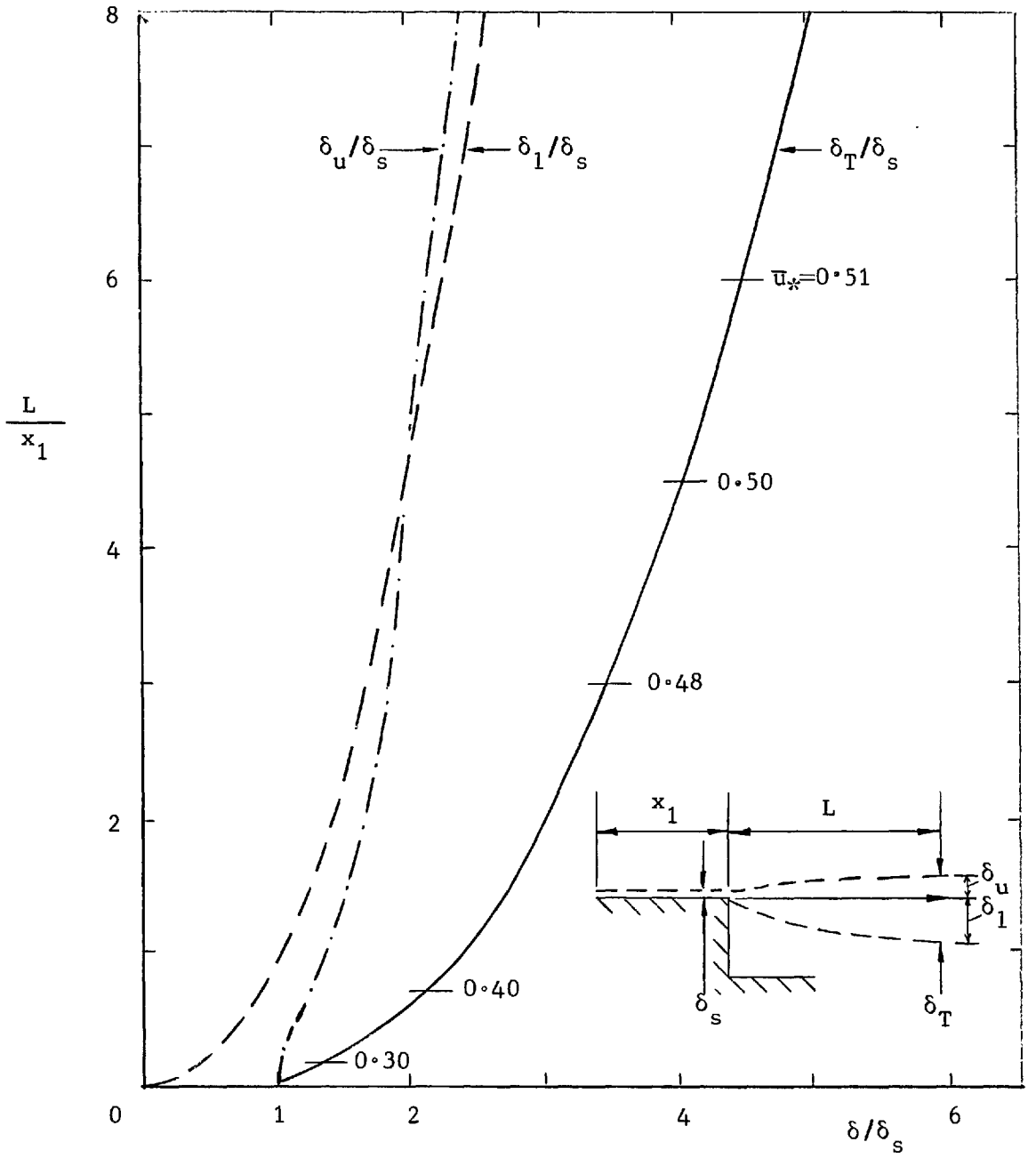

FIG. 4. Growth of the mixing layer.

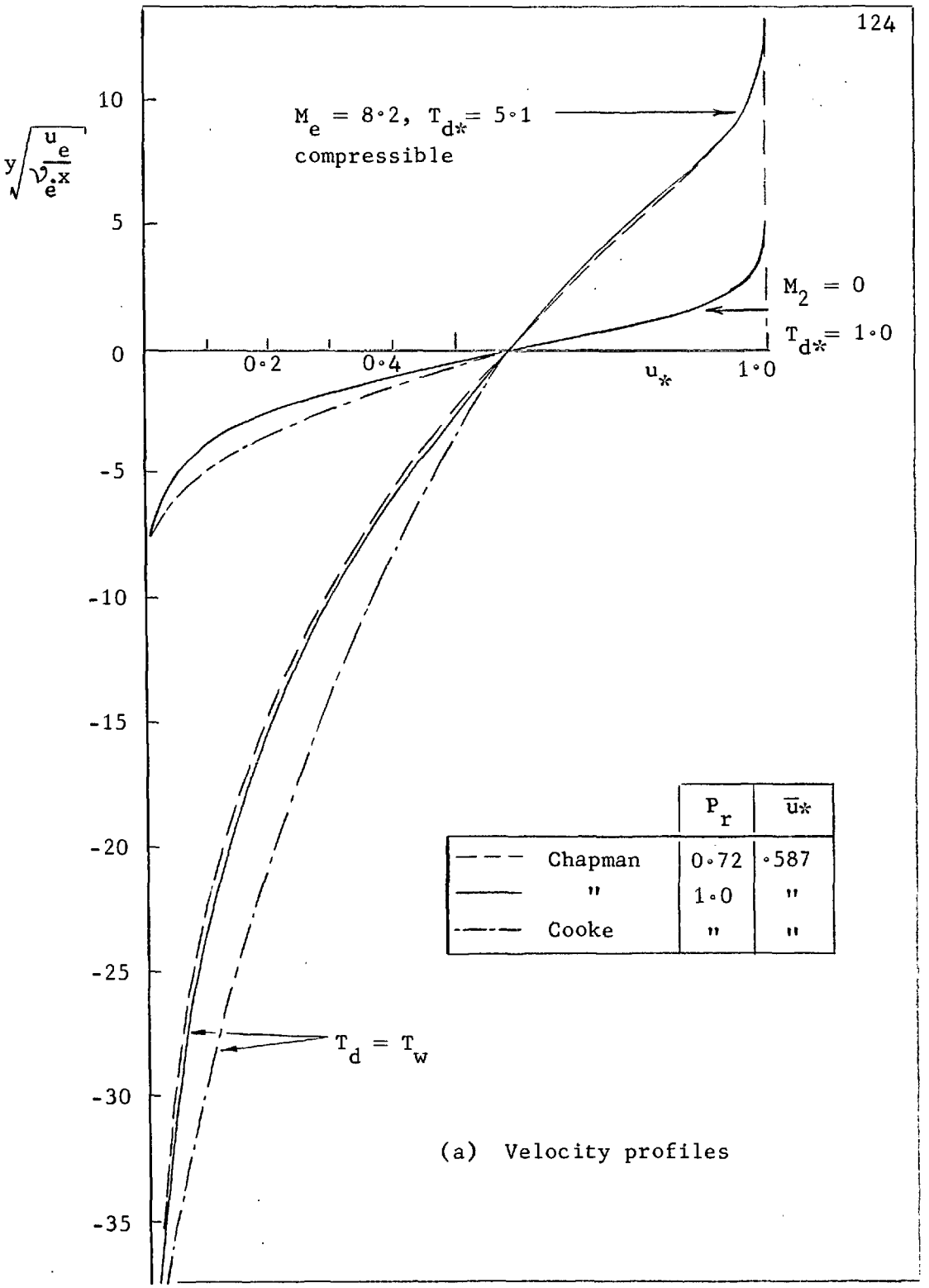

FIG. 5. Mixing layer velocity and density profiles.

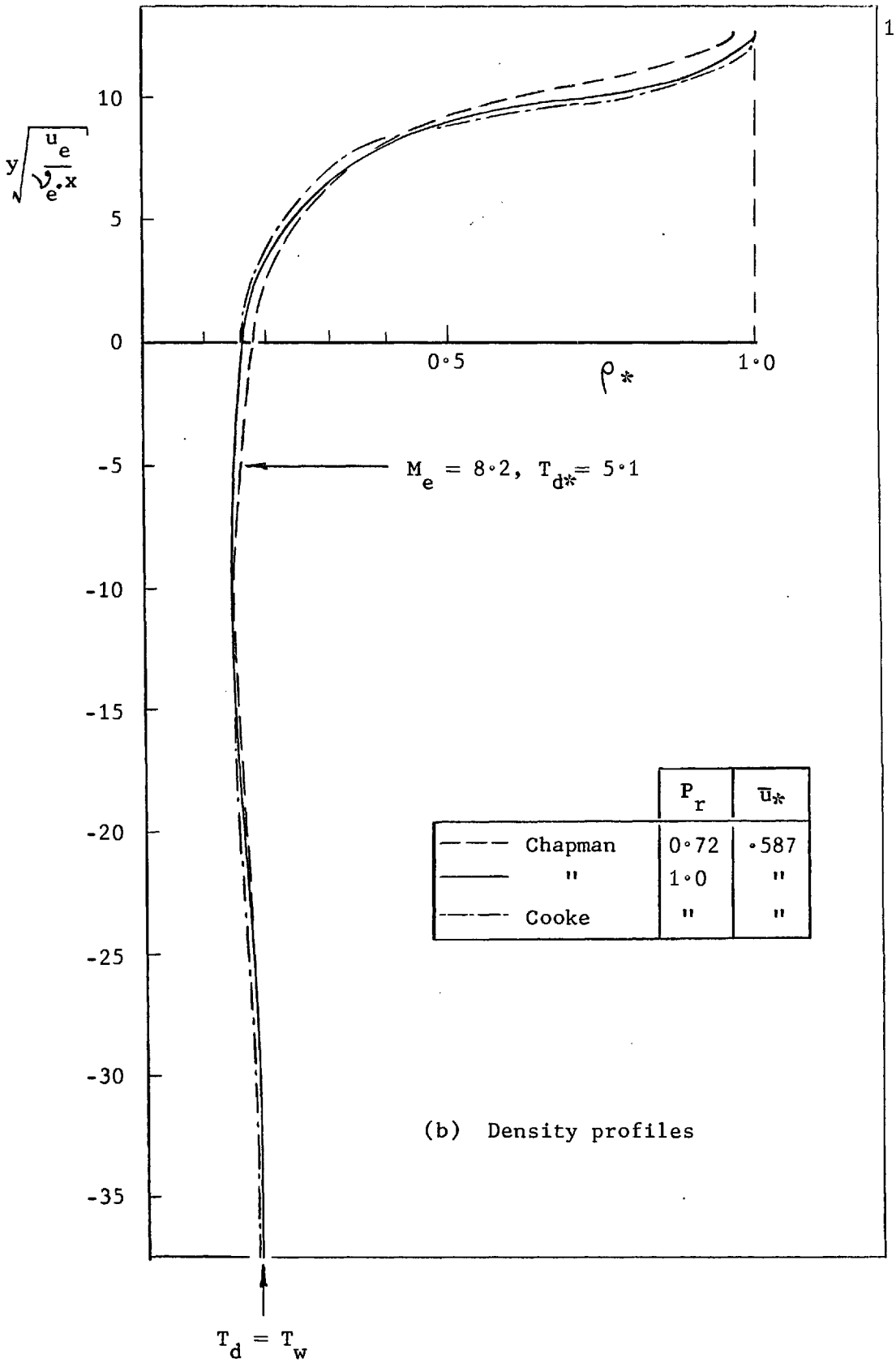

(b) Density profiles

FIG. 5. concluded.

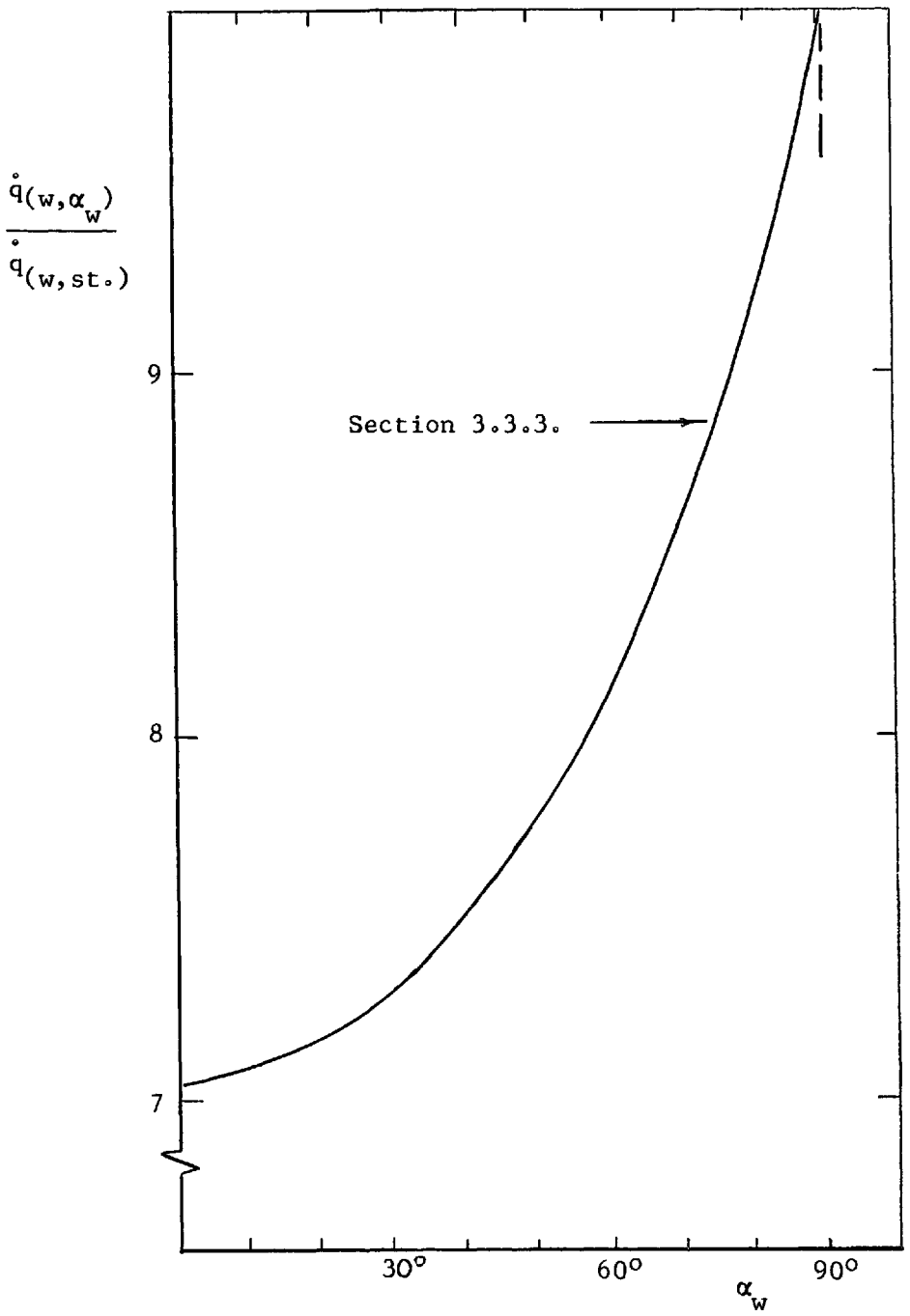

FIG. 6. Variation of peak heat transfer rate with flap angle.

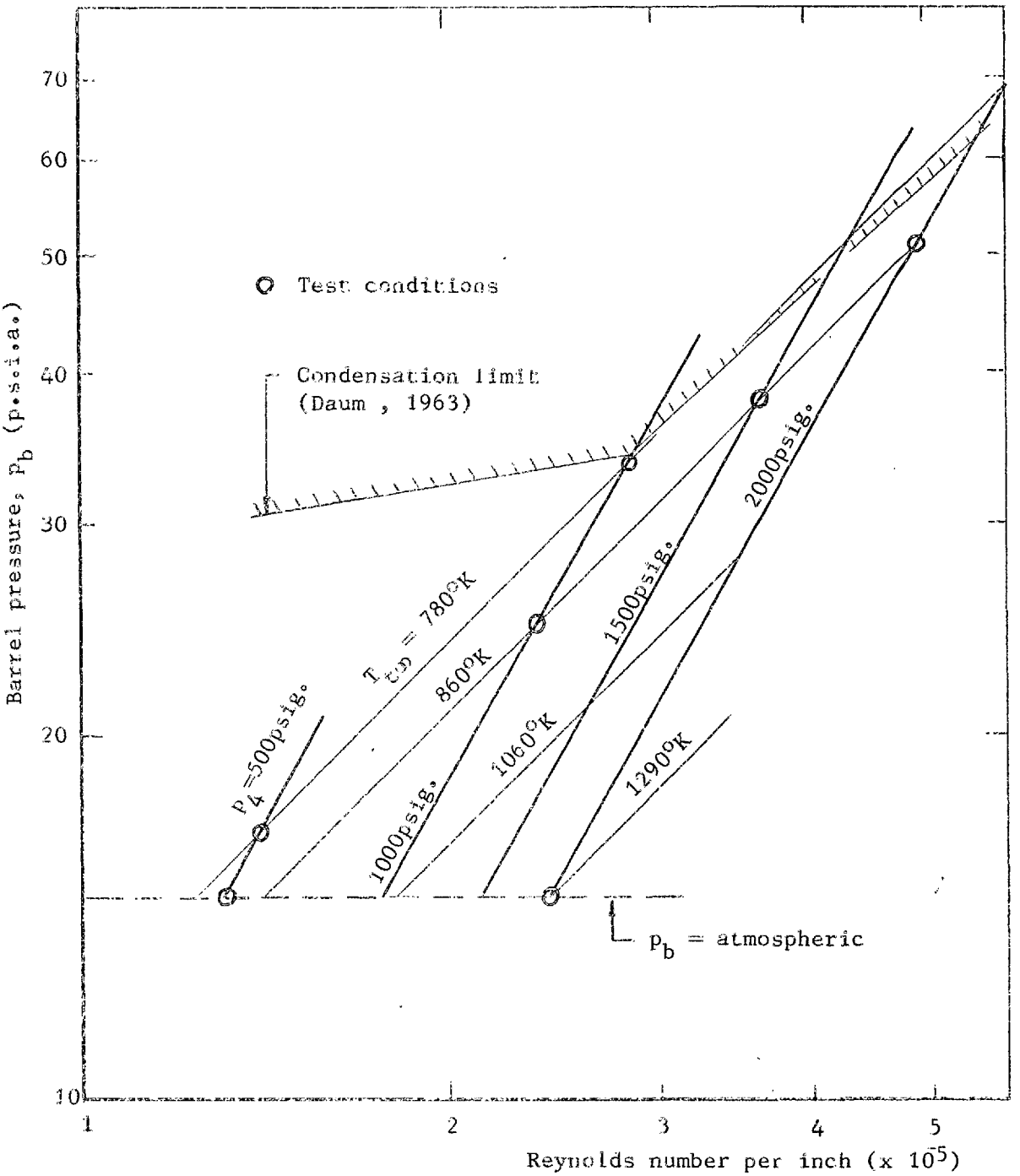

FIG. 7. Free stream unit Reynolds number at $M_\infty = 8.2$.

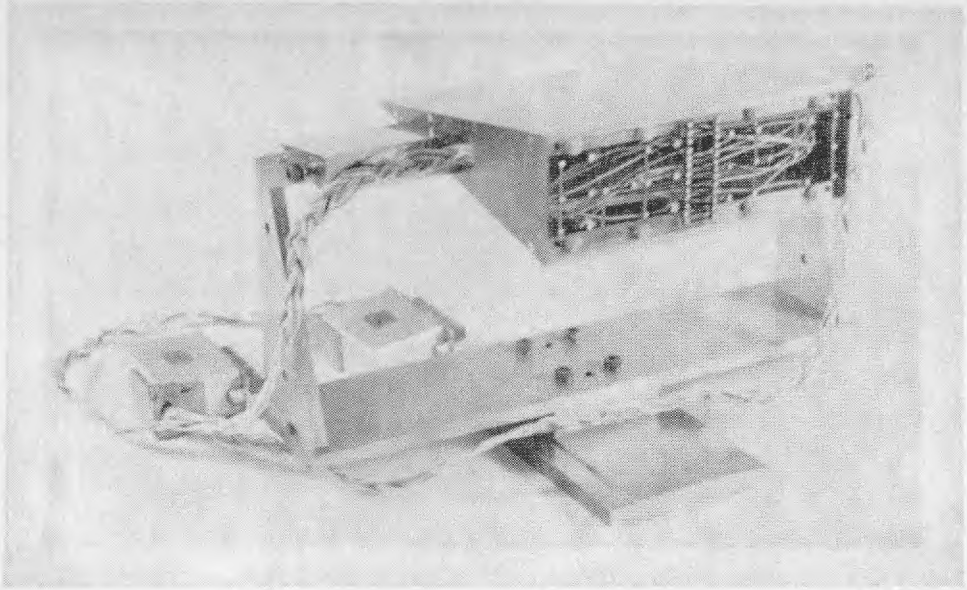

(a) Wedge. (Base instrumented for heat transfer)

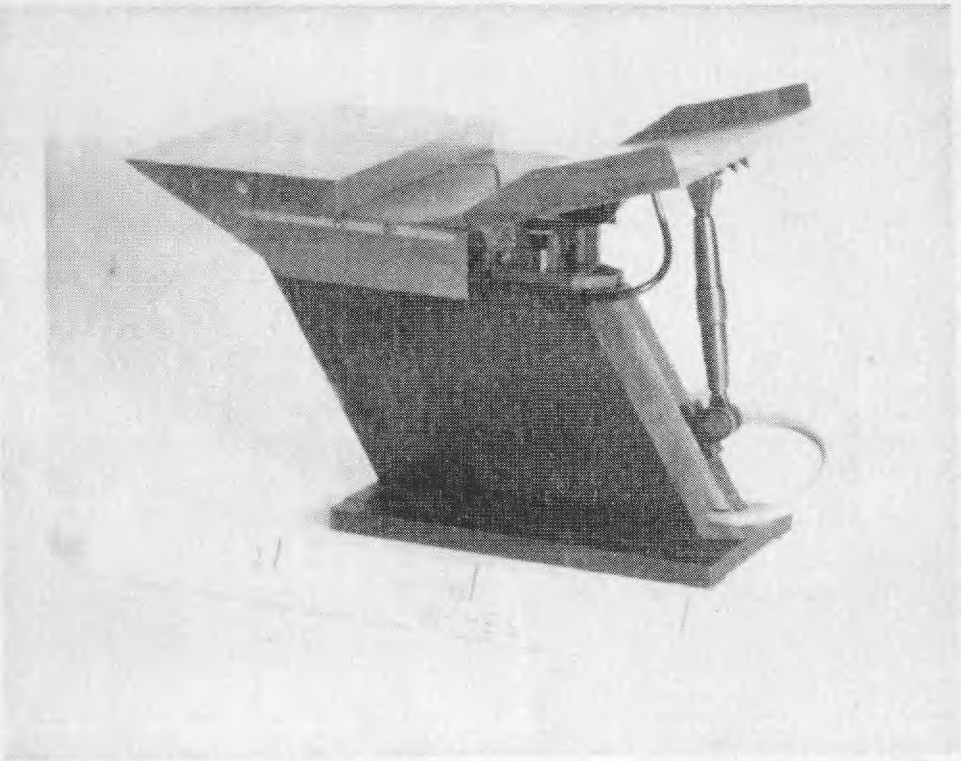

(b) Rearward-facing step. (Pressure instrumented)

FIG. 8. Wedge and rearward-facing step models.

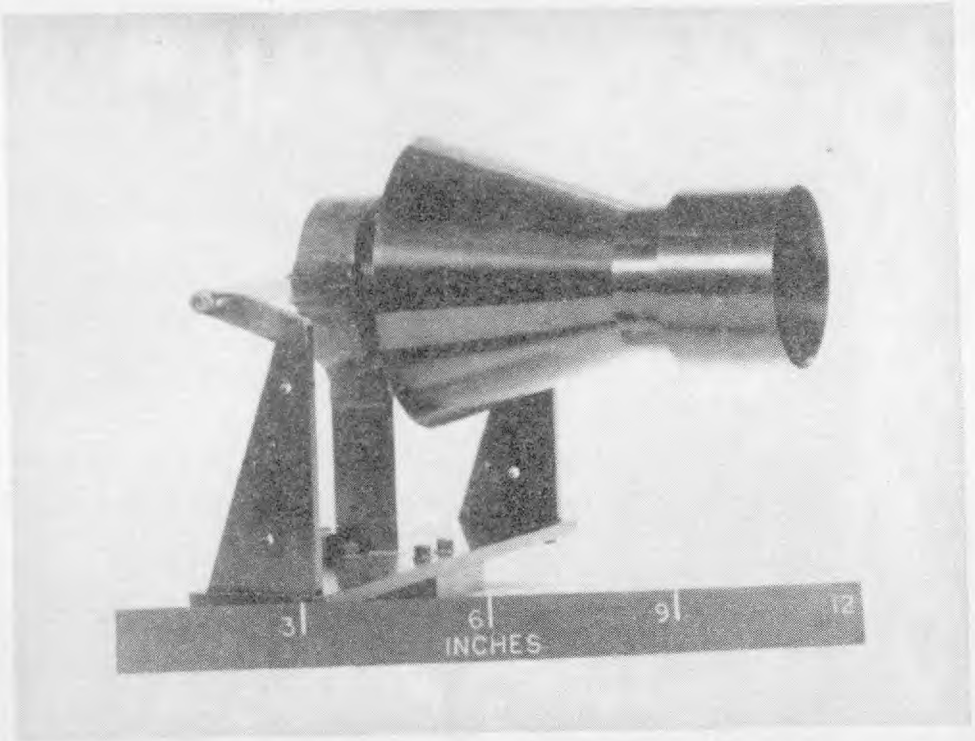

(a) Axisymmetric.

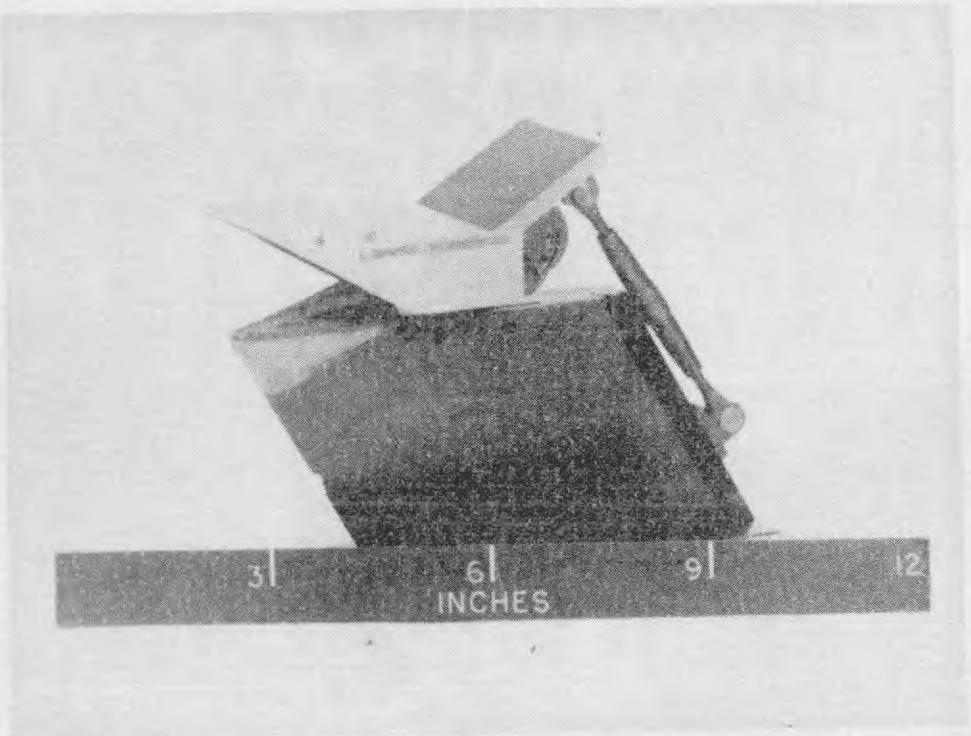

(b) Half-scale.

FIG. 9. Axisymmetric and half-scale rearward-facing step models.

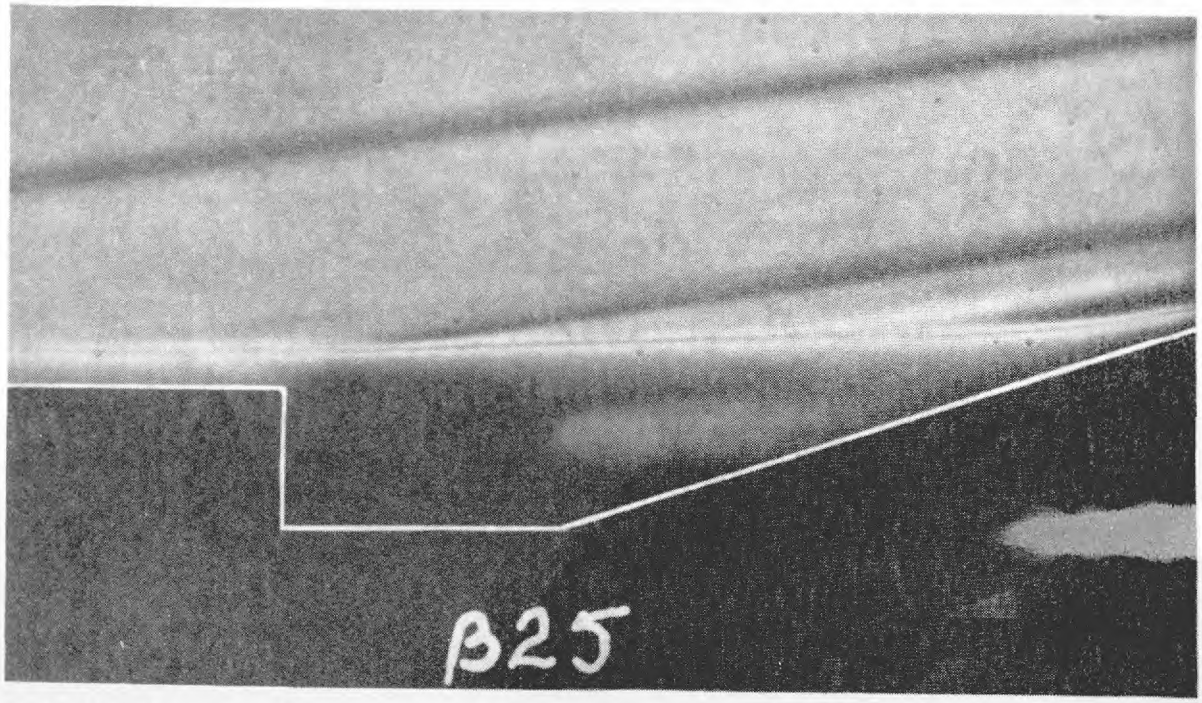

(a) Powder visualisation of the recirculating flow, M = 8·2.

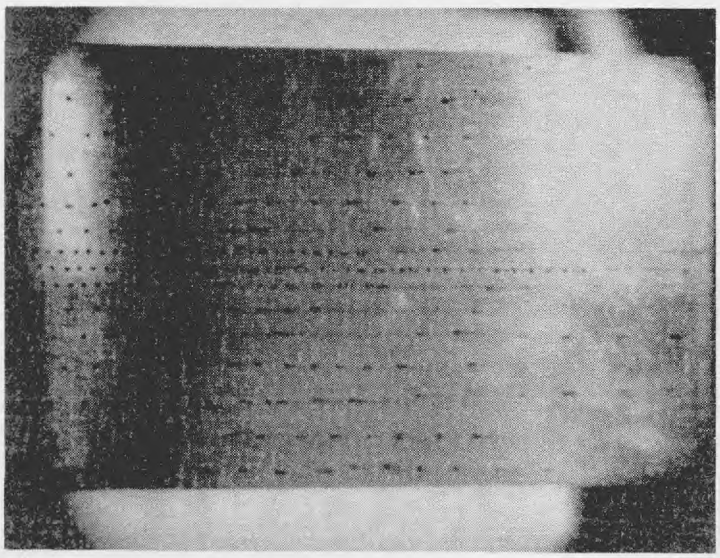

(b) Oil spot surface visualisation.
(no side plates)

step

FIG. 10. Flow visualisation techniques.

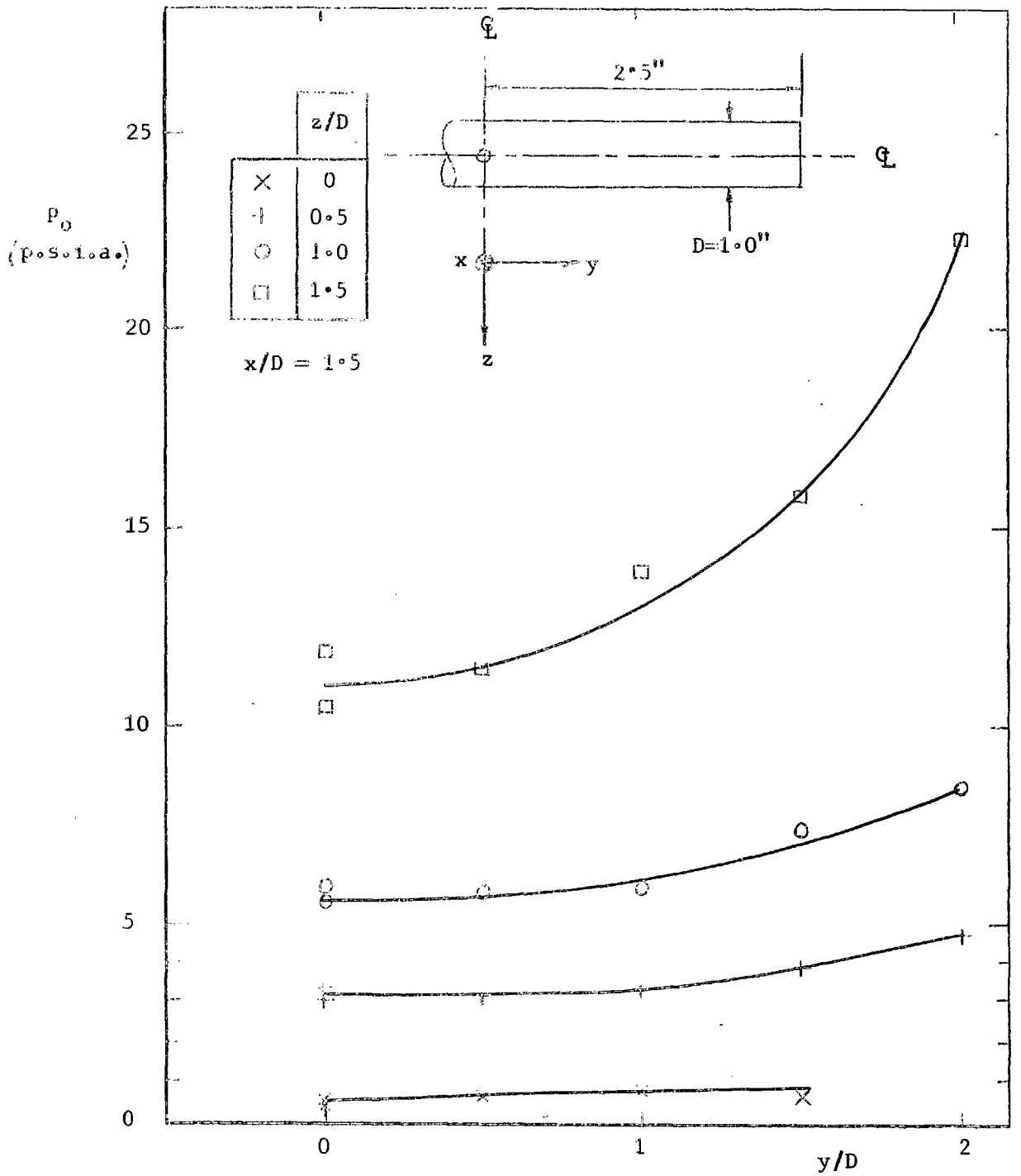

(a) Spanwise traverses

FIG. 11. Pitot pressure traverses behind a cylinder at $M_\infty = 8{\cdot}2$ and $R_e/\text{in.} = 0{\cdot}24 \times 10^6$.

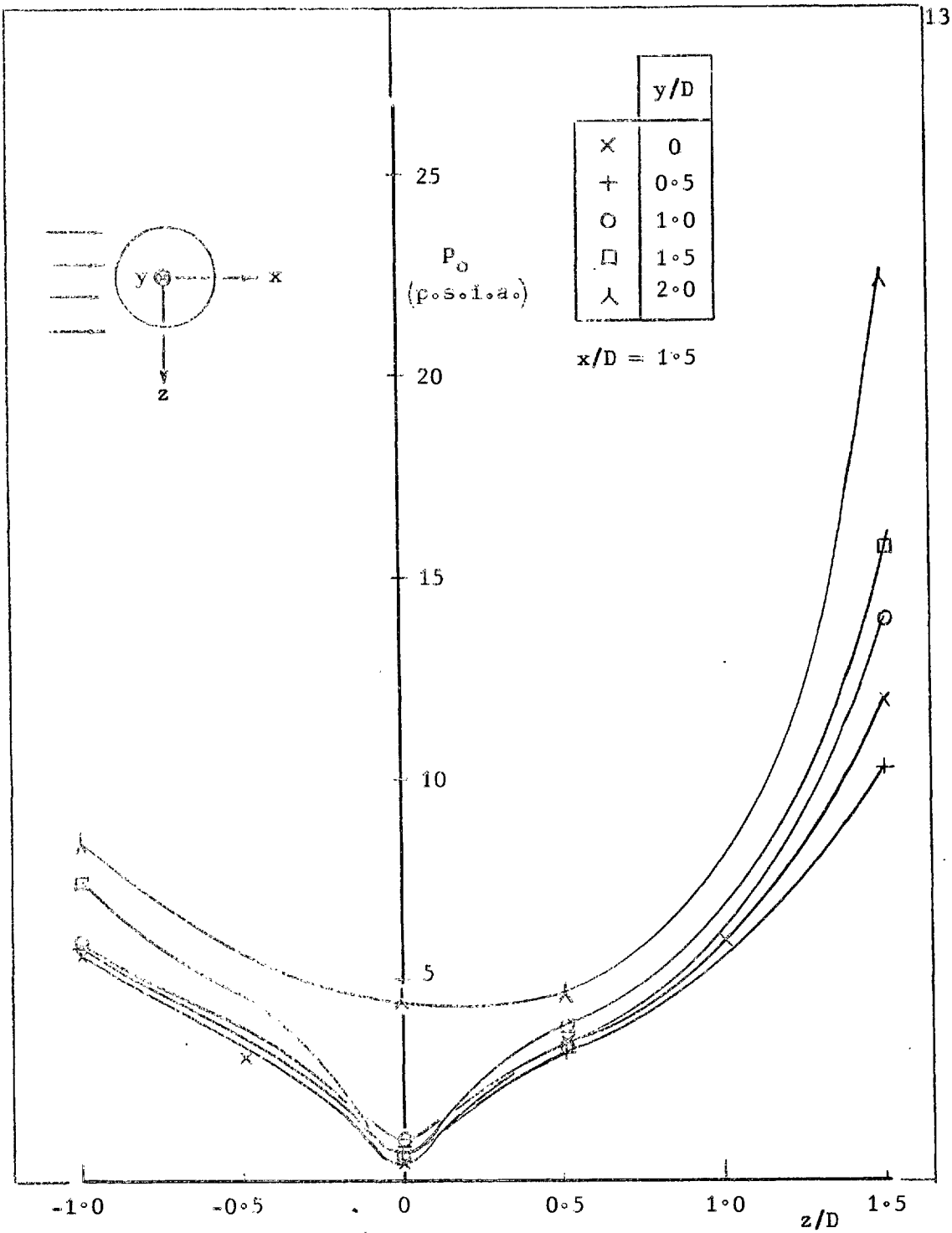

(b) Traverses across the wake

FIG. 11. concluded.

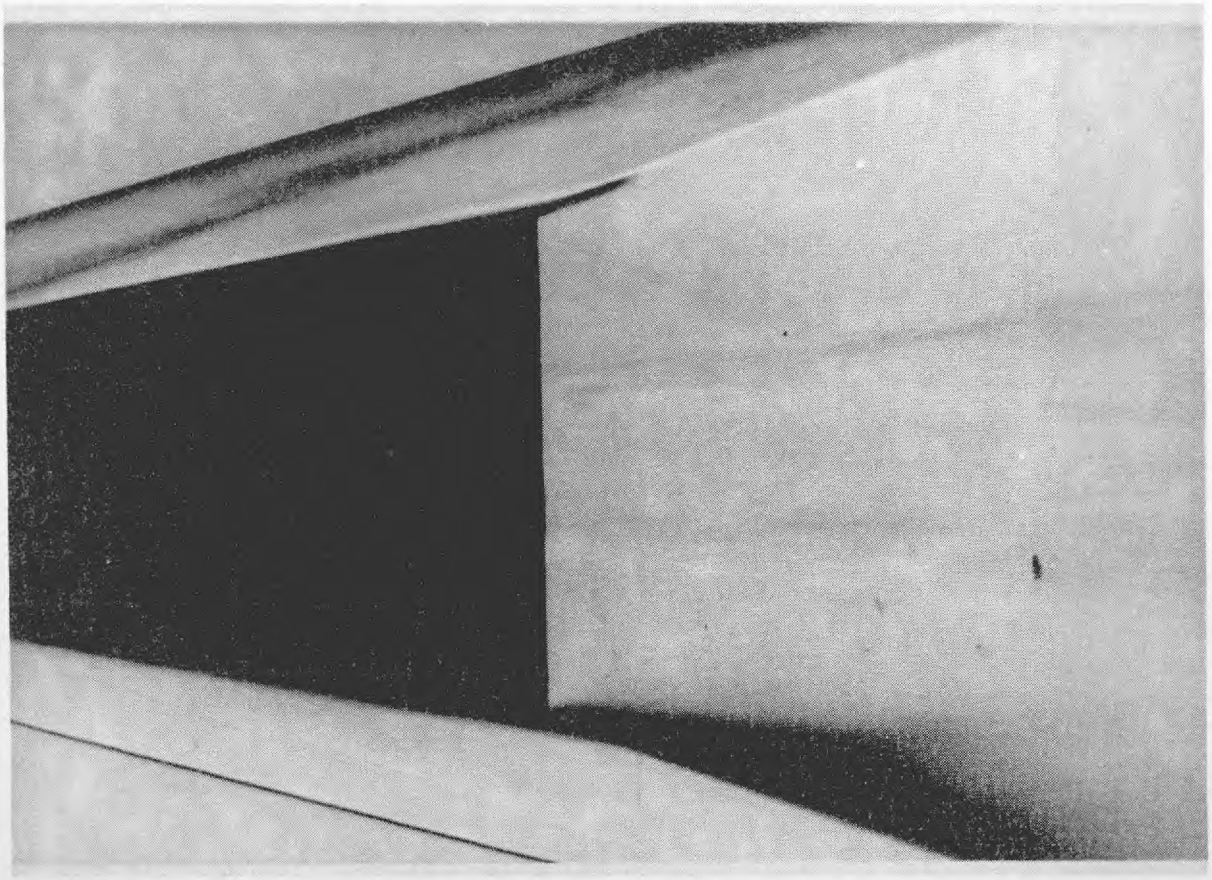

FIG. 12. Schlieren photograph of wedge separated flow at M = 8.2.

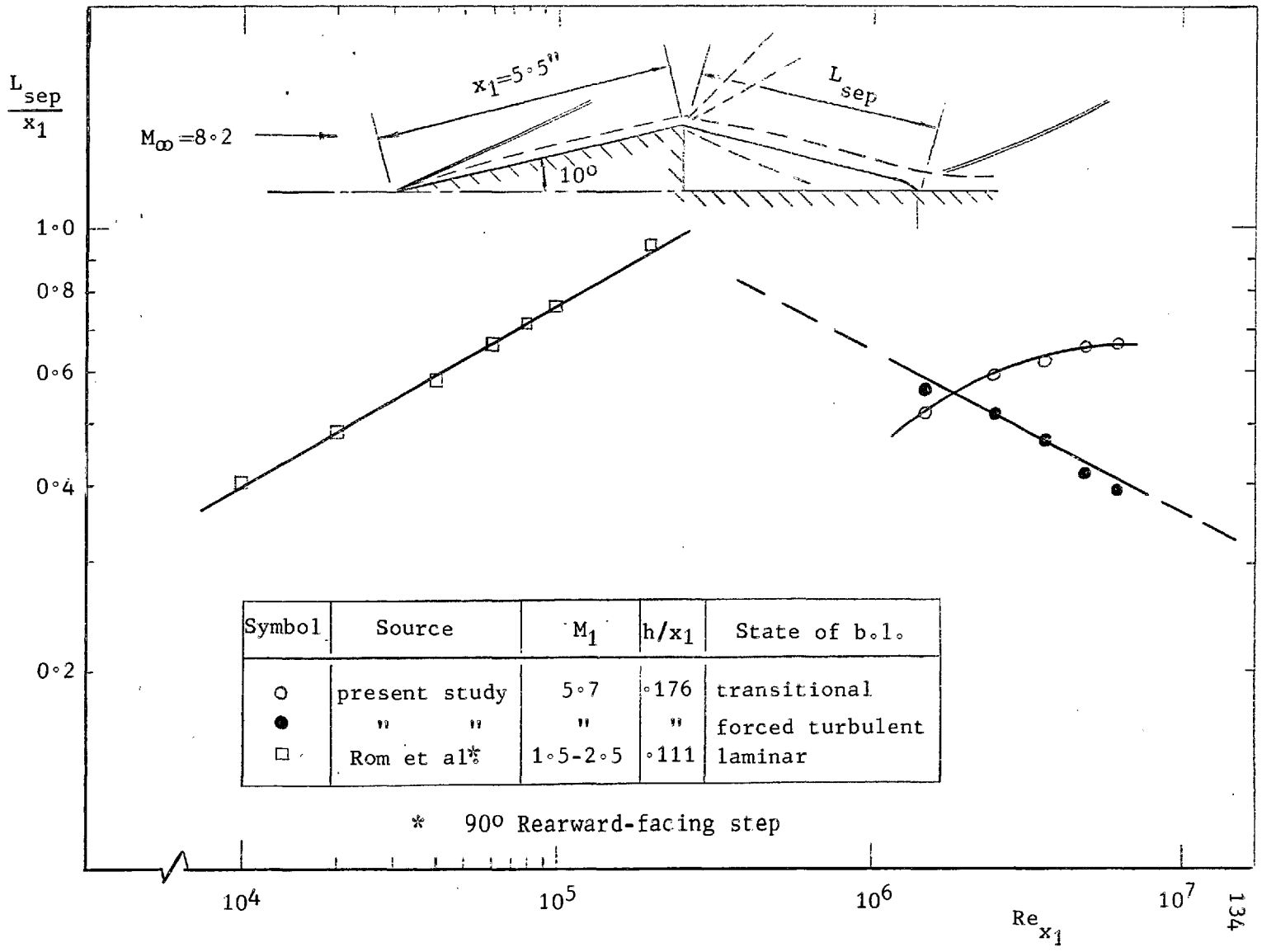

FIG. 13. Correlation of the wedge separated length in terms of Reynolds number.

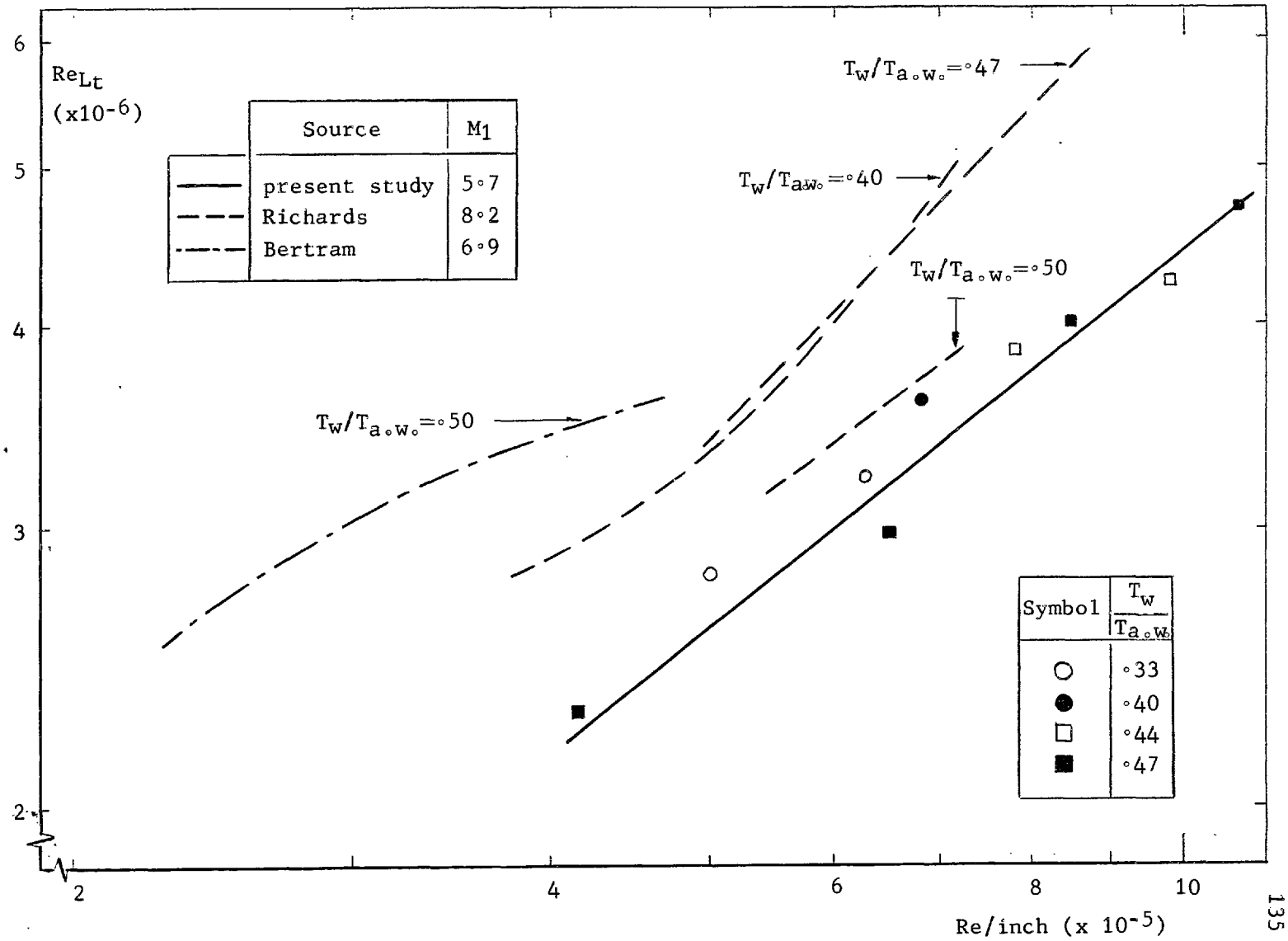

FIG. 14. Variation of transition with unit Reynolds number for an attached boundary layer.

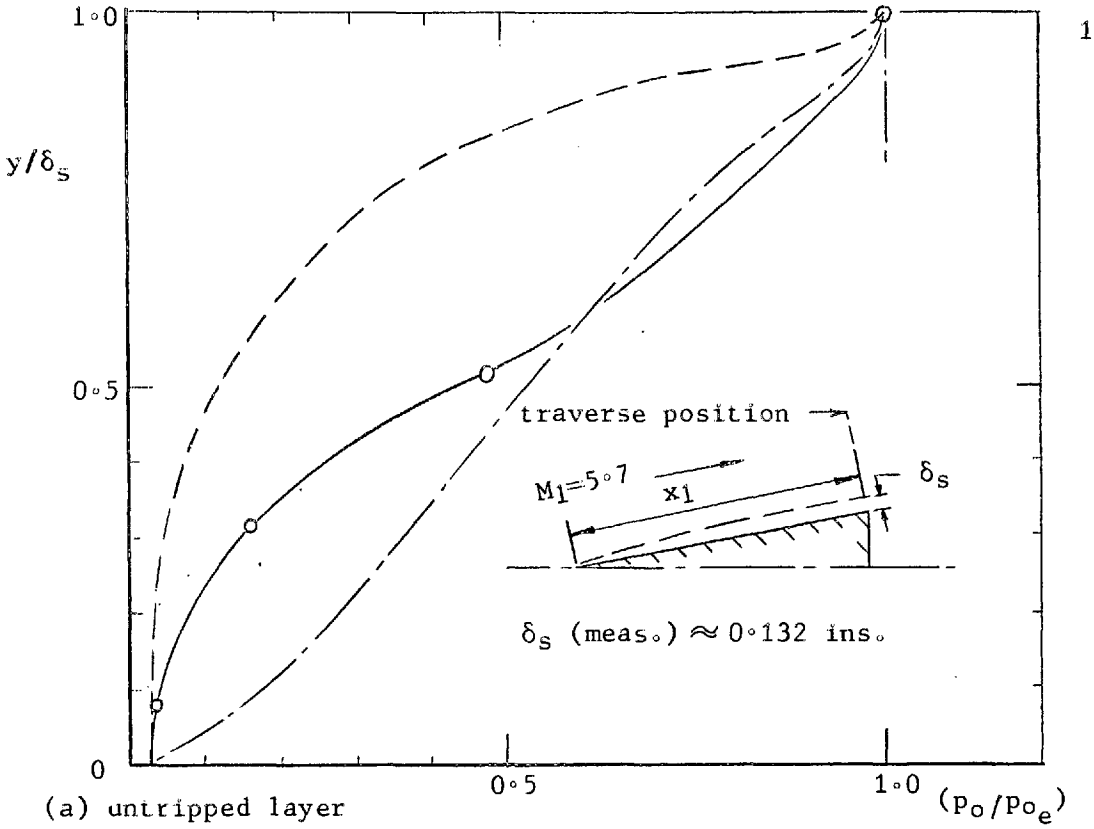

(a) untripped layer

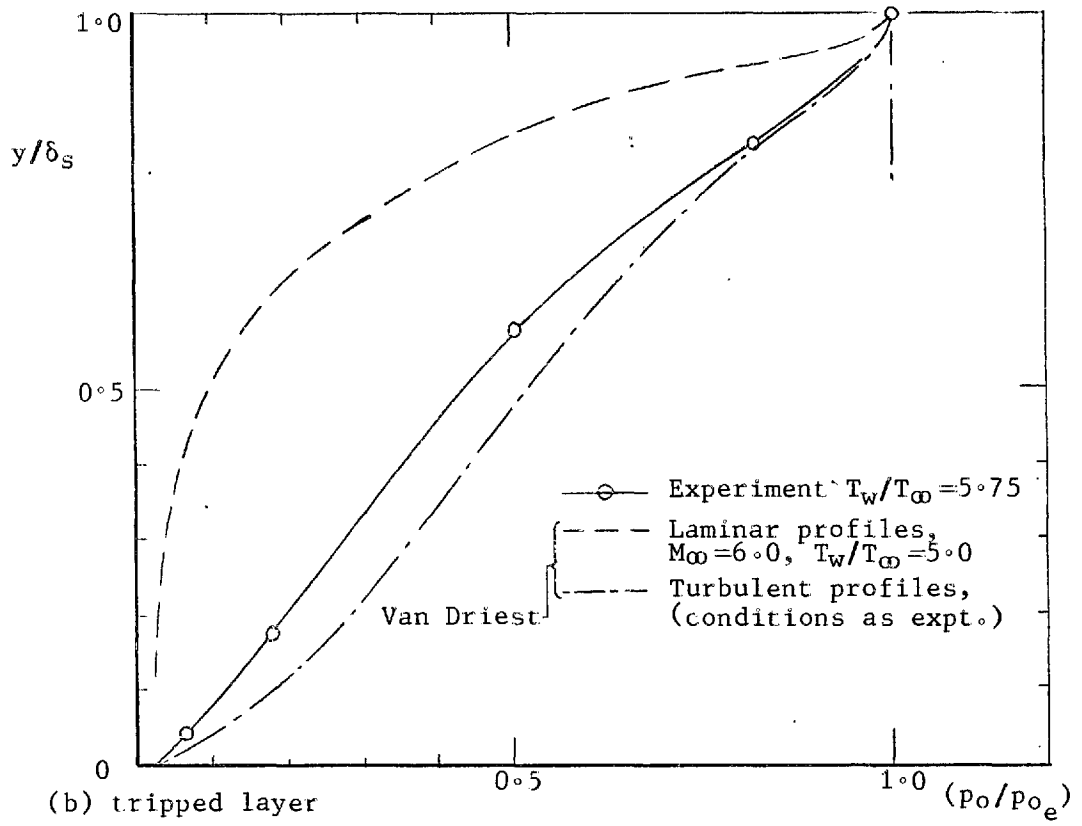

(b) tripped layer

FIG. 15. Pitot profiles of the wedge boundary layer at M = 5·7 and $Re_{x1} = 1{\cdot}45 \times 10^6$.

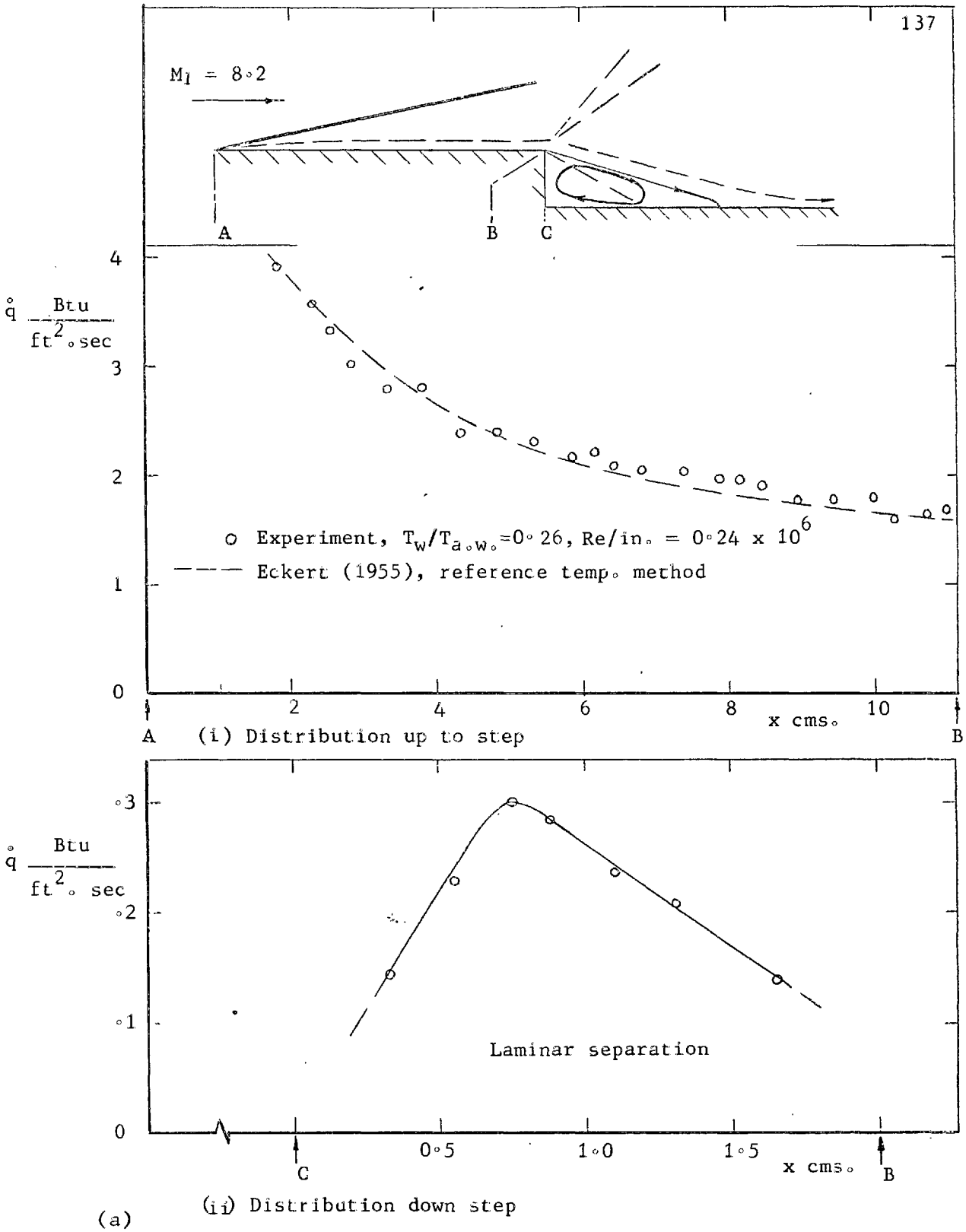

(a)

FIG. 16. Centre line heat transfer distributions down a step and wedge base for laminar and transitional separations.

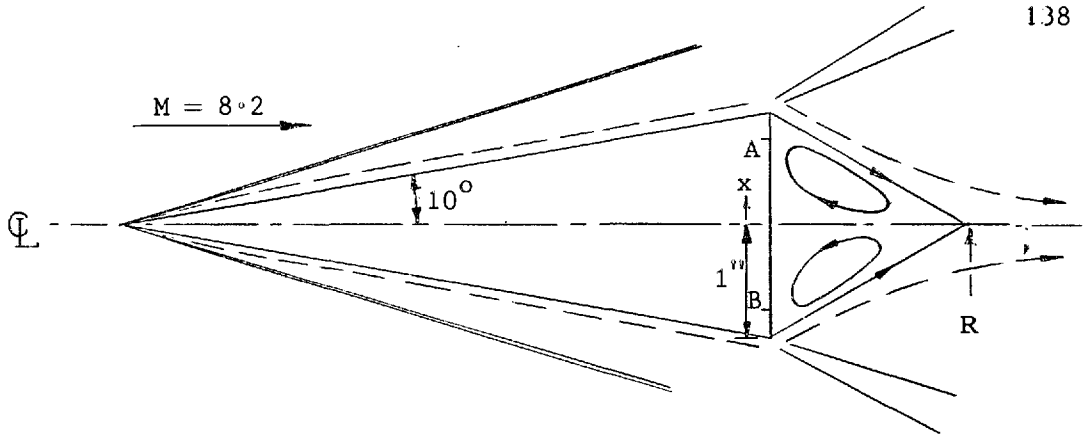

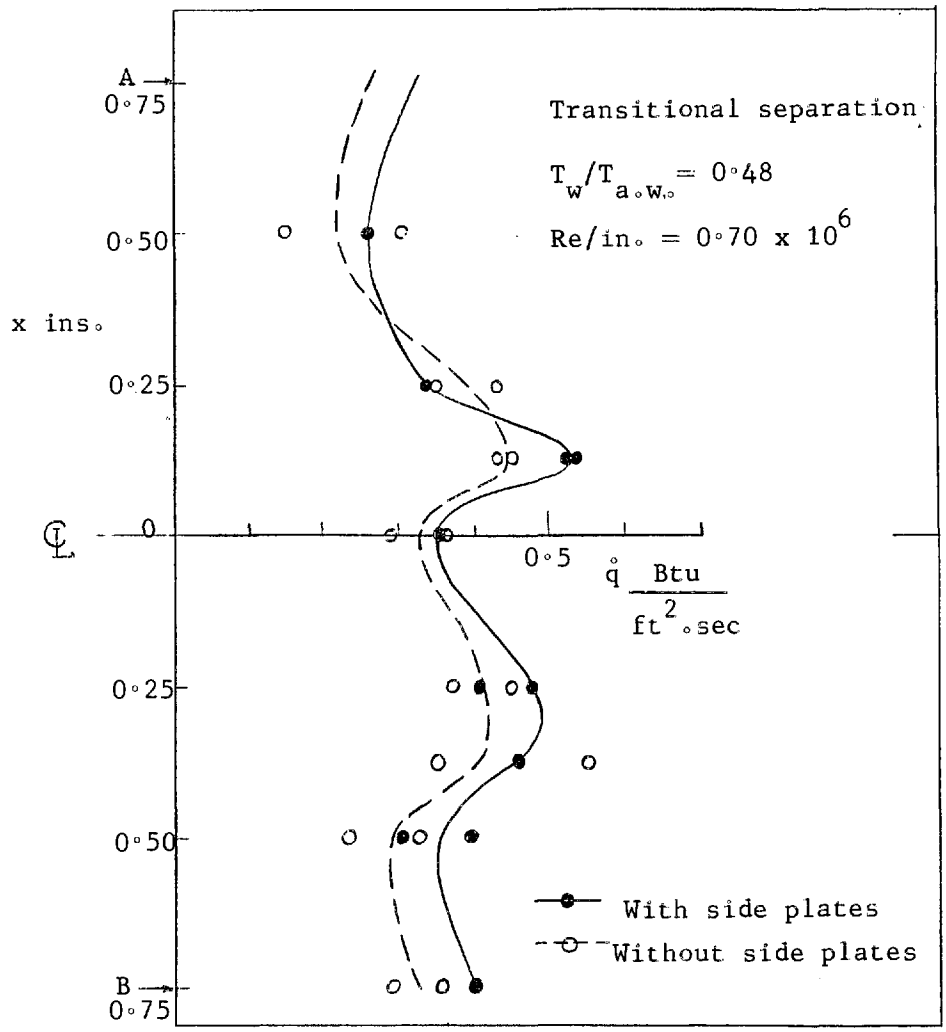

(b) Distribution down wedge base

FIG. 16. concluded.

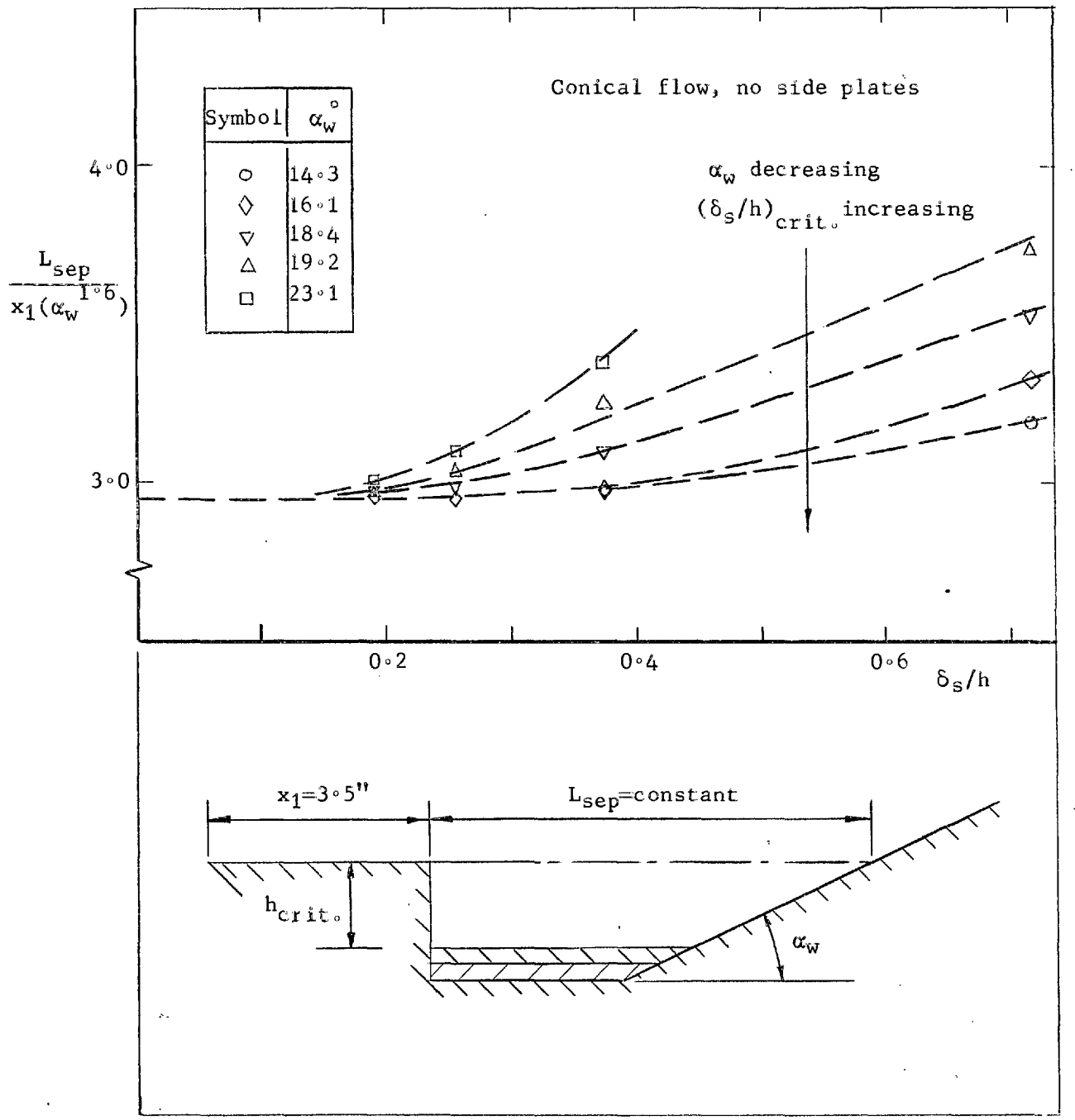

(a) critical step height

FIG. 17. Effect of step height on the straight-separated flow at M = 9°7 and Re/in. = 0°24 x 10^6 .

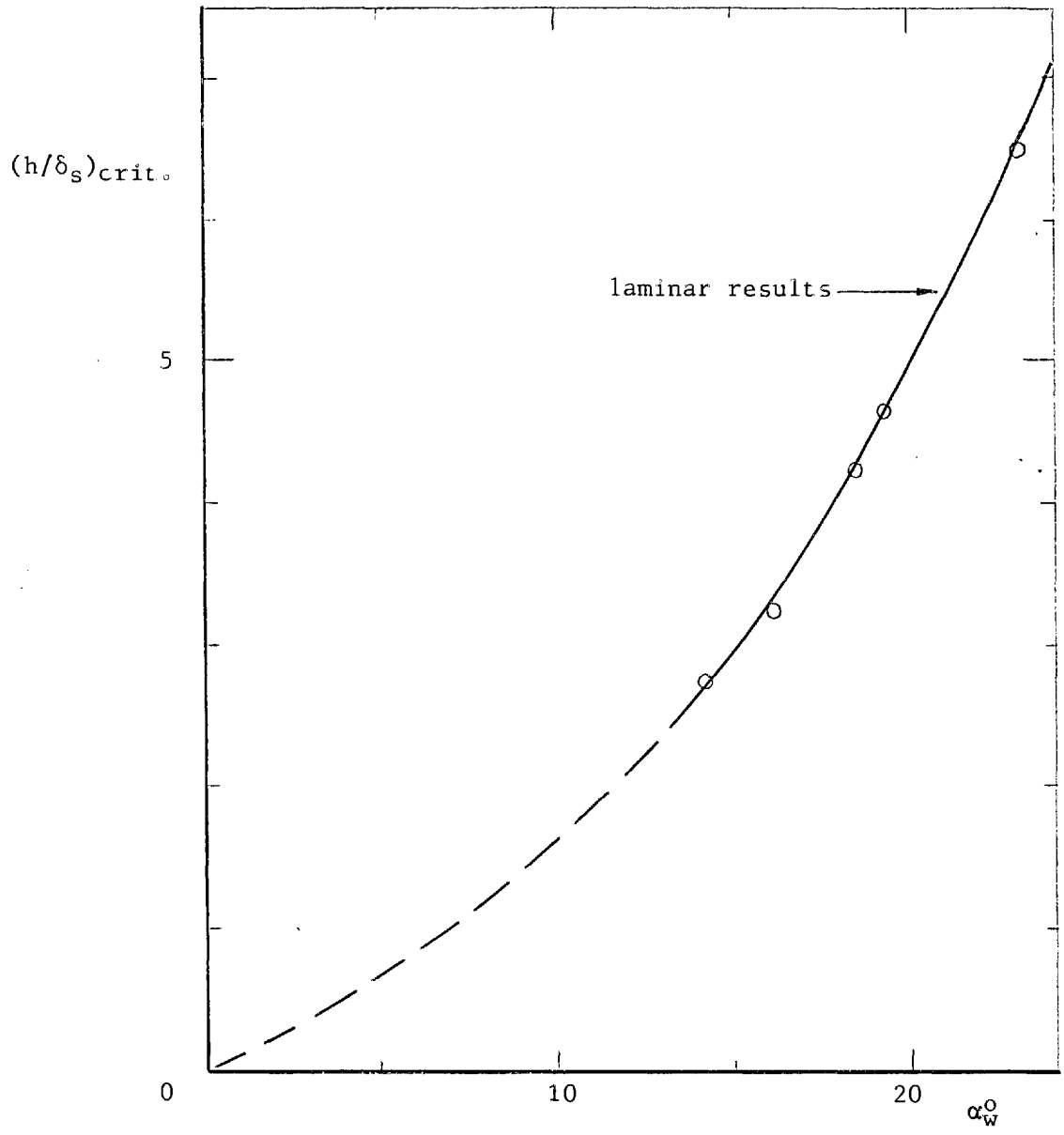

(b) critical $\frac{\text{step height}}{\text{b.l. thickness}}$ ratio vs. α_w

FIG. 17. concluded.

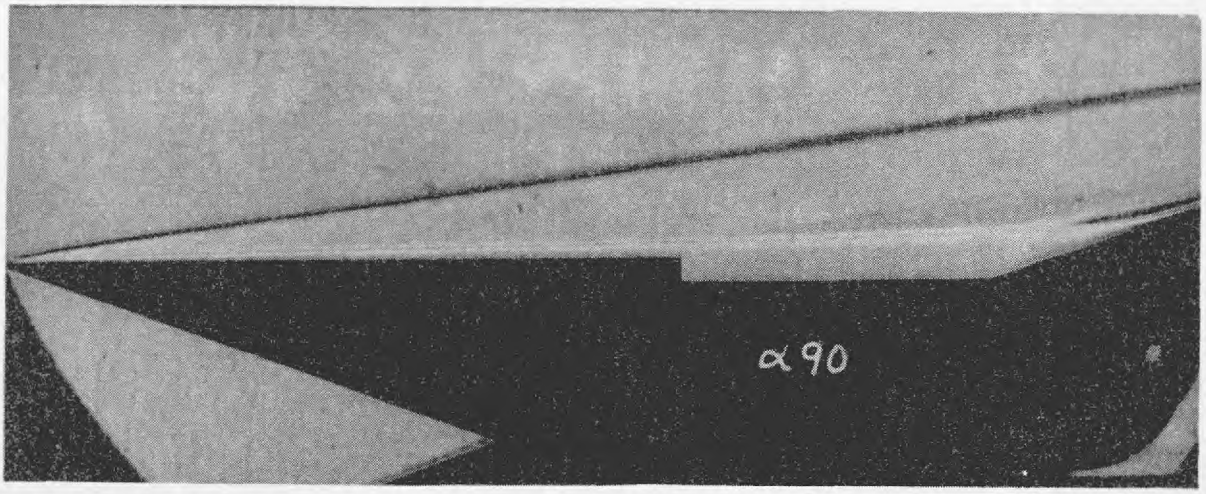

(i) $h = 0{\cdot}125$ins. $L_{sep} = 2{\cdot}00$ins.

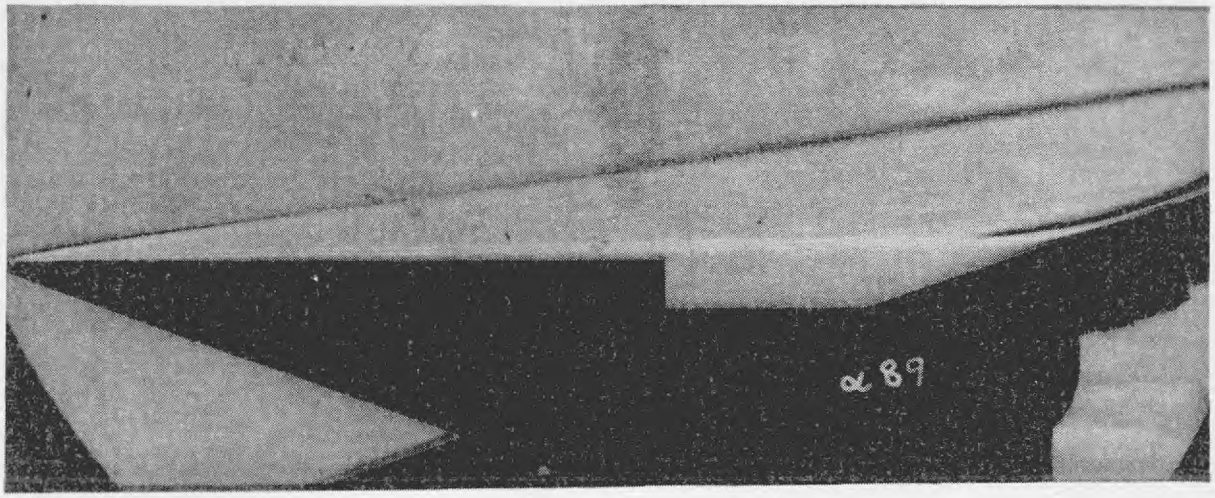

(ii) $h = 0{\cdot}25$ins. $L_{sep} = 1{\cdot}76$ins.

$\alpha_w = 18{\cdot}4^{\circ}$, x_1 and Re/in. = constant.

(a)

FIG. 18. Schlieren photographs demonstrating step height effect on straight separations at $M = 9{\cdot}7$.

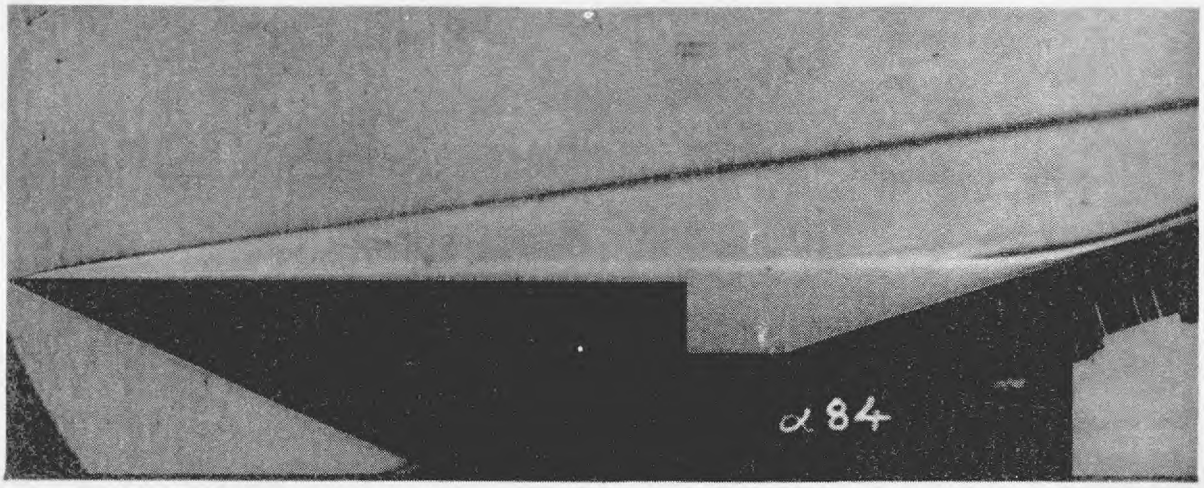

(iii) h = 0·375ins. L_{sep} = 1·64ins.

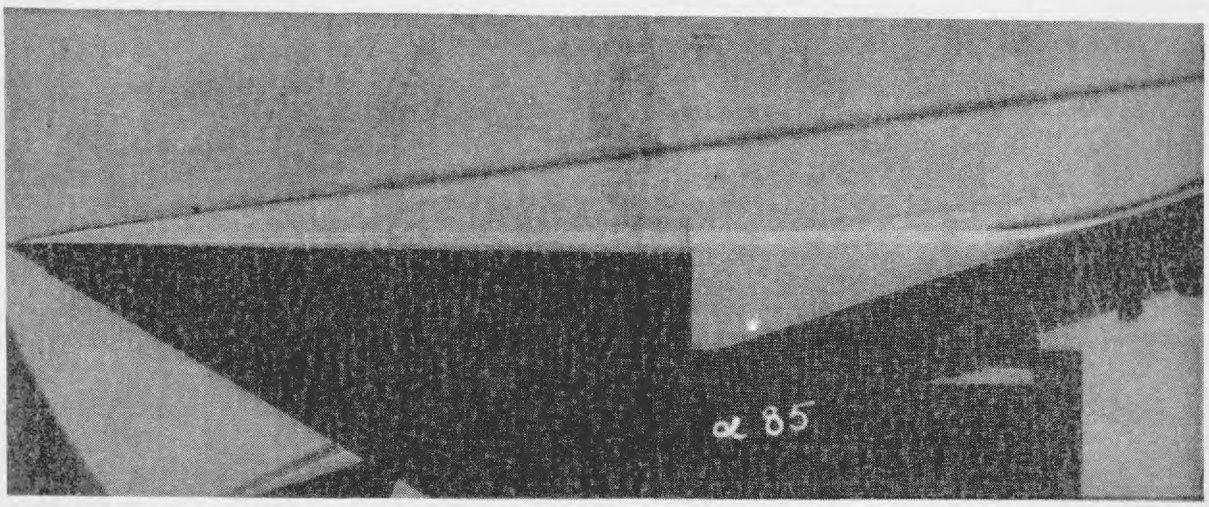

(iv) h = 0·50ins. L_{sep} = 1·64ins.

(b)

FIG. 18. concluded.

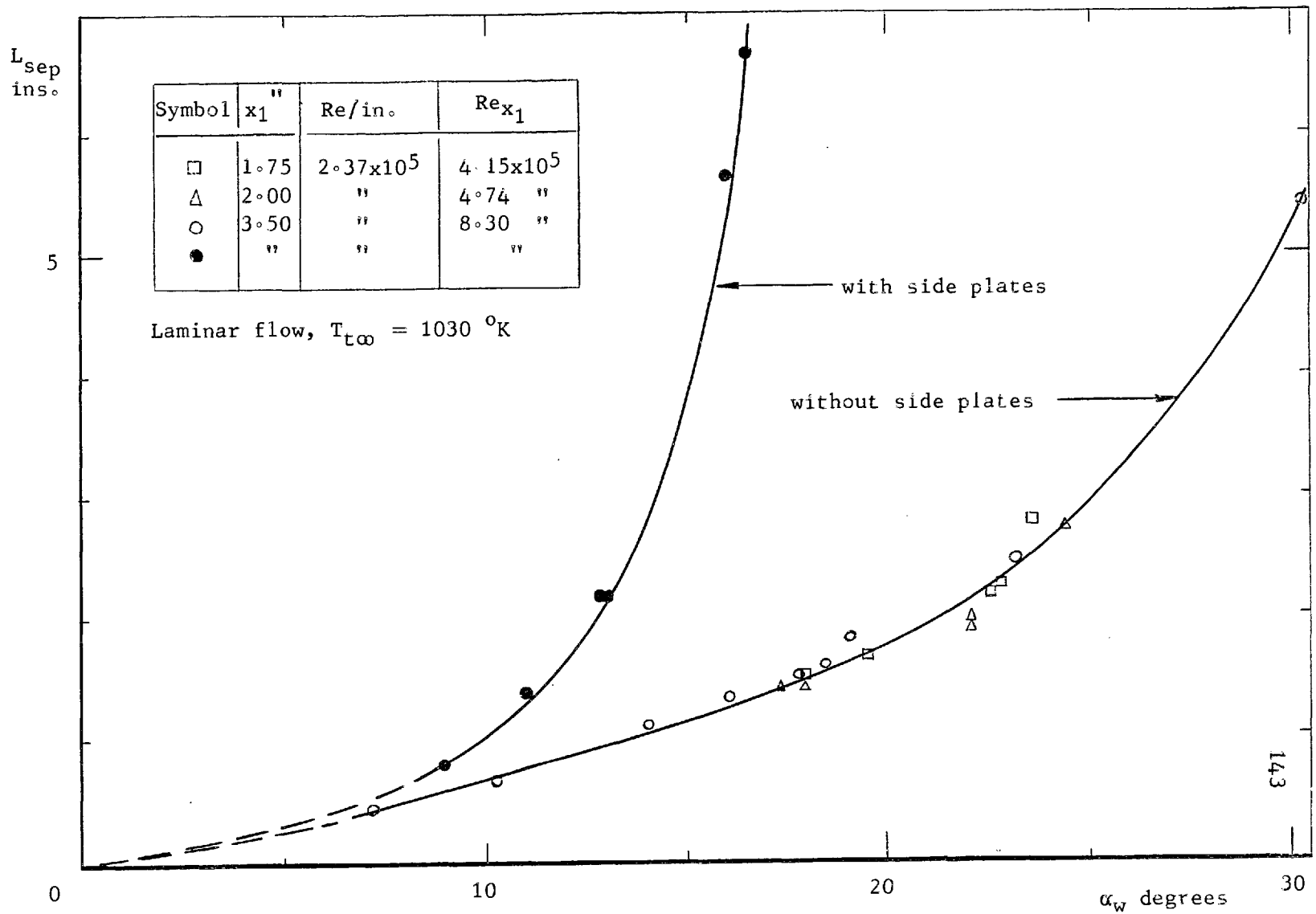

FIG. 19. Correlation of straight-separated length and reattachment angle for conical flow at M = 9.7

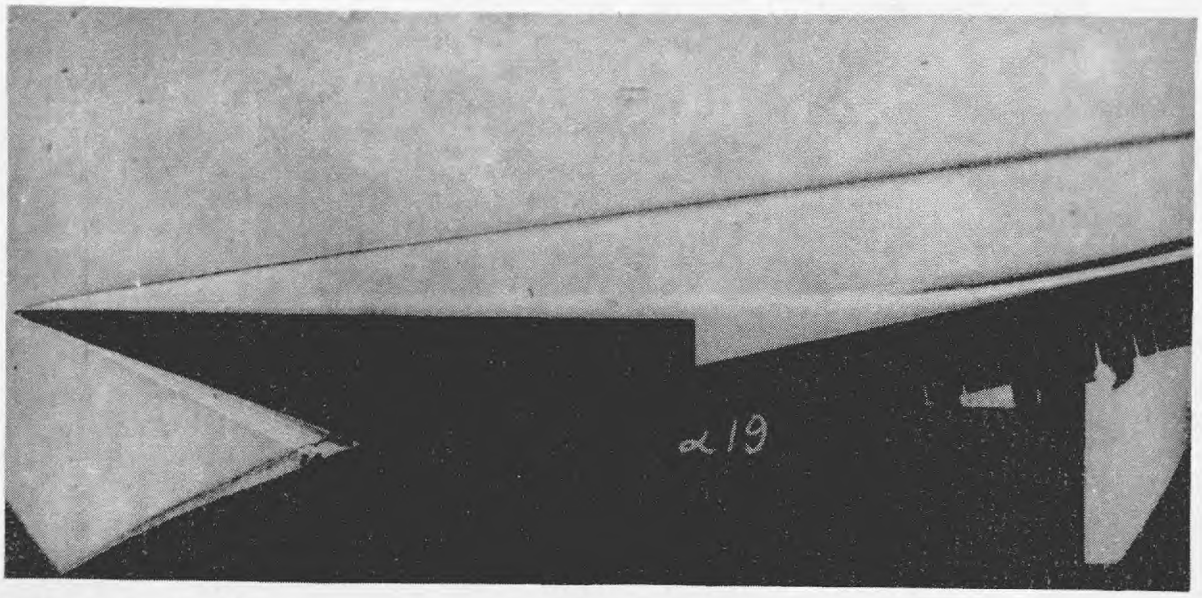

(i) $\alpha_w = 12{\cdot}9^o$ $L_{sep} = 1{\cdot}10$ins.

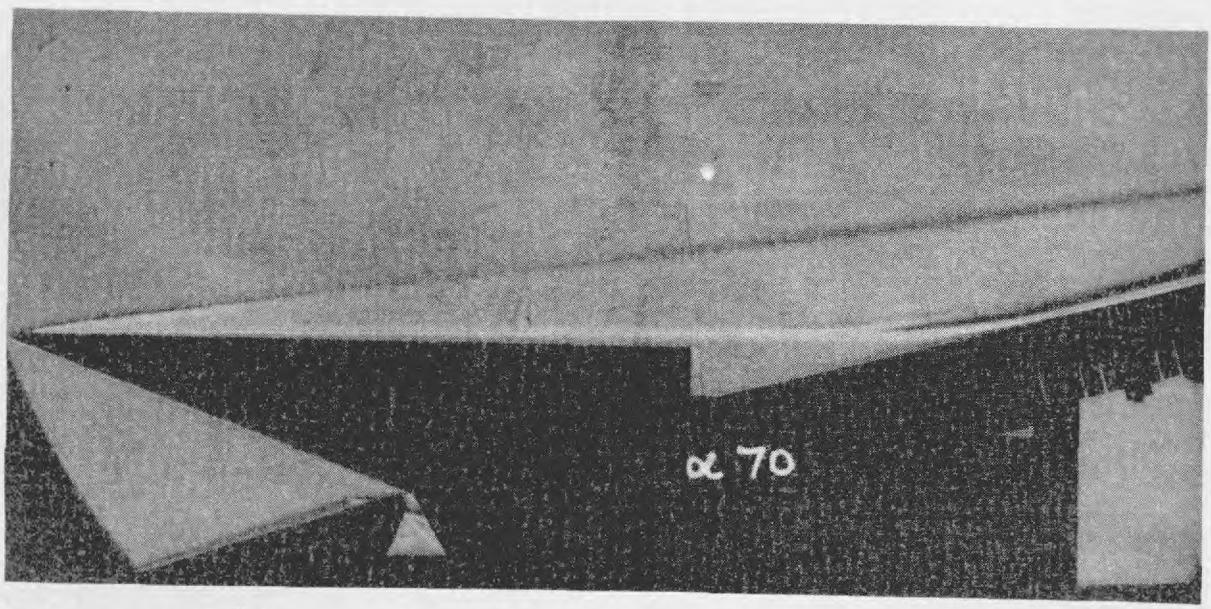

(ii) $\alpha_w = 14{\cdot}3^o$ $L_{sep} = 1{\cdot}13$ins.

(a) $h = 0{\cdot}25$ins., x_1 and Re/in. = constant

FIG. 20. Schlieren photographs illustrating the variation of separated length with flap angle at $M = 9{\cdot}7$.

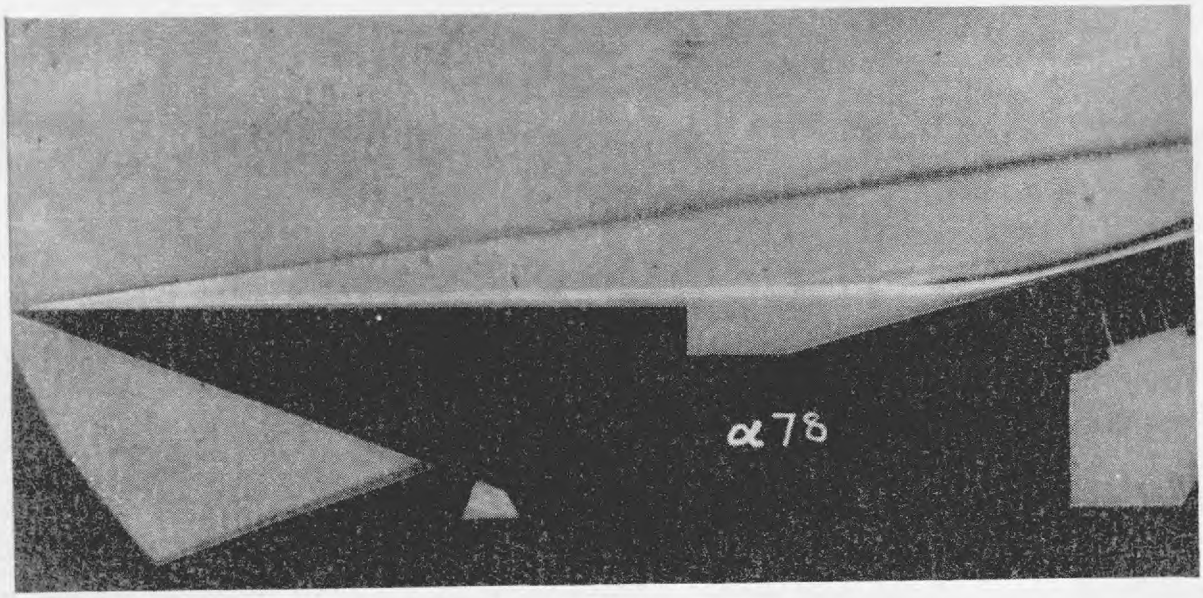

(iii) $\alpha_w = 16{\cdot}1^{\circ}$ $L_{sep} = 1{\cdot}33$ins.

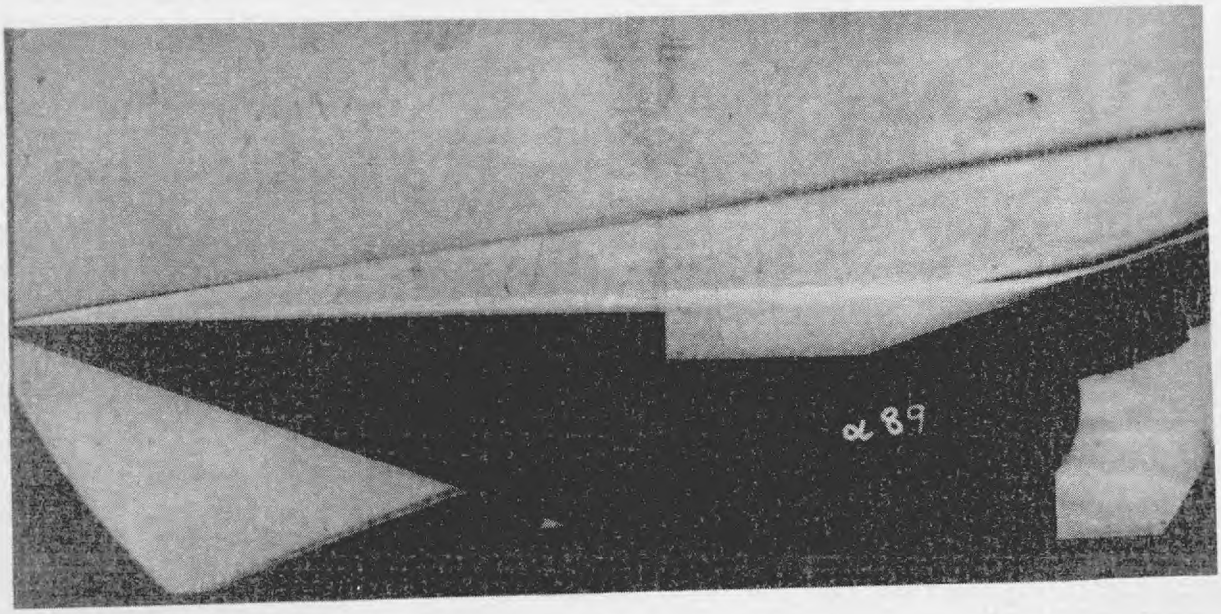

(iv) $\alpha_w = 18{\cdot}4^{\circ}$ $L_{sep} = 1{\cdot}76$ins.

(b)

FIG. 20. continued.

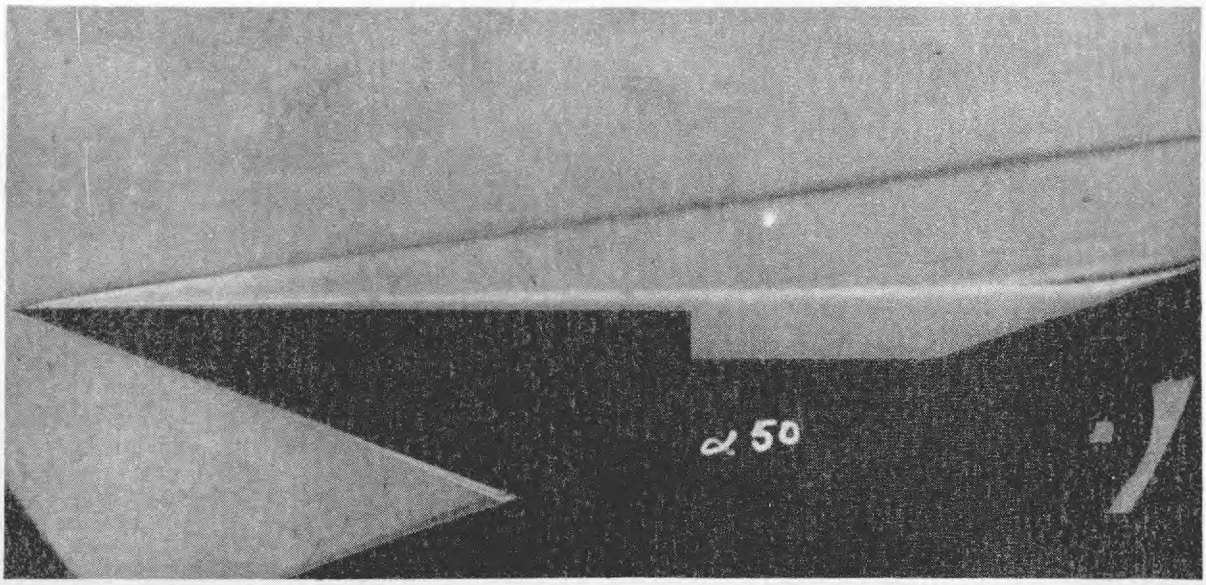

(v) $\alpha_w = 19{\cdot}2^o$ $L_{sep} = 2{\cdot}00$ins.

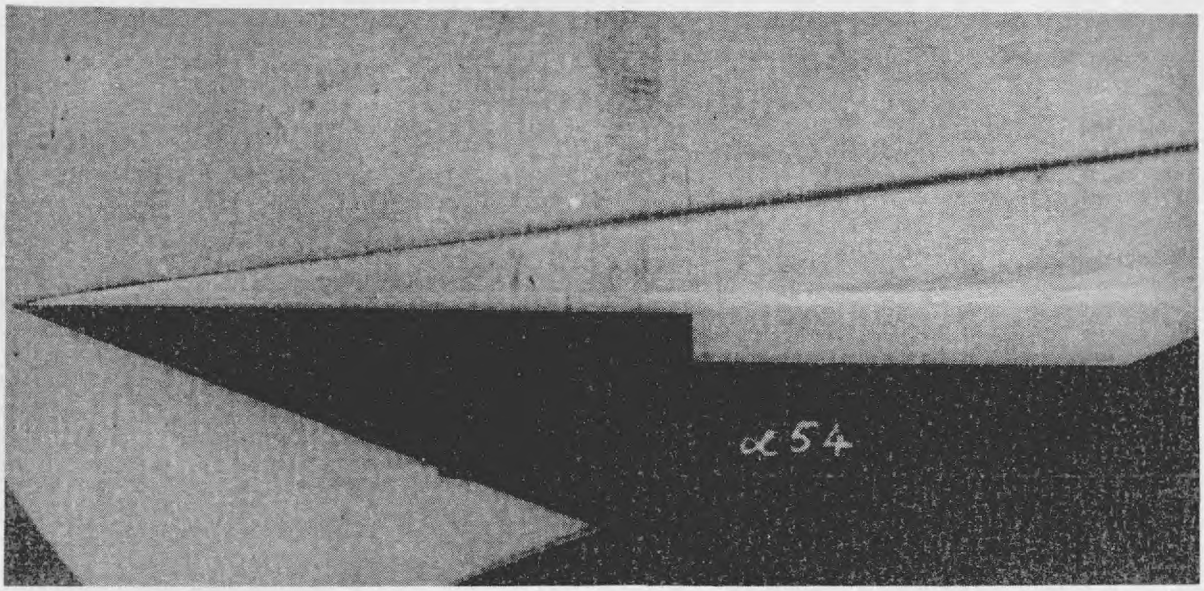

(vi) $\alpha_w = 23{\cdot}1^o$ $L_{sep} = 2{\cdot}77$ins.

(c)

FIG. 20. concluded.

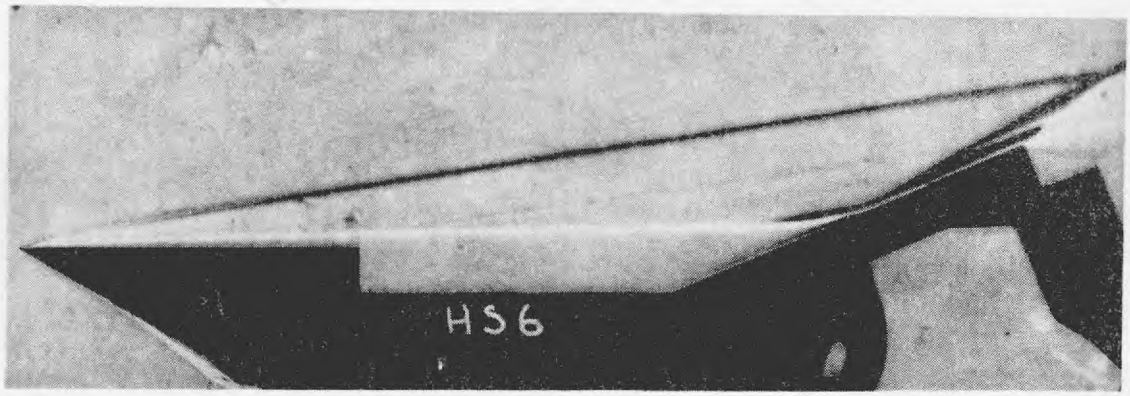

(i) $x_1 = 1{\cdot}75$ins. $L_{sep} = 2{\cdot}10$ins. $\alpha_w = 22{\cdot}5^{\circ}$

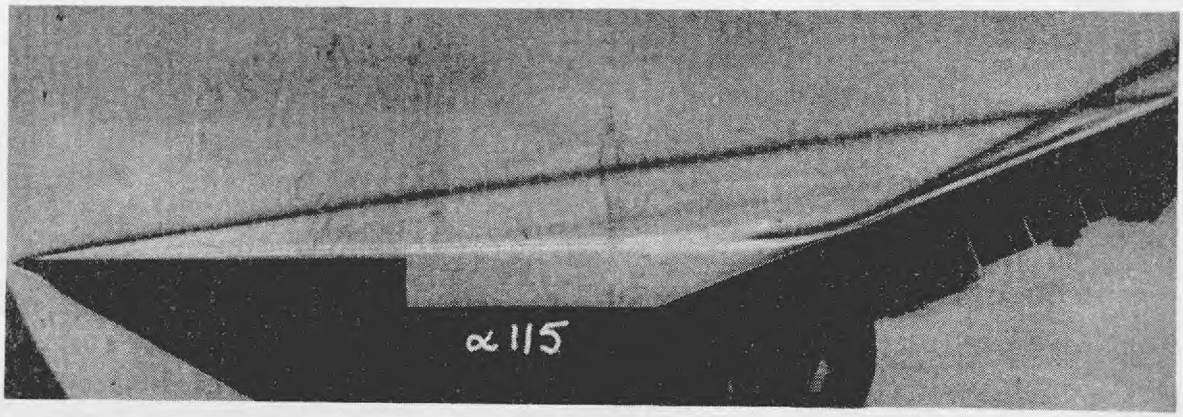

(ii) $x_1 = 2{\cdot}0$ins. $L_{sep} = 1{\cdot}97$ins. $\alpha_w = 22{\cdot}0^{\circ}$

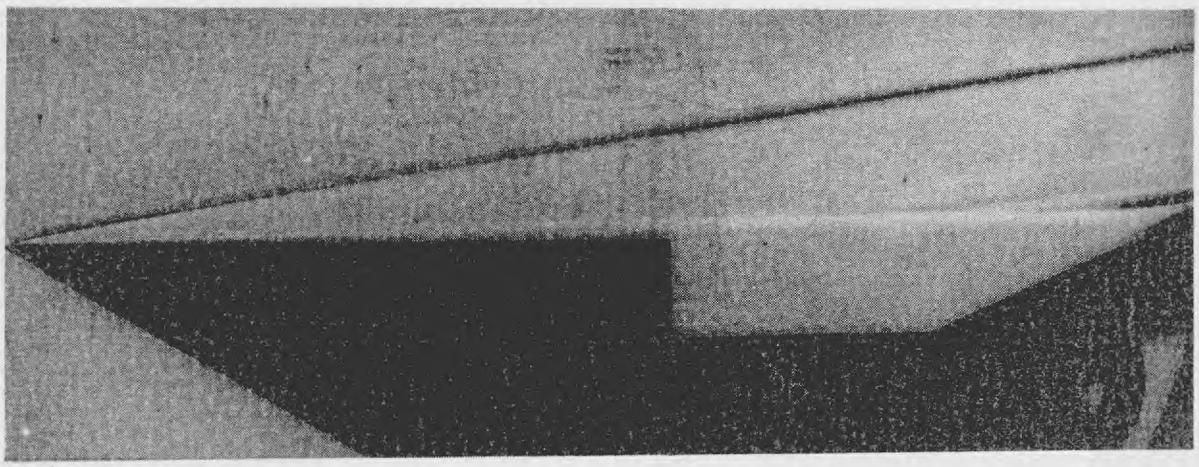

(iii) $x_1 = 3{\cdot}5$ins. $L_{sep} = 2{\cdot}45$ins. $\alpha_w = 23{\cdot}1^{\circ}$

For constant α_w and Re/in. L_{sep} changes little with x_1

FIG. 21. The independence of length of separation on attached flow length in a $M = 9{\cdot}7$, conical flow.

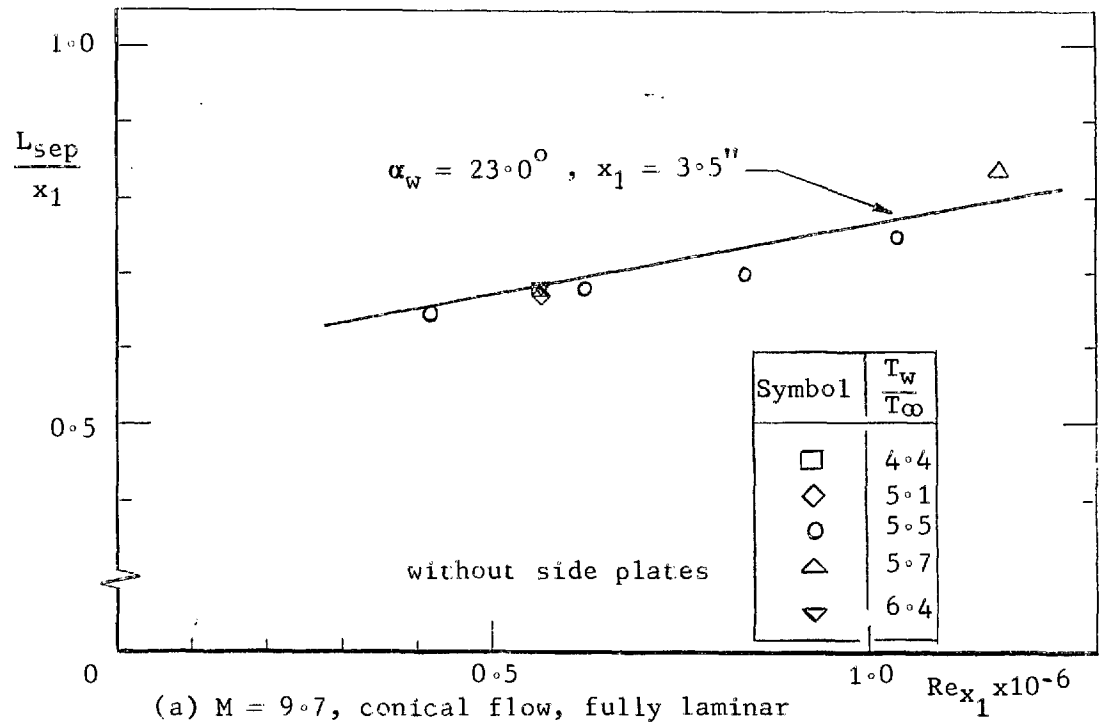

(a) M = 9.7, conical flow, fully laminar

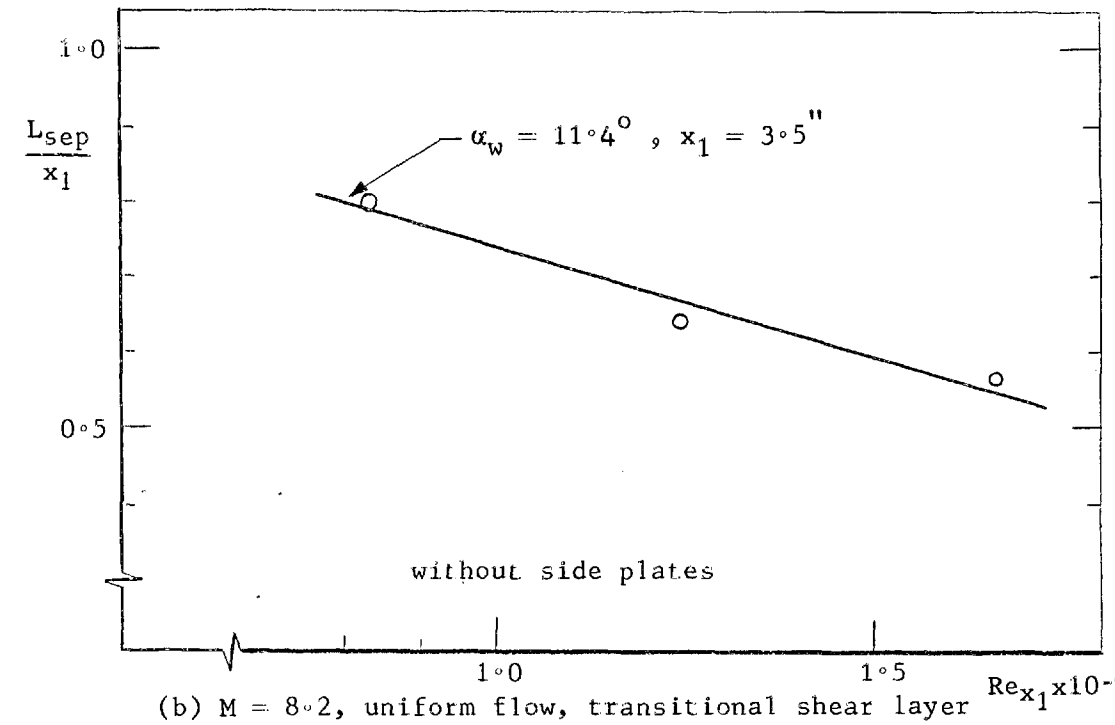

(b) M = 8.2, uniform flow, transitional shear layer

FIG. 22. Reynolds number effect on the length of straight separations at M = 8.2 and 9.7 .

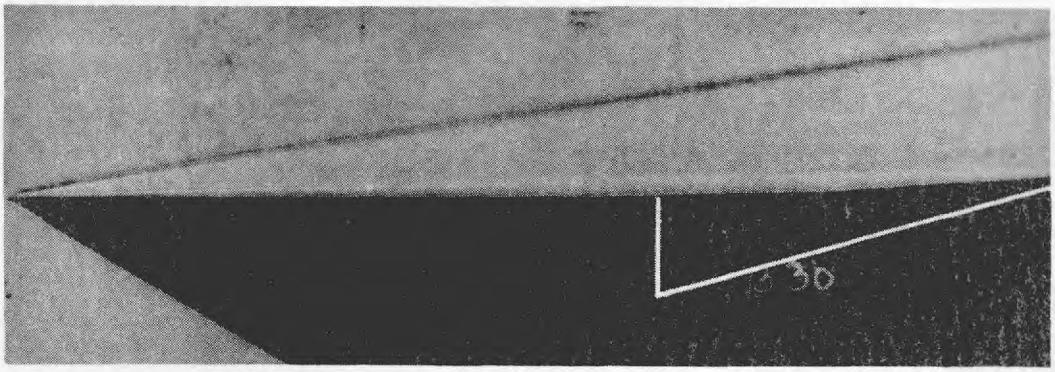

(i) Side plates enclosing the 'dead air' region and the reattachment pressure rise.

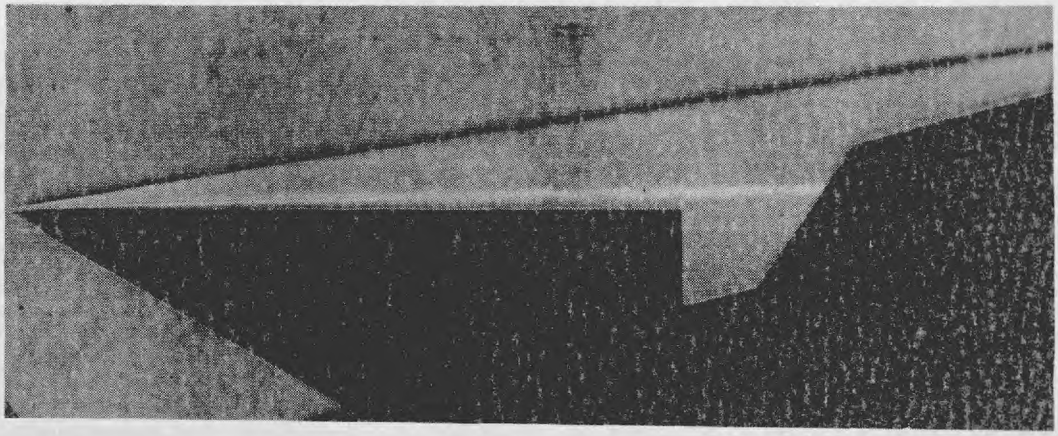

(ii) Side plates extending through, and downstream of, the reattachment pressure rise.

$\alpha_w = 13{\cdot}0^\circ$ $\qquad \frac{L_{sep}}{x_1} = 0{\cdot}62$

$x_1 = 3{\cdot}5\text{ins.}$ $\qquad h = 0{\cdot}5\text{ins.}$

FIG. 23. Side plate similarity in conical flow at $M = 9{\cdot}7$.

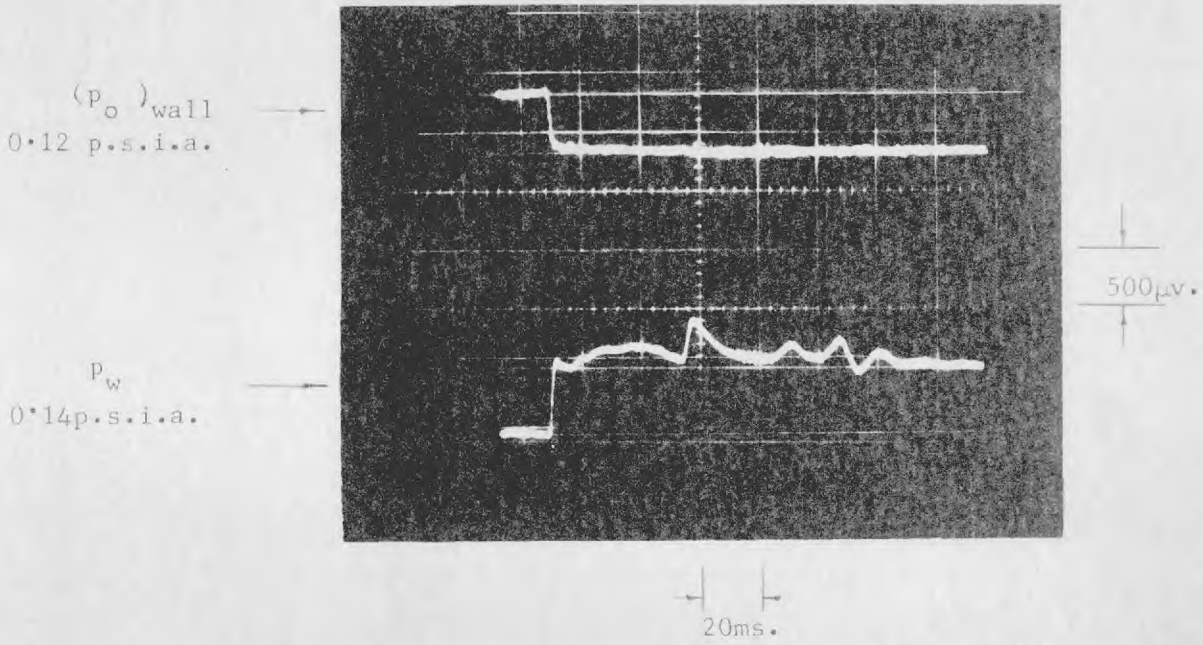

(i) C.E.C. transducers (0 - 10p.s.i.a. range)

M = 9·7

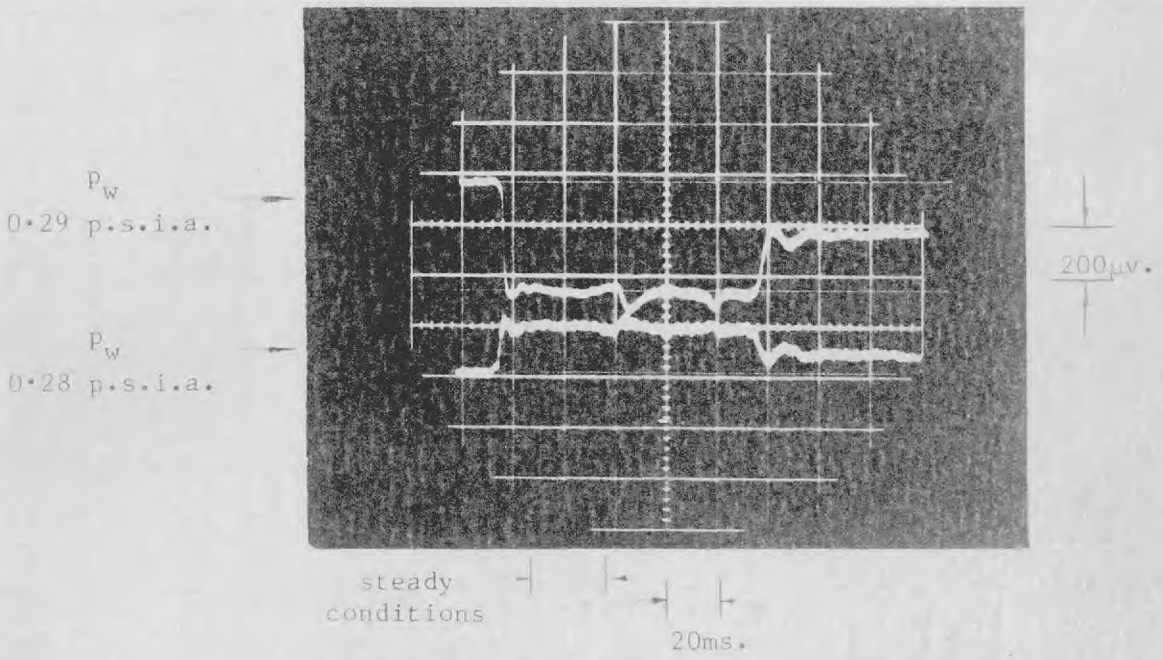

(ii) Solartron transducers(0-15 and 0-30p.s.i.a.)

FIG. 24. Oscilloscope traces of the pressure transducer outputs.

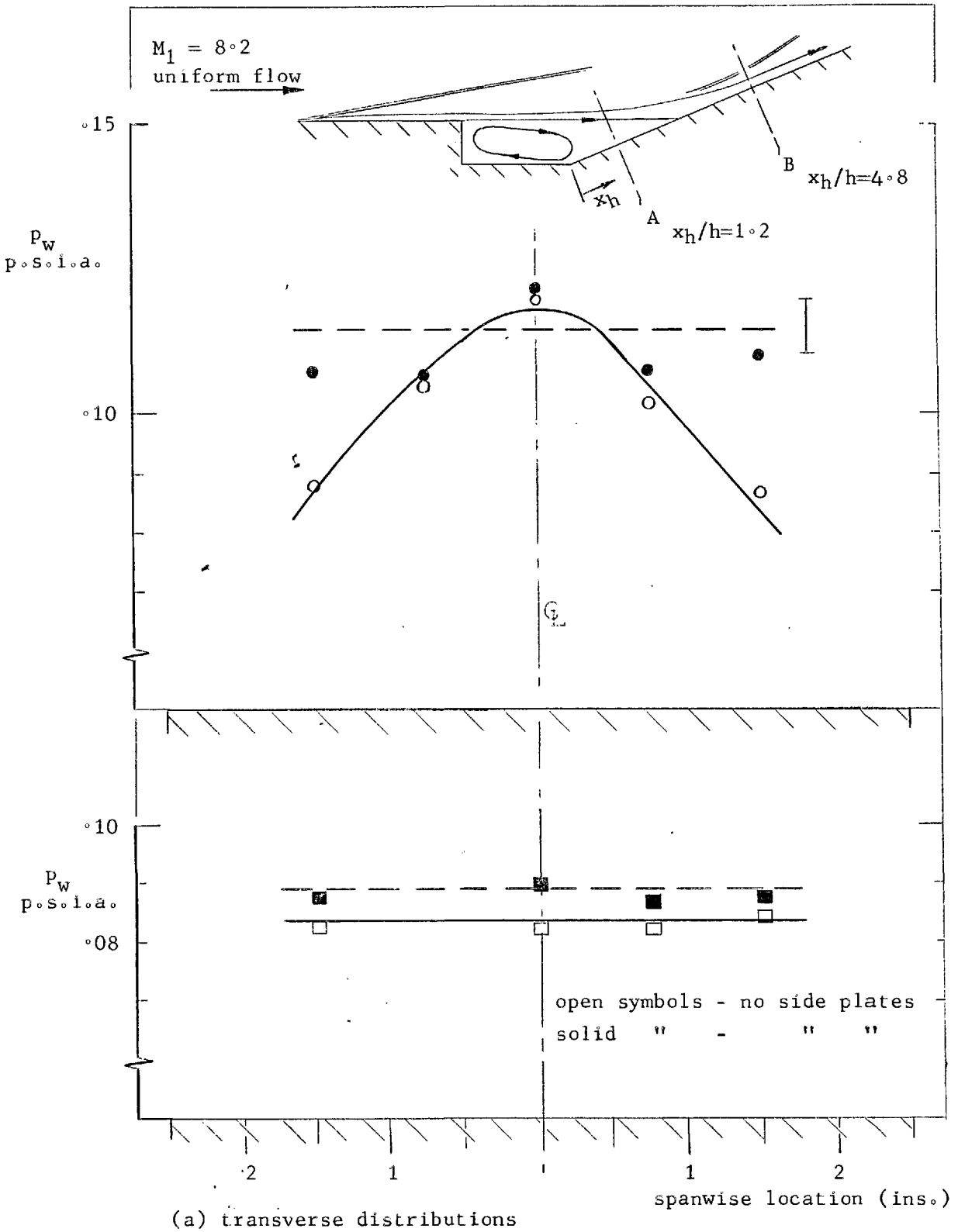

(a) transverse distributions

FIG. 25. Transverse and streamwise pressure distributions in separated flow at M = 8·2 - side plate effects.

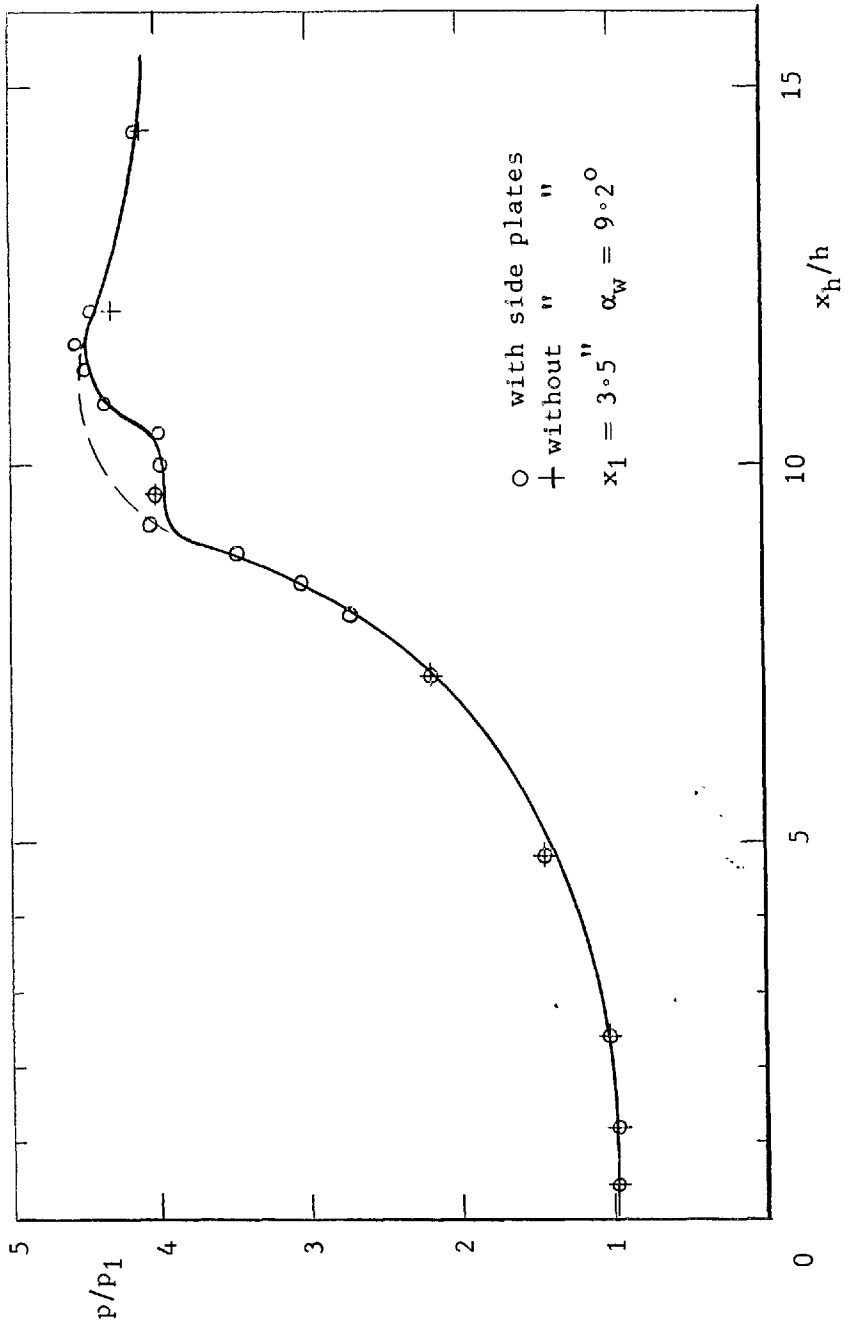

(b) reattachment centre-line pressure distribution

FIG. 25. concluded.

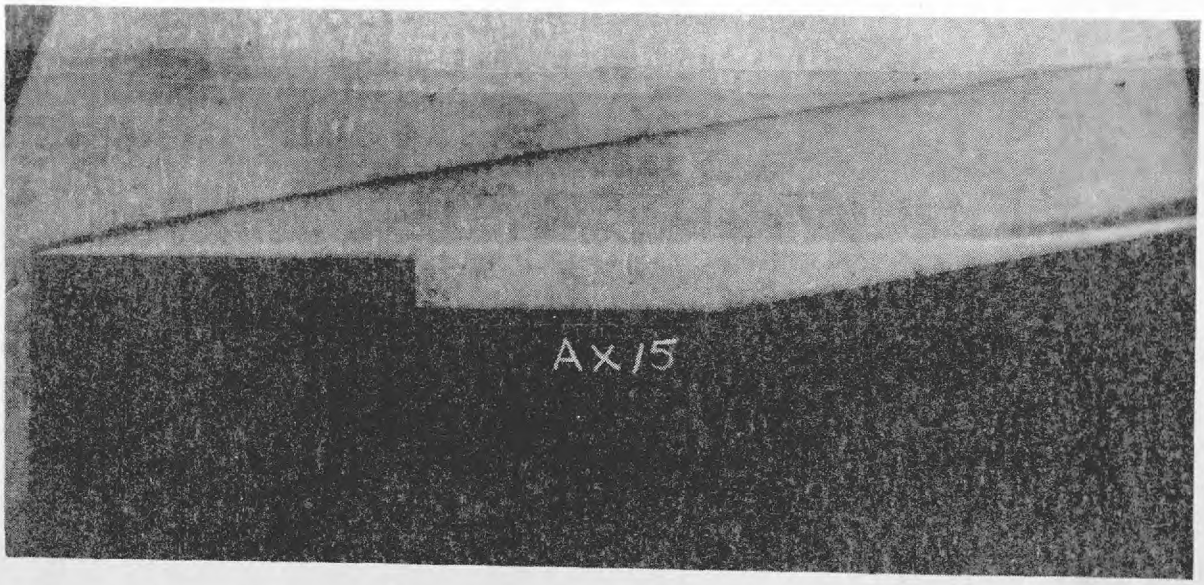

(i) Re/in. = $0{\cdot}24 \times 10^6$ $\qquad L_{sep}/x_1 = 1{\cdot}51$

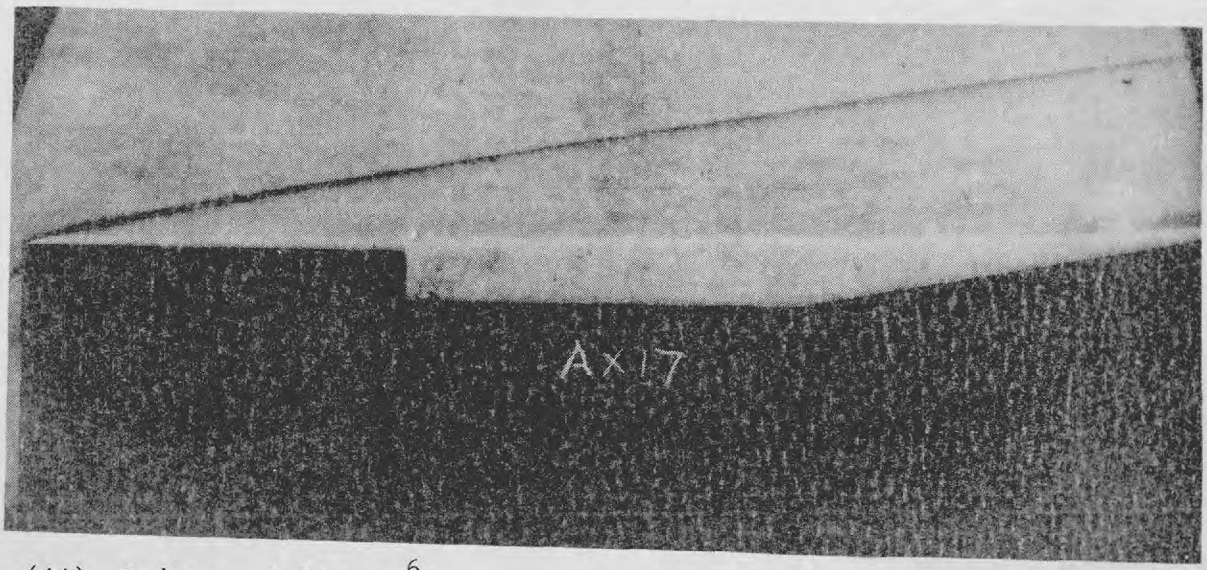

(ii) Re/in. = $0{\cdot}36 \times 10^6$ $\qquad L_{sep}/x_1 = 1{\cdot}76$

$x_1 = 2{\cdot}0$ins., $\quad \alpha_w = 10{\cdot}5^\circ$

For laminar reattachments; L_{sep}/x_1 increases with Reynolds number

FIG. 26. Photographs of a straight, laminar separation from the axisymmetric rearward-facing step model at M = 8·2.

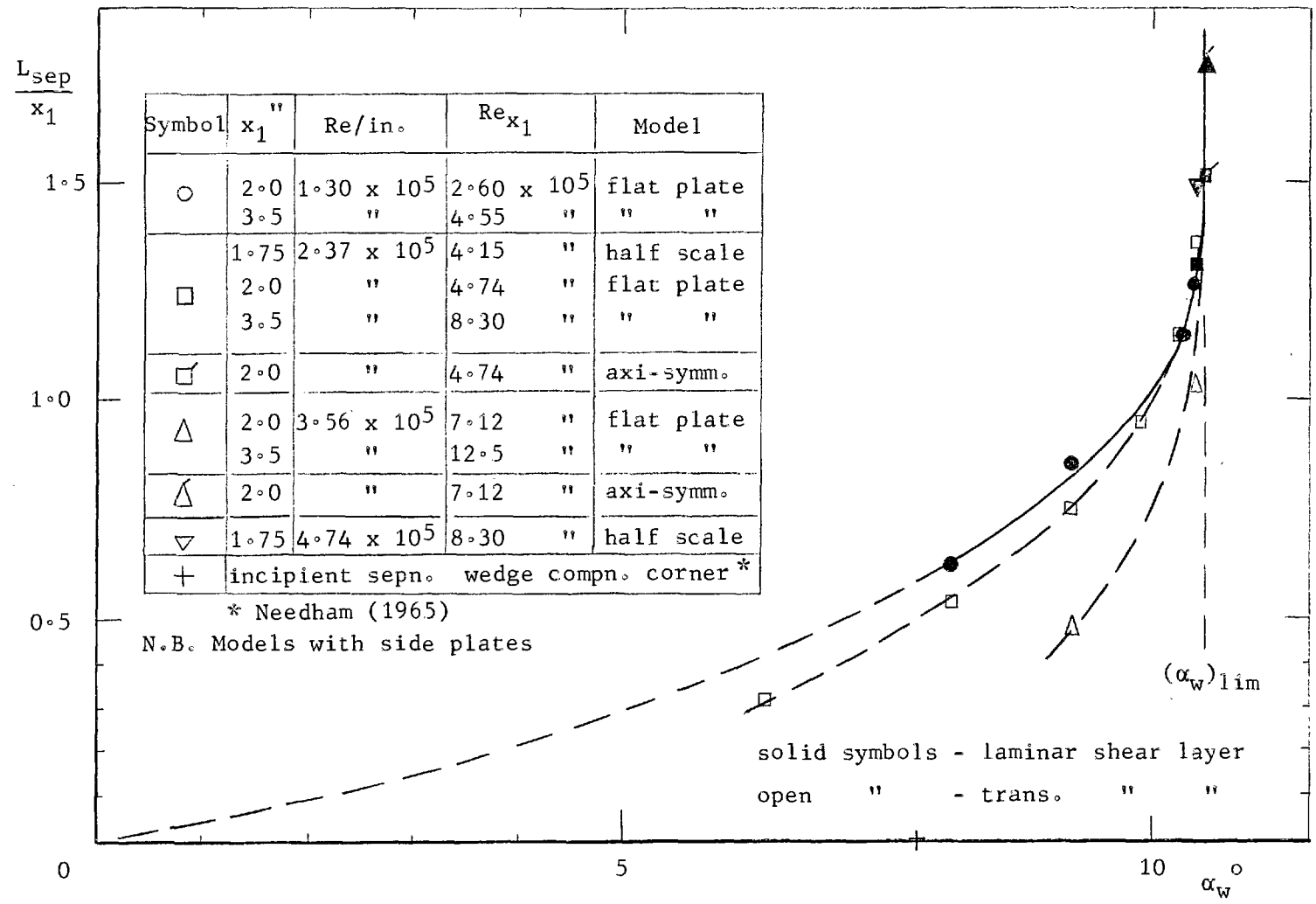

FIG· 27· Correlation of straight-separated length and reattachment angle in uniform flow at M = 8·2 ·

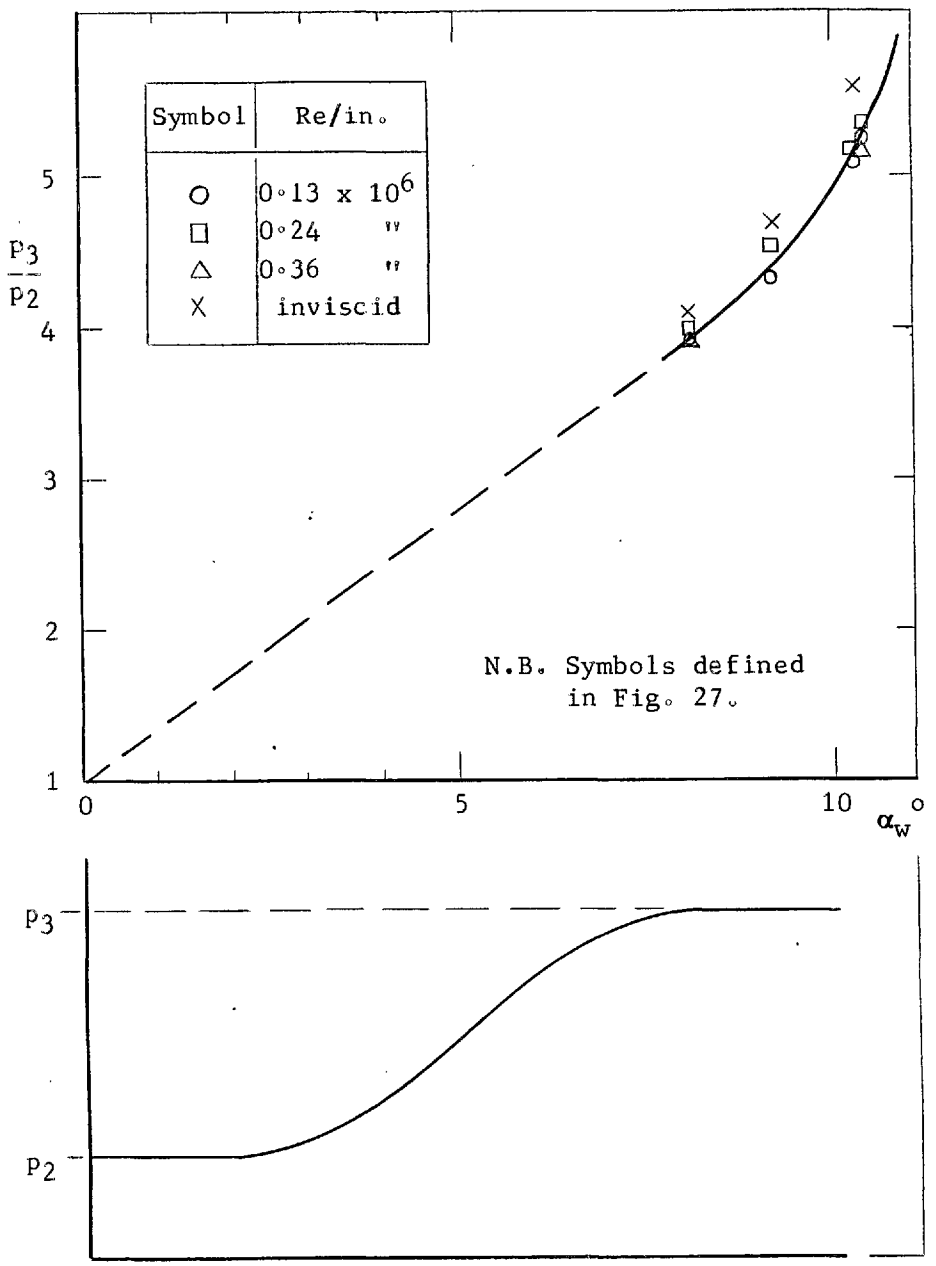

FIG. 28. Relation between reattachment peak pressure ratio and flap angle at M = 8·2 .

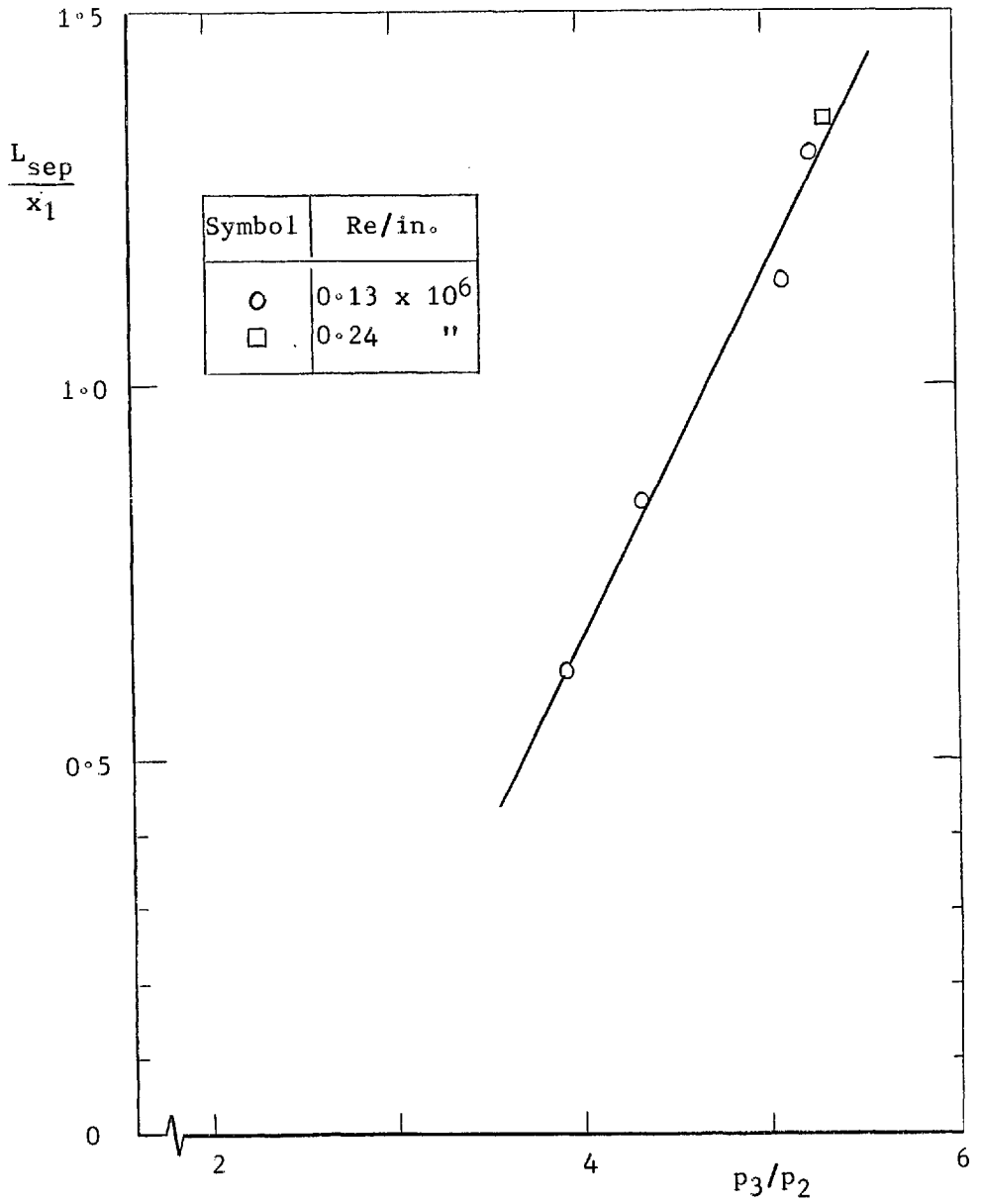

FIG. 29. Variation of laminar separated length with reattachment pressure rise for M = 8.2 .

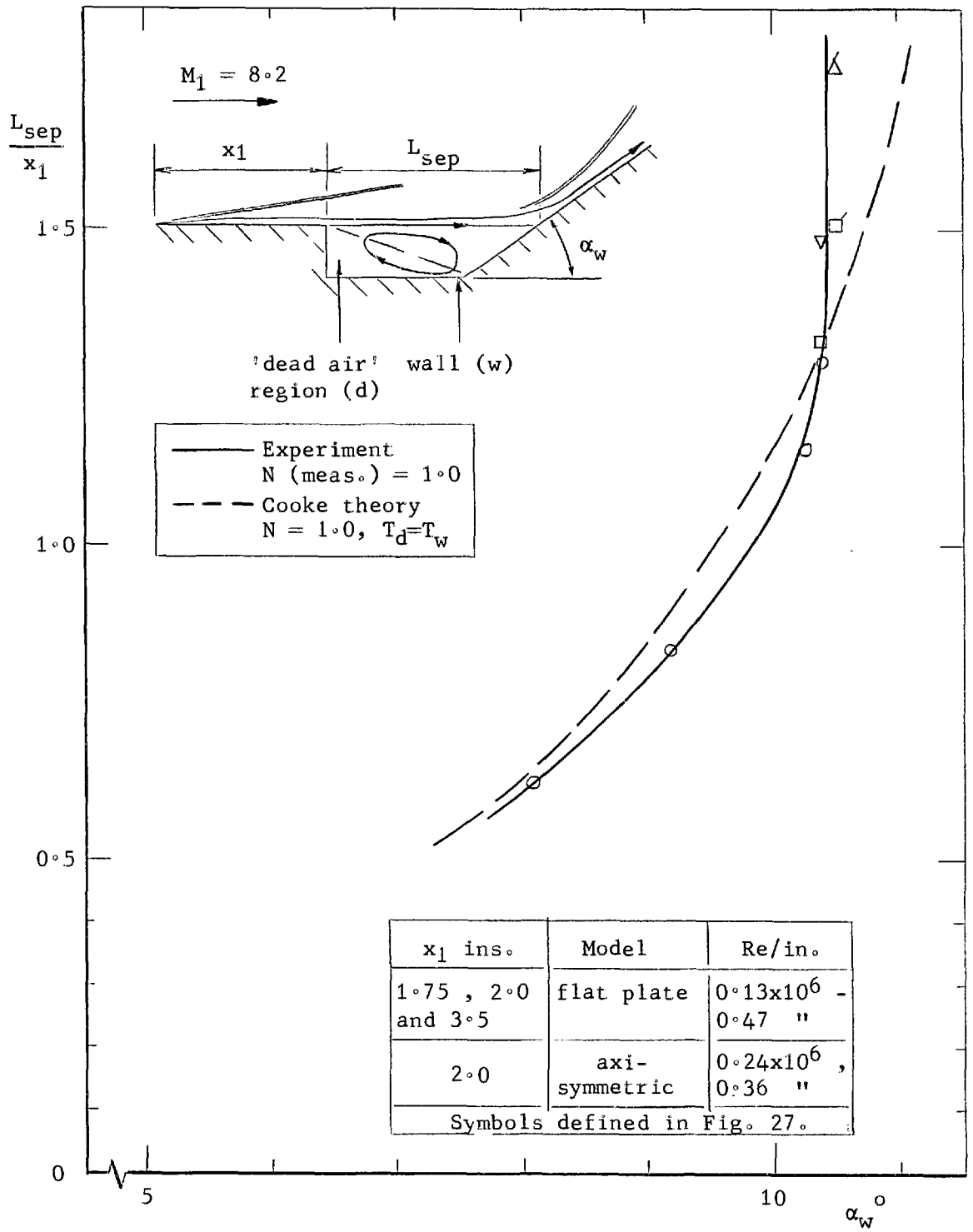

x_1 ins.	Model	Re/in.
1.75 , 2.0 and 3.5	flat plate	0.13×10^6 - 0.47×10^6 "
2.0	axi-symmetric	0.24×10^6 , 0.36×10^6 "
Symbols defined in Fig. 27.		

FIG. 30. Correlation of laminar separated length in terms of reattachment angle and comparison with theory.

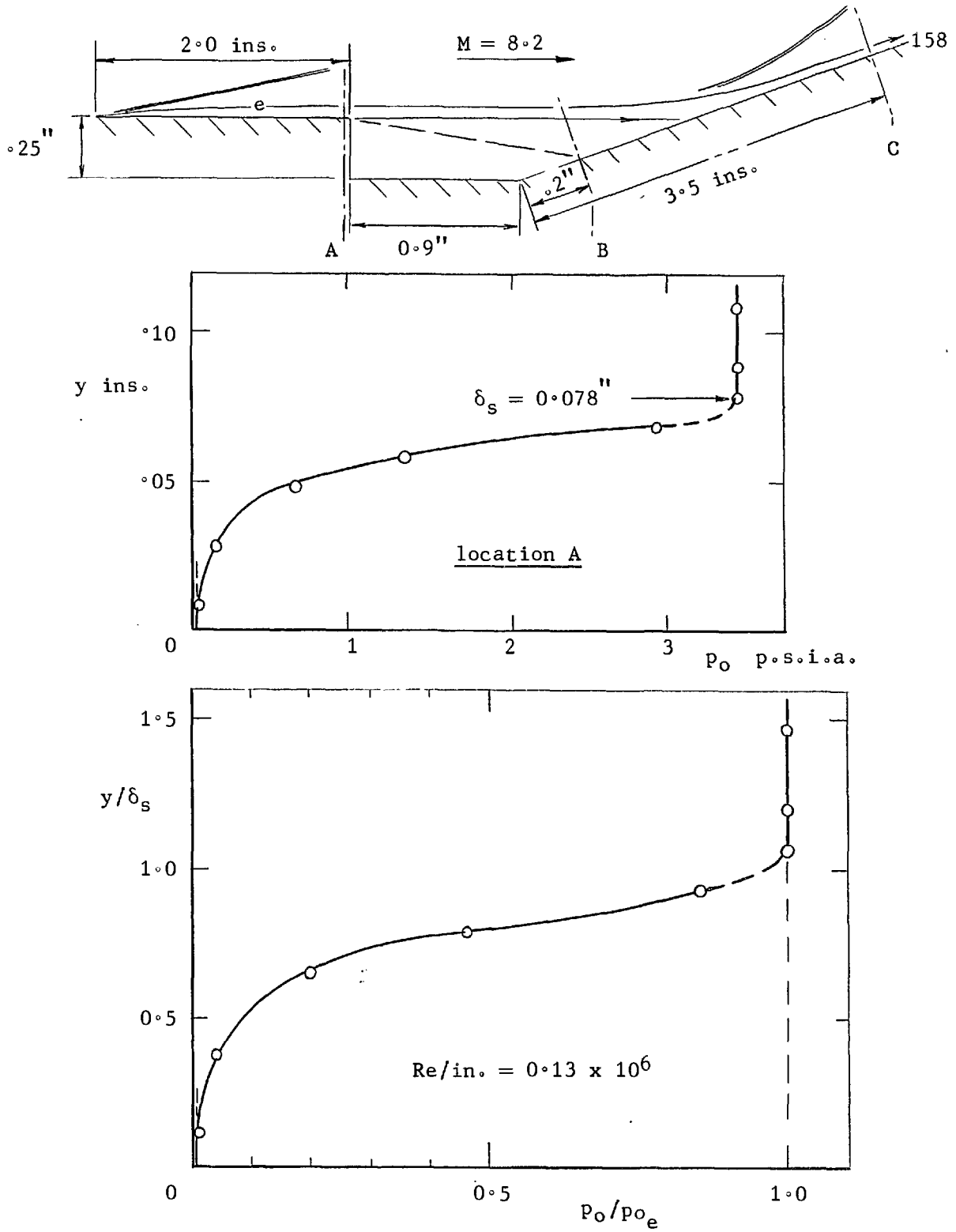

(a) pitot pressure profile of the attached layer

FIG. 31. Pitot pressure and Mach number profiles in the attached and separated regions of laminar flow.

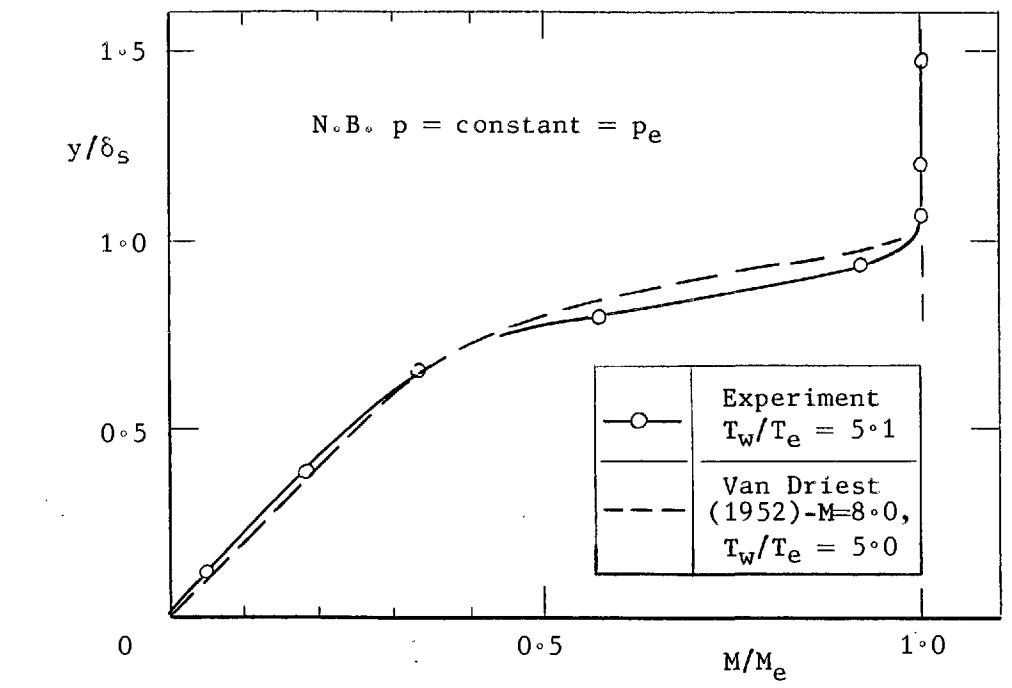

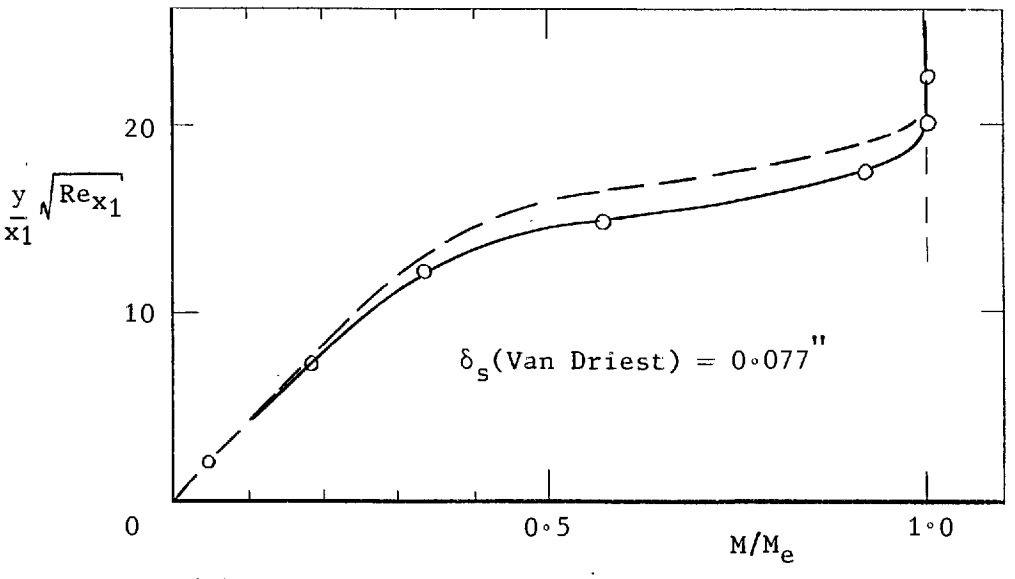

(a) concluded

Mach number profiles of the attached layer

FIG. 31. continued.

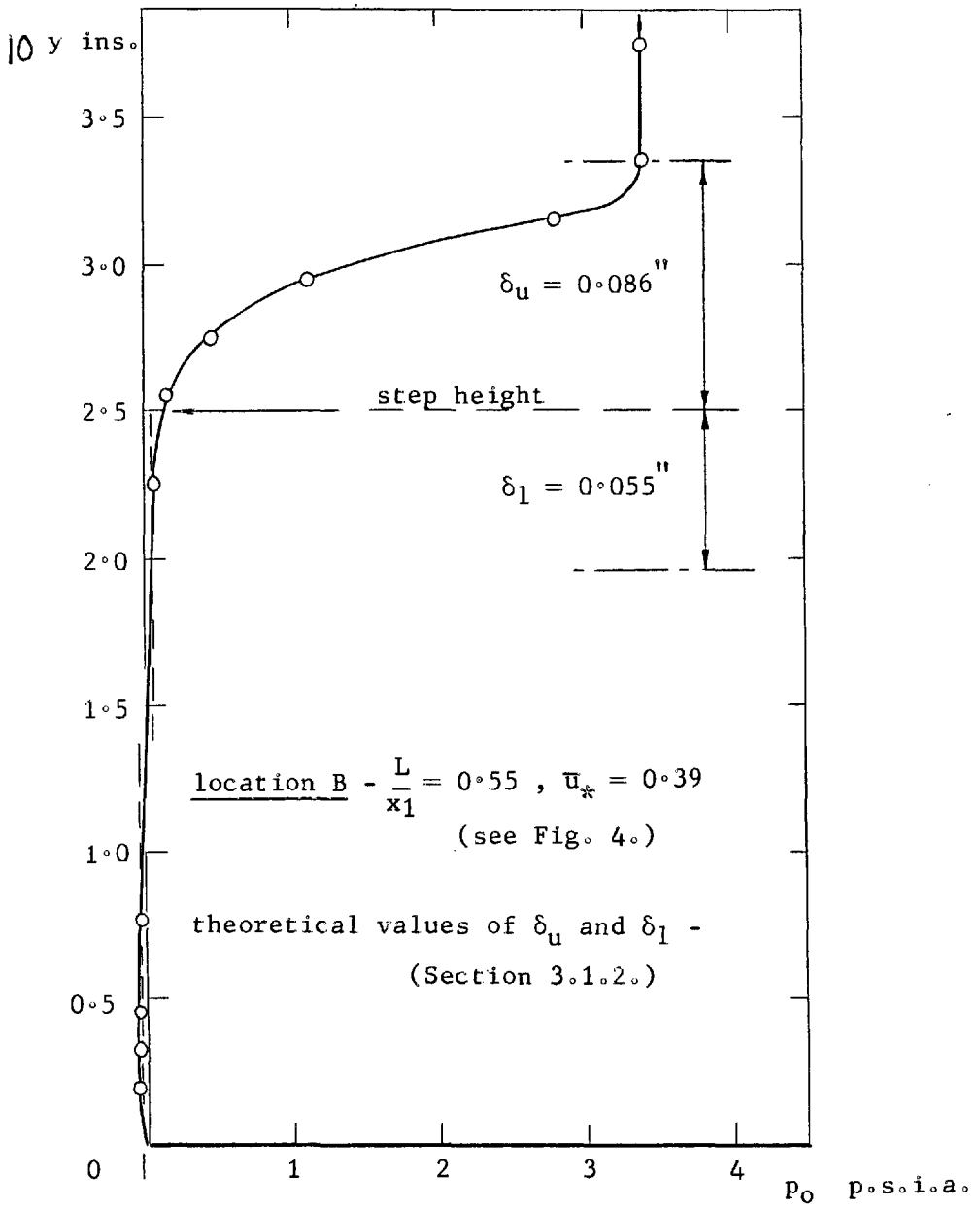

(b) pitot pressure profile of the separated layer

FIG. 31. continued.

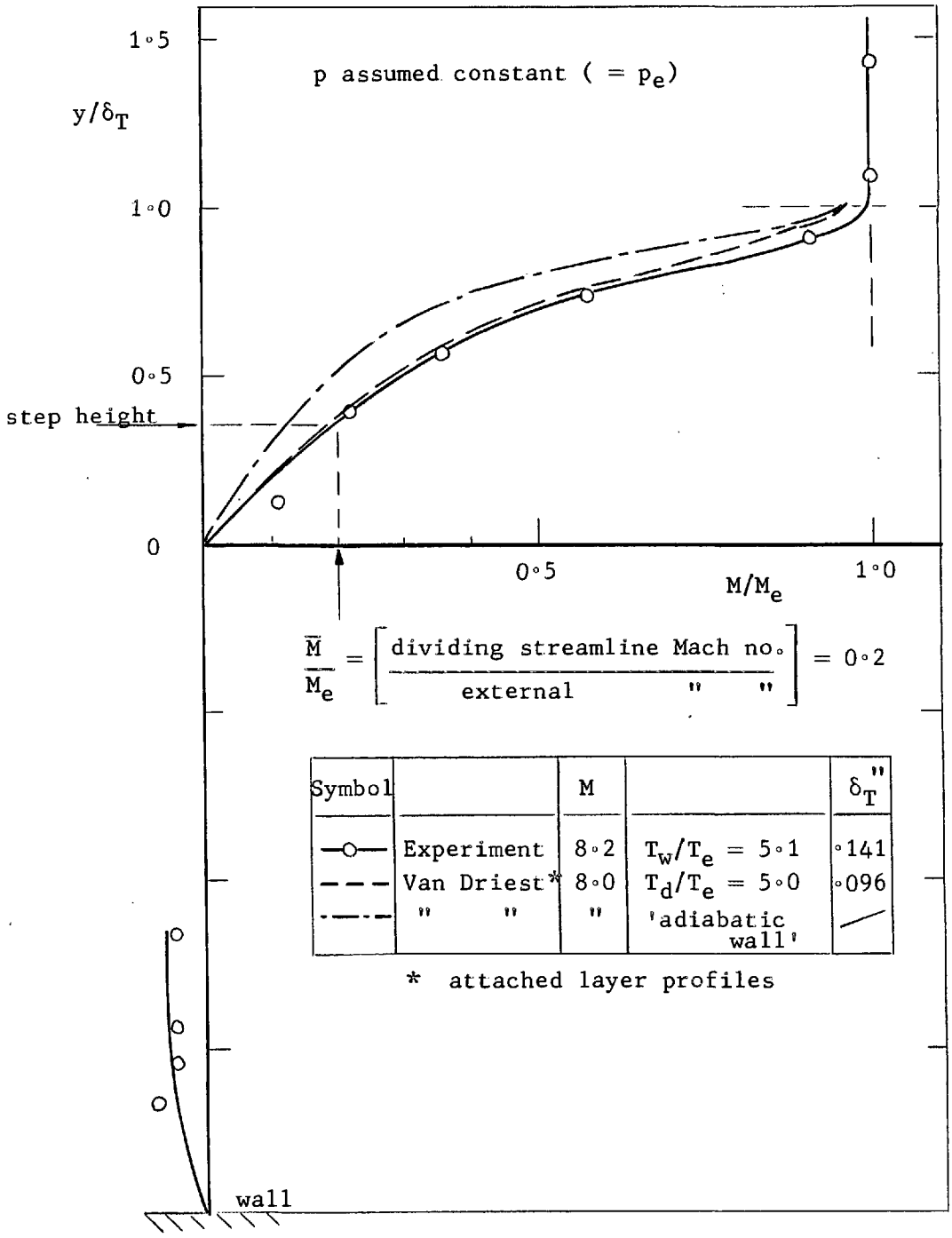

(b) concluded
Mach number profiles of the separated layer

FIG. 31. continued.

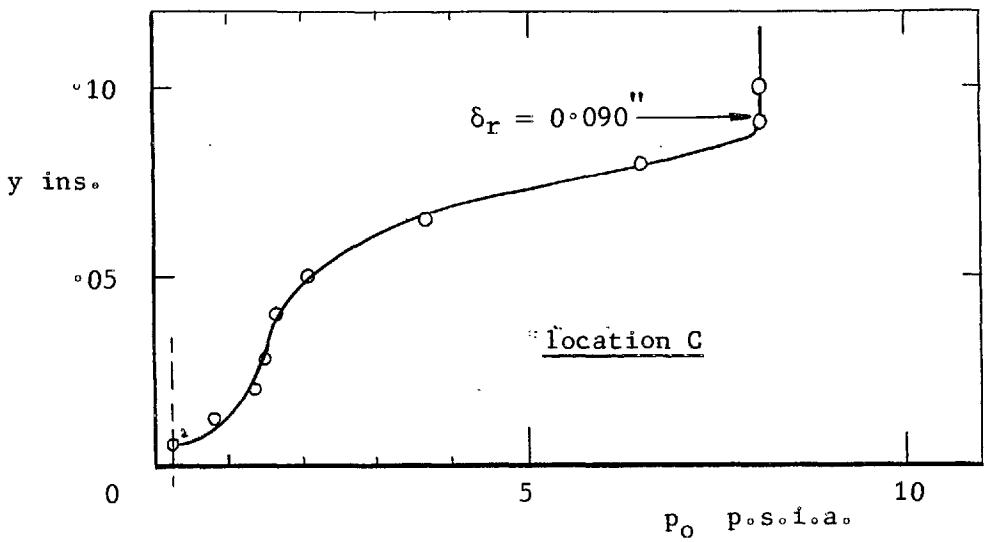

(i) pitot pressure

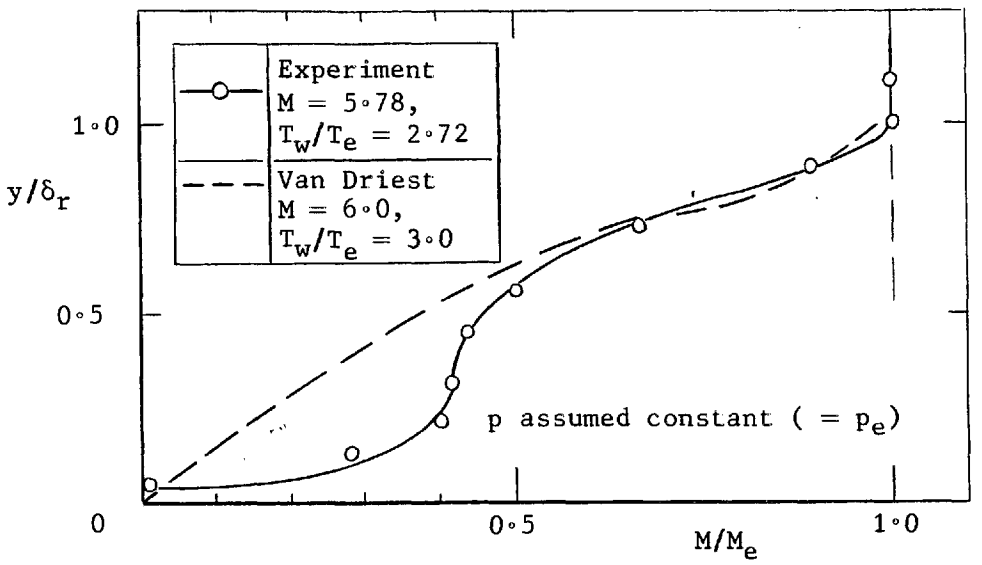

(ii) Mach number

(c) profiles of the reattached layer

FIG. 31. concluded.

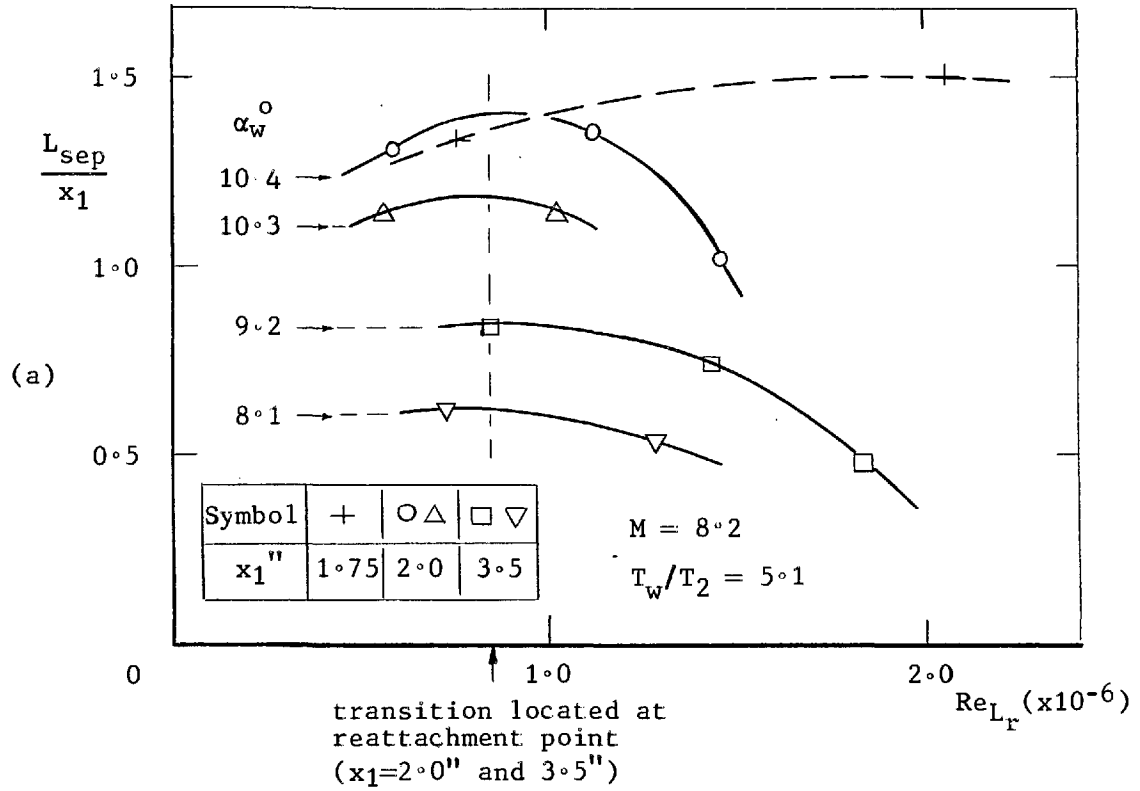

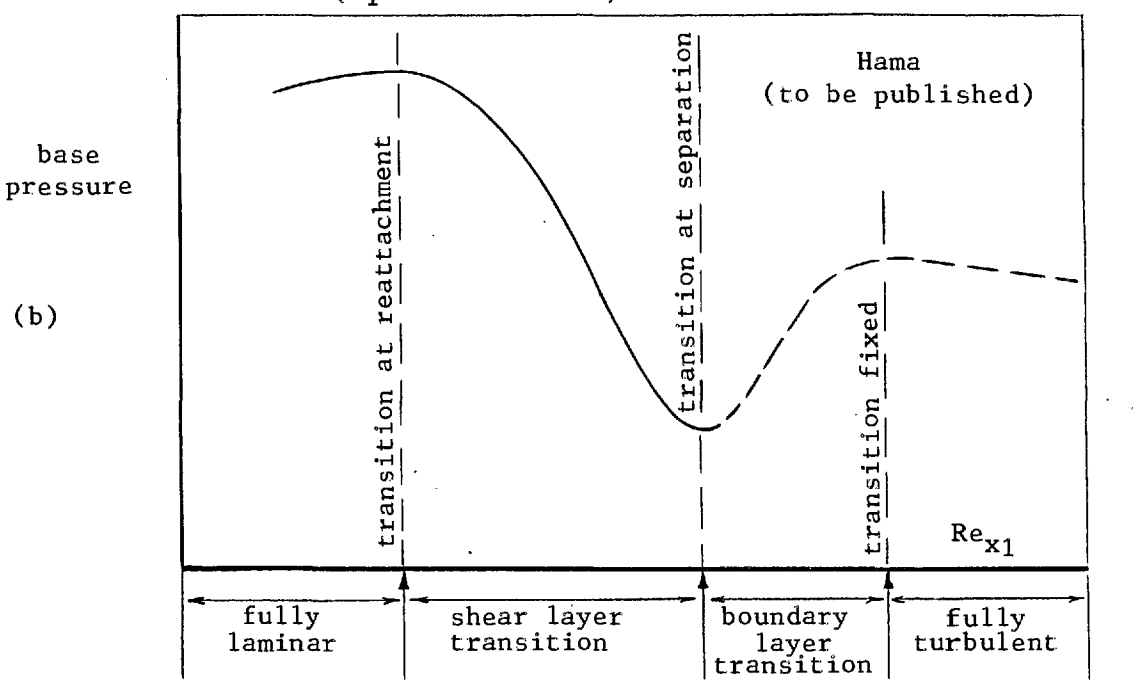

FIG. 32. Variation of base properties in relation to transition location.

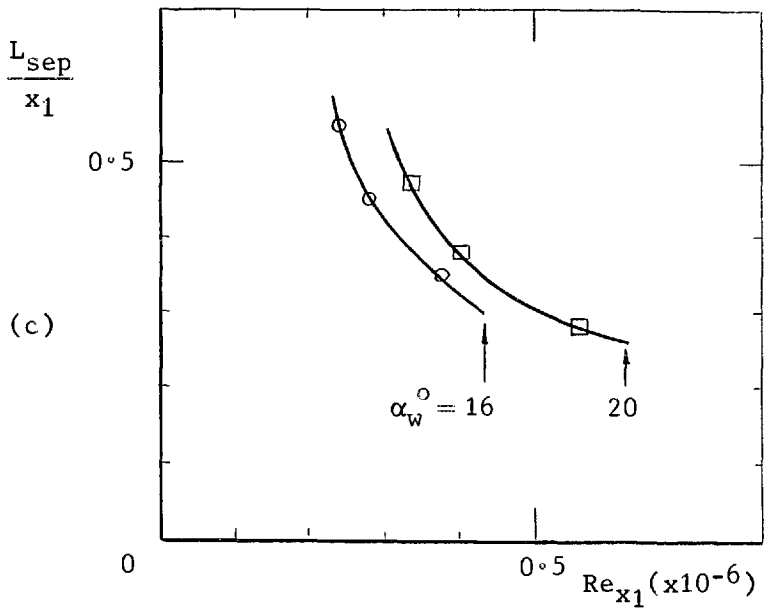

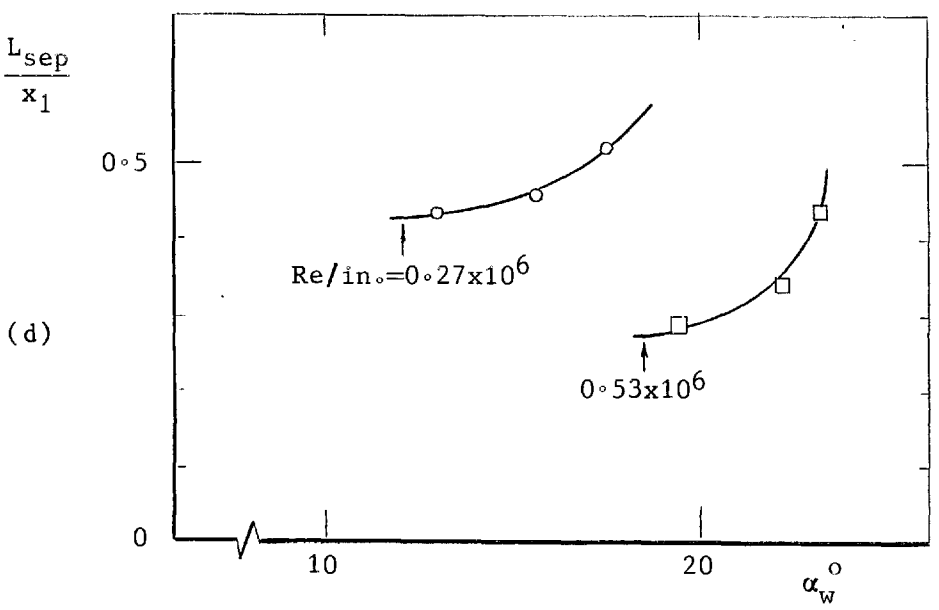

Hurlburt(1966) , M = 3.0

FIG. 32. concluded.

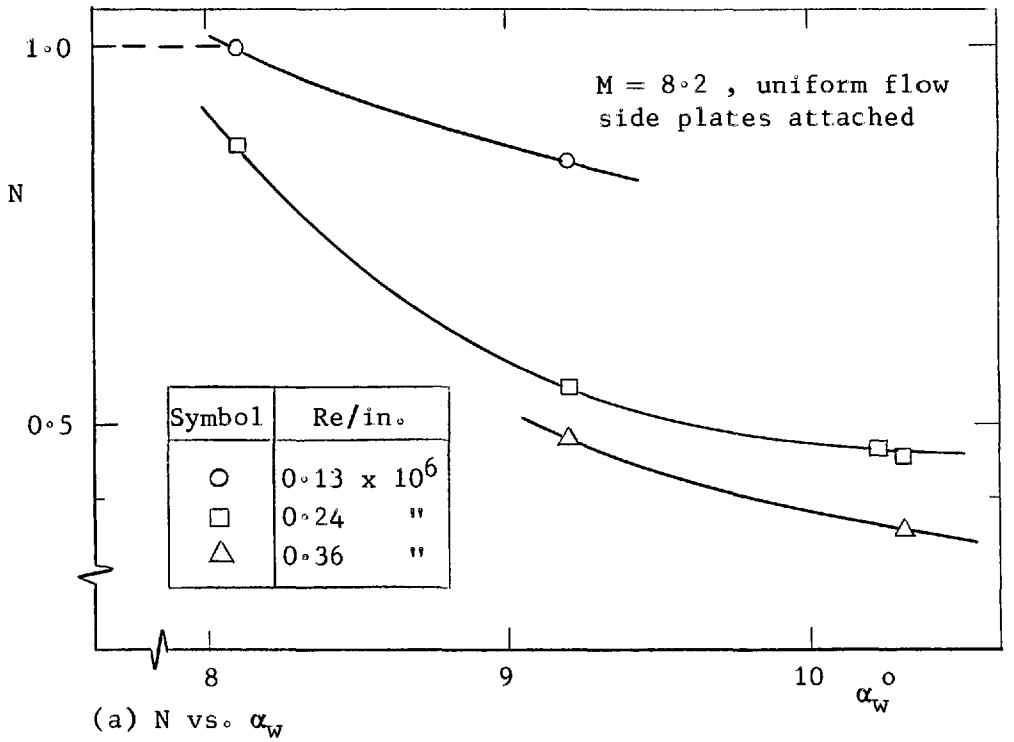

(a) N vs. α_w

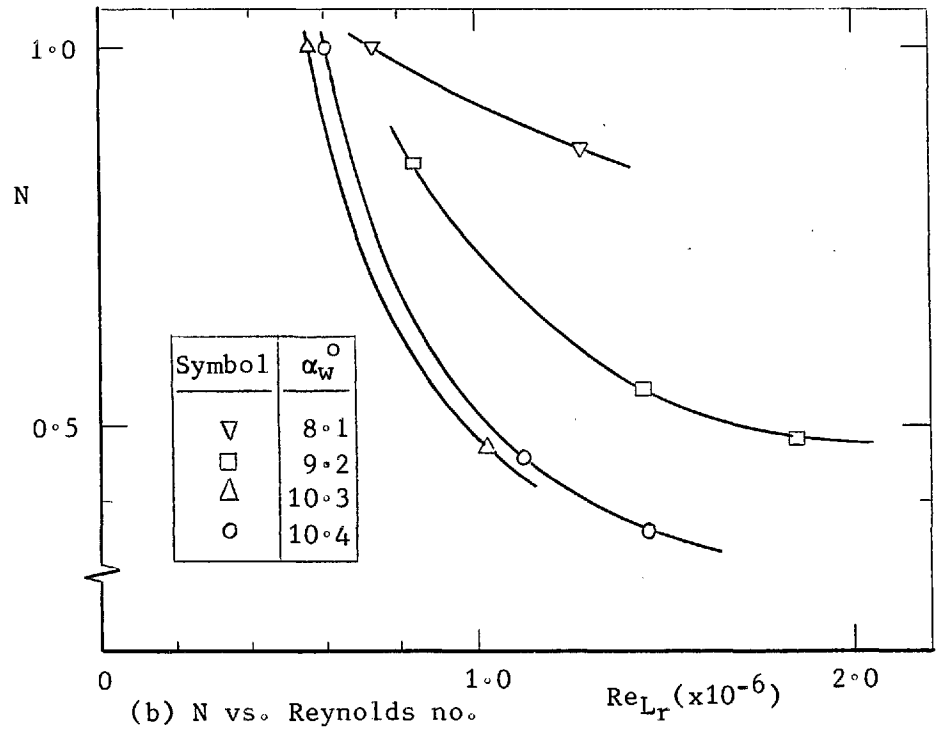

(b) N vs. Reynolds no.

FIG. 33. Reattachment pressure rise parameter as a function of flap angle and Reynolds number.

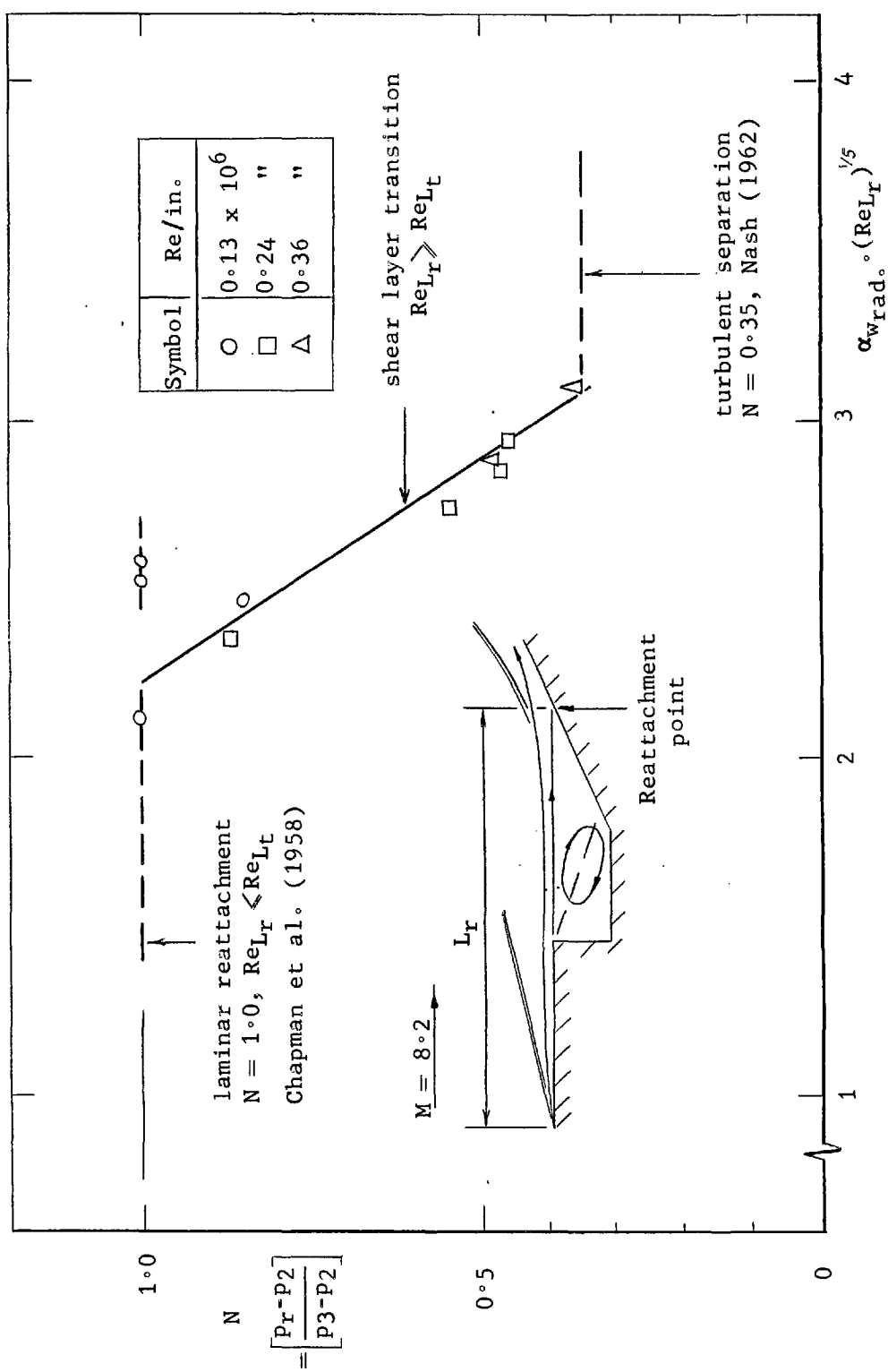

FIG. 34. Correlation of the reattachment parameter in the laminar, transitional and turbulent regimes at M = 8.2.

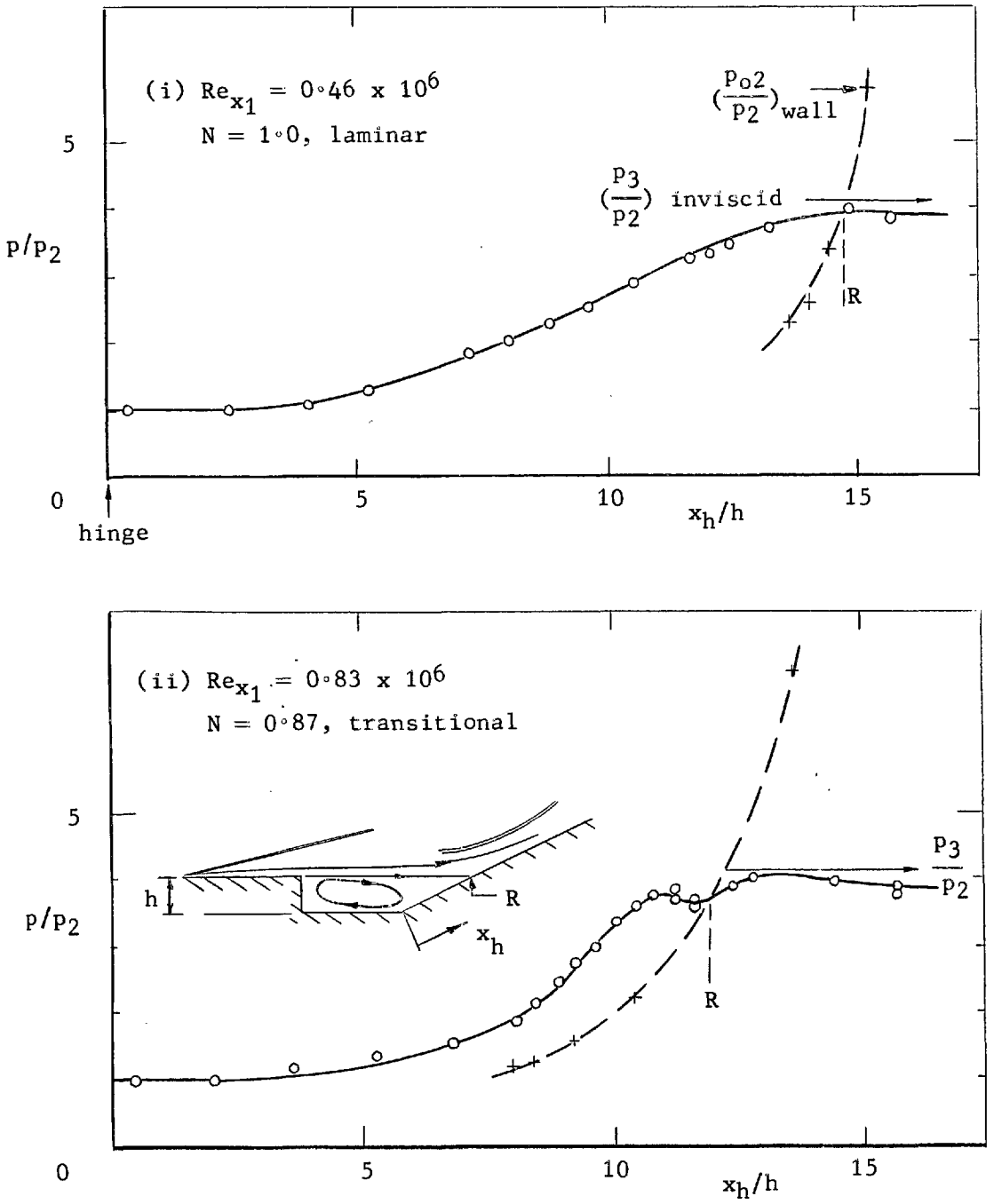

(a) $\alpha_w = 8{\cdot}1^{\circ}$, $x_1 = 3{\cdot}5''$, $T_w/T_2 = 5{\cdot}1$

FIG. 35. Pressure distributions in the separated region and location of the reattachment point at M = 8·2.

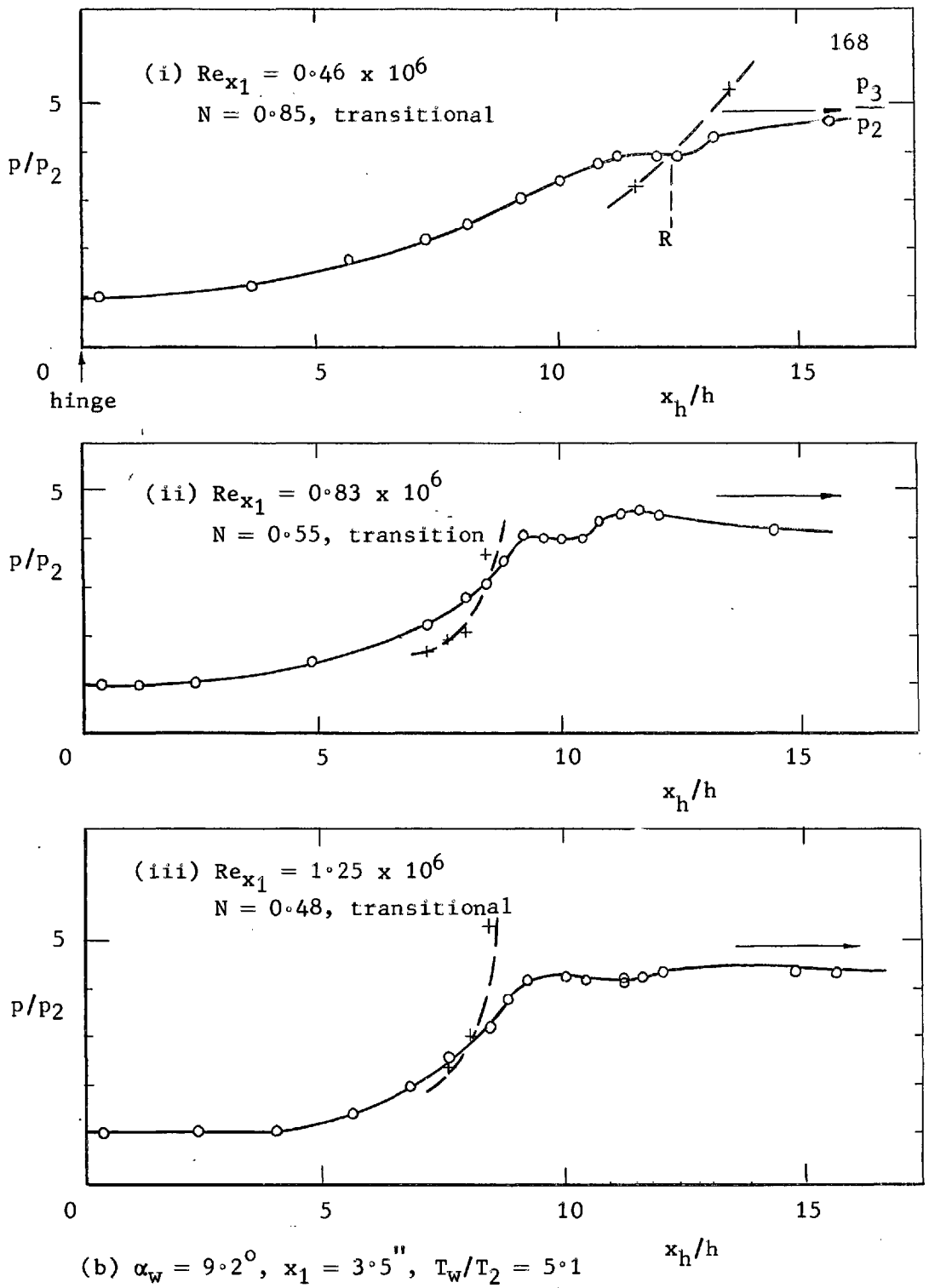

(b) $\alpha_w = 9·2^o$, $x_1 = 3·5''$, $T_w/T_2 = 5·1$

FIG. 35. continued.

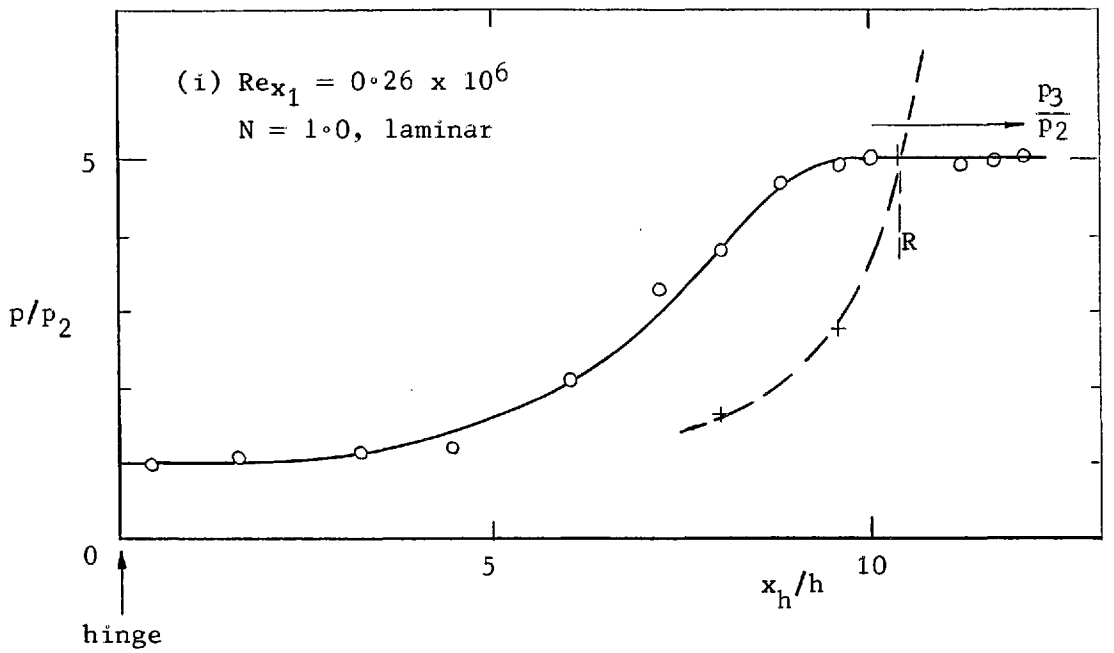

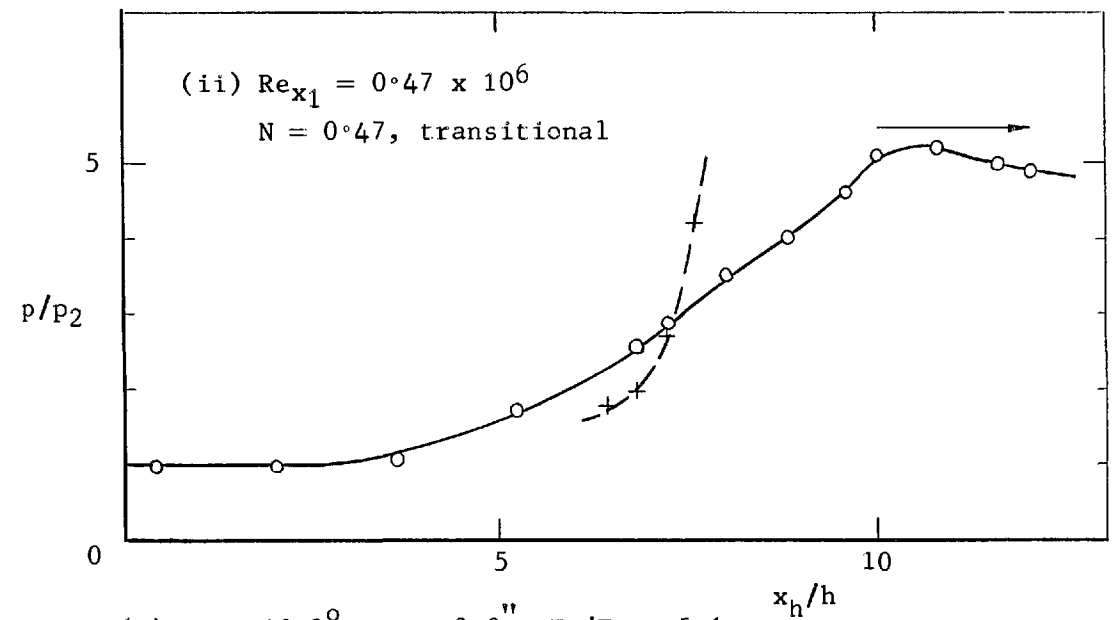

(c) $\alpha_w = 10{\cdot}3^{\circ}$, $x_1 = 2{\cdot}0''$, $T_w/T_2 = 5{\cdot}1$

FIG. 35. continued.

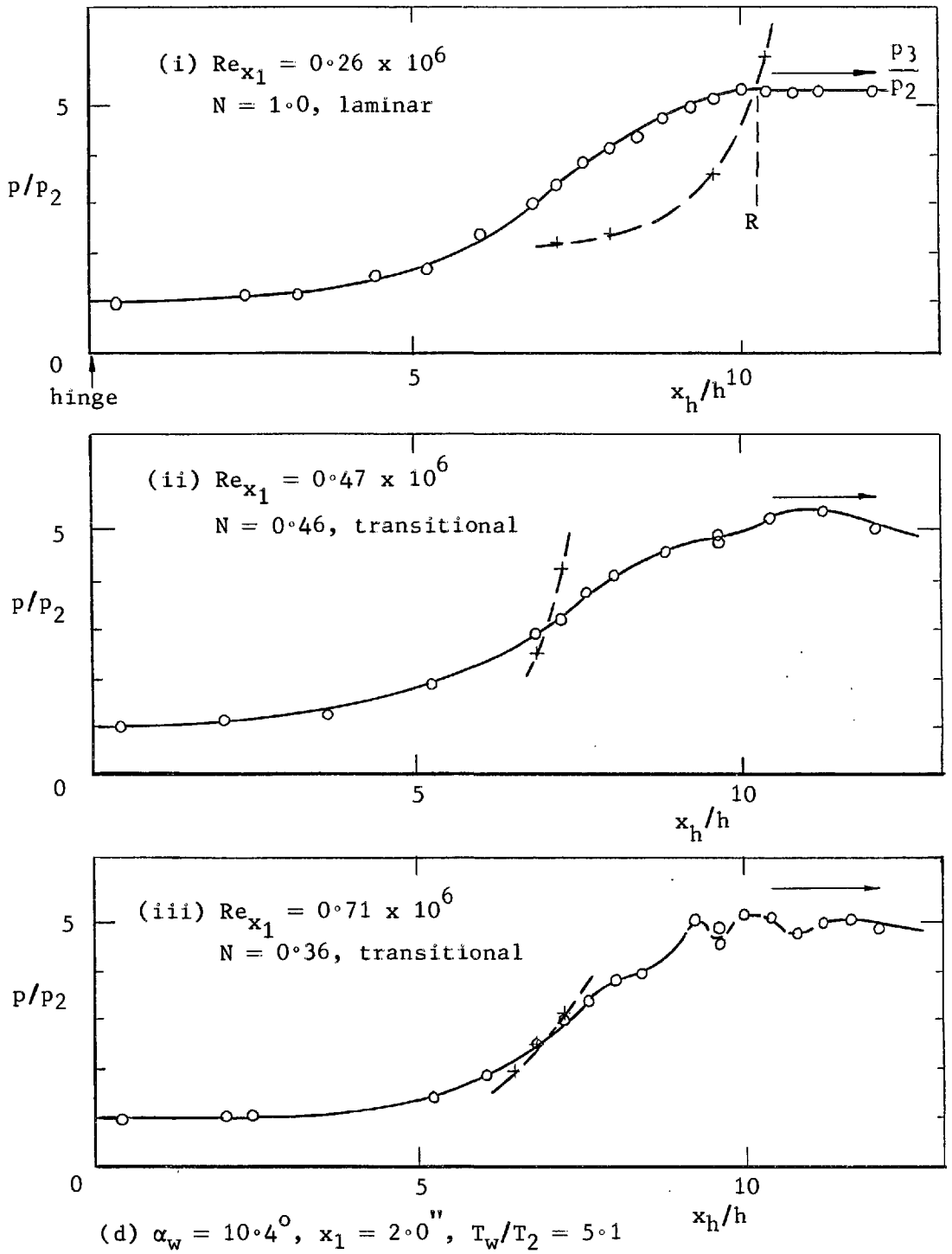

(d) $\alpha_w = 10{\cdot}4^\circ$, $x_1 = 2{\cdot}0''$, $T_w/T_2 = 5{\cdot}1$

FIG. 35. concluded.

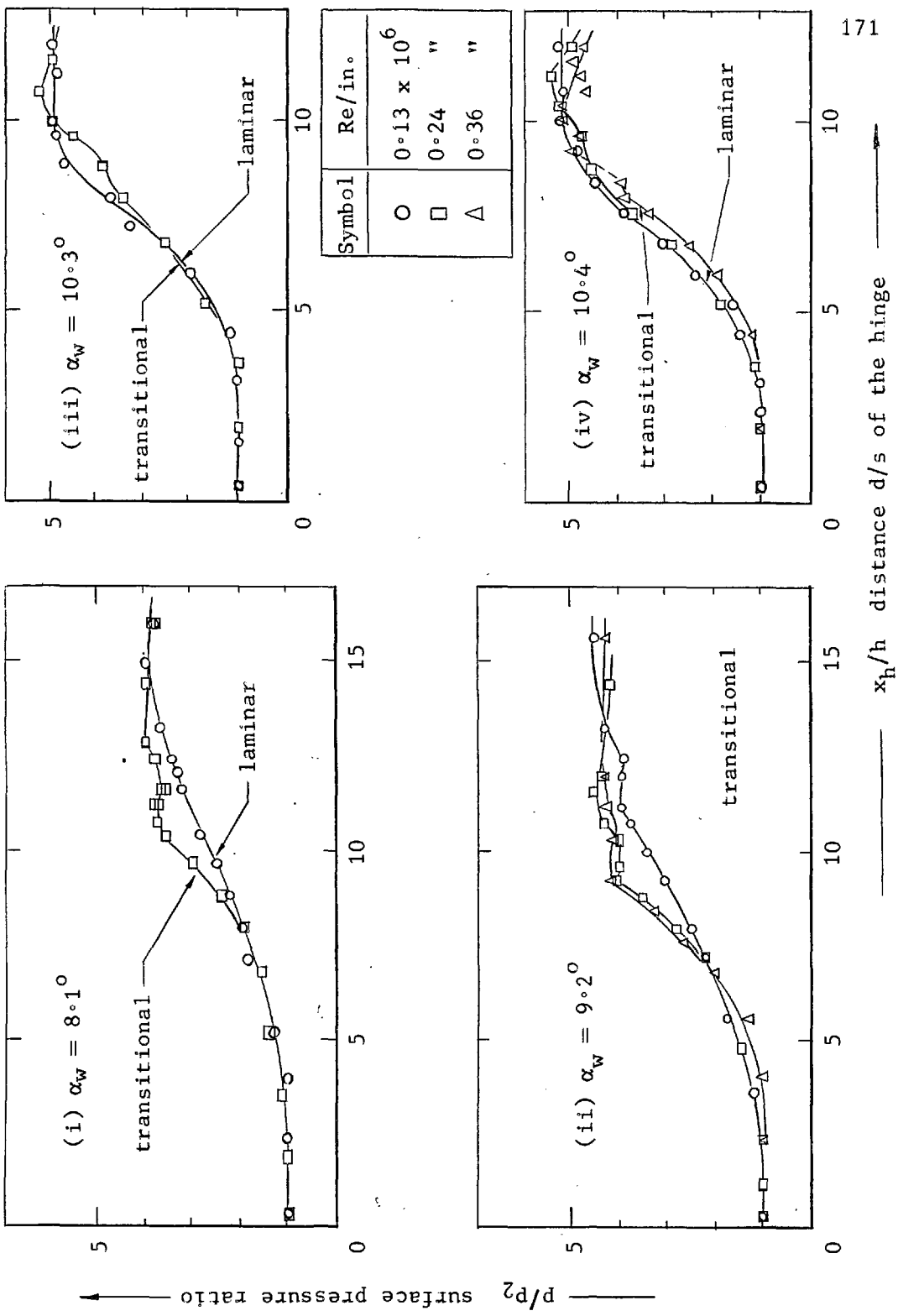

FIG. 36. Laminar and transitional pressure distributions for various values of Reynolds number at M = 8·2.

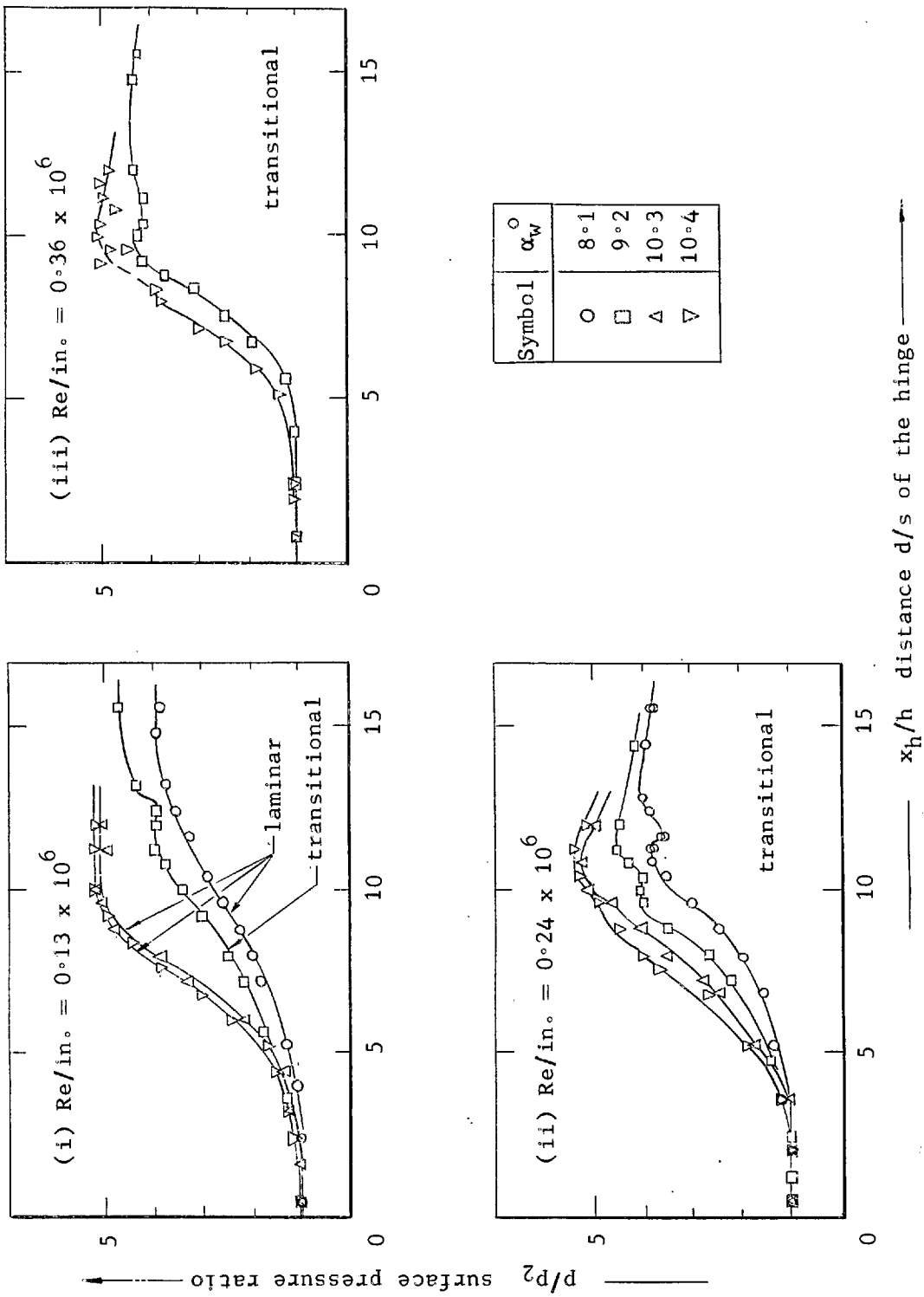

FIG. 37. The effect of flap angle on the pressure distributions in the step-separated flow at M = 8·2.

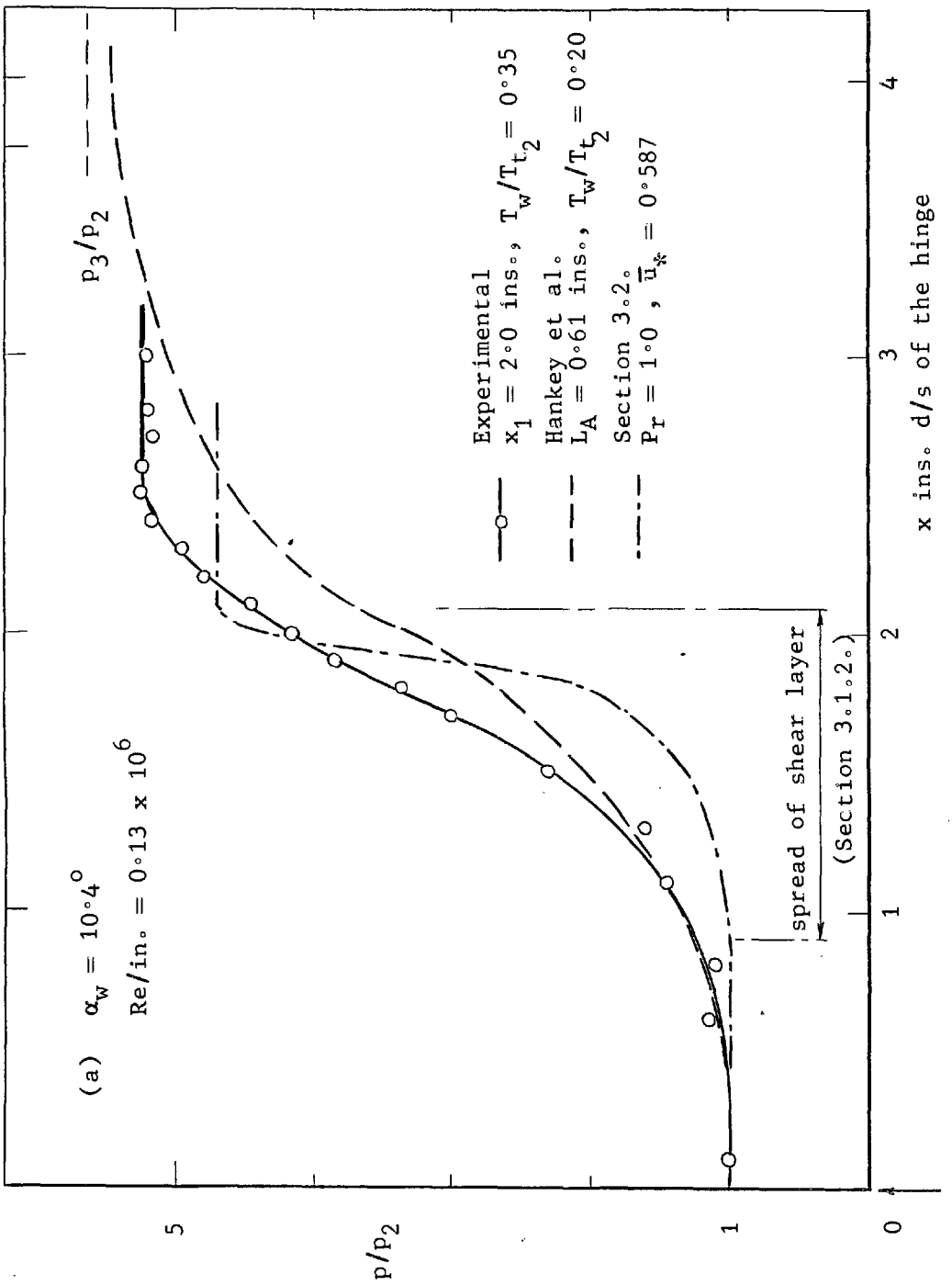

FIG. 38. Laminar pressure distribution of the straight-separating flow - comparison of experiment with theory at M = 8·2.

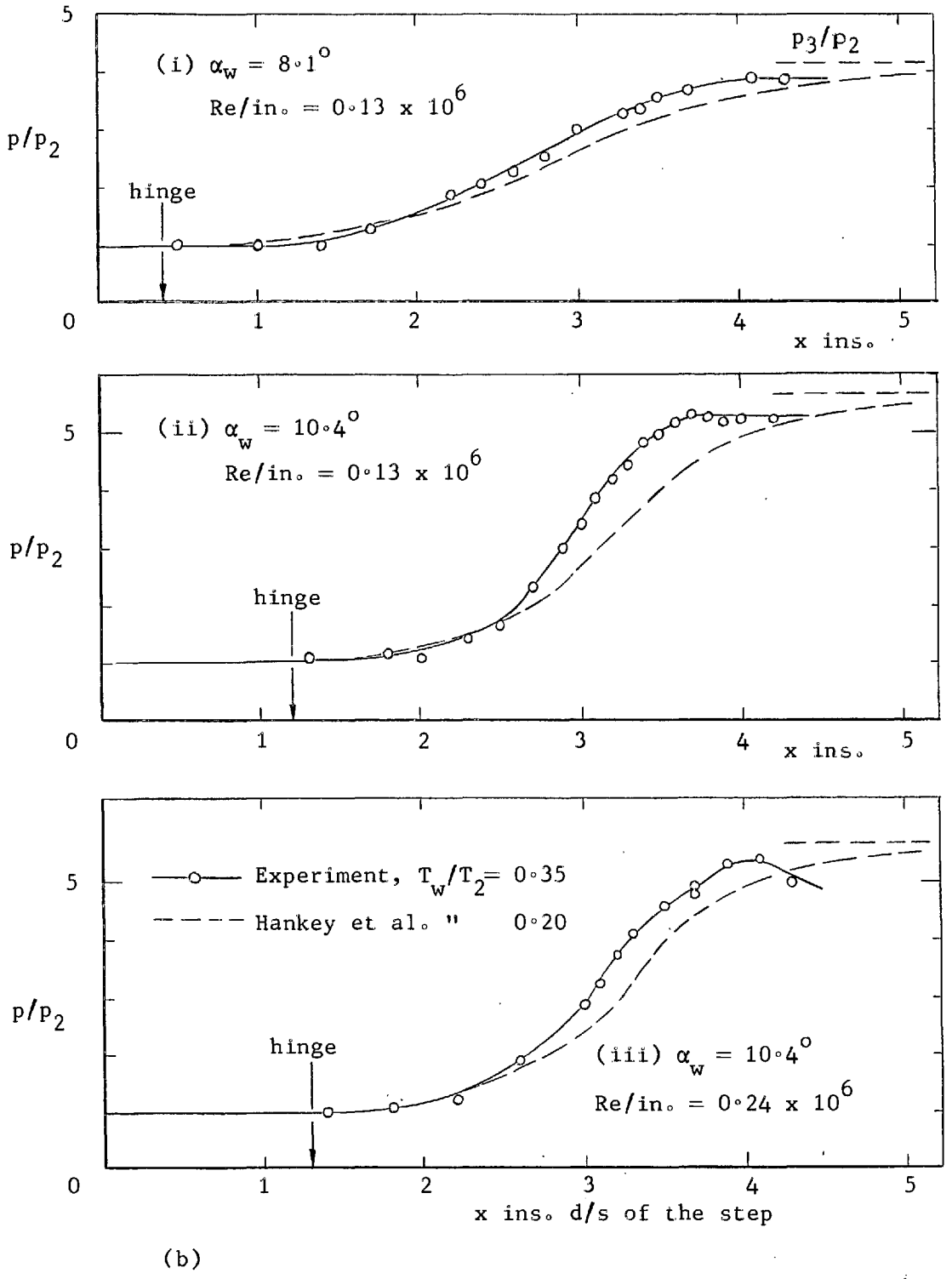

(b)

FIG. 38. concluded.

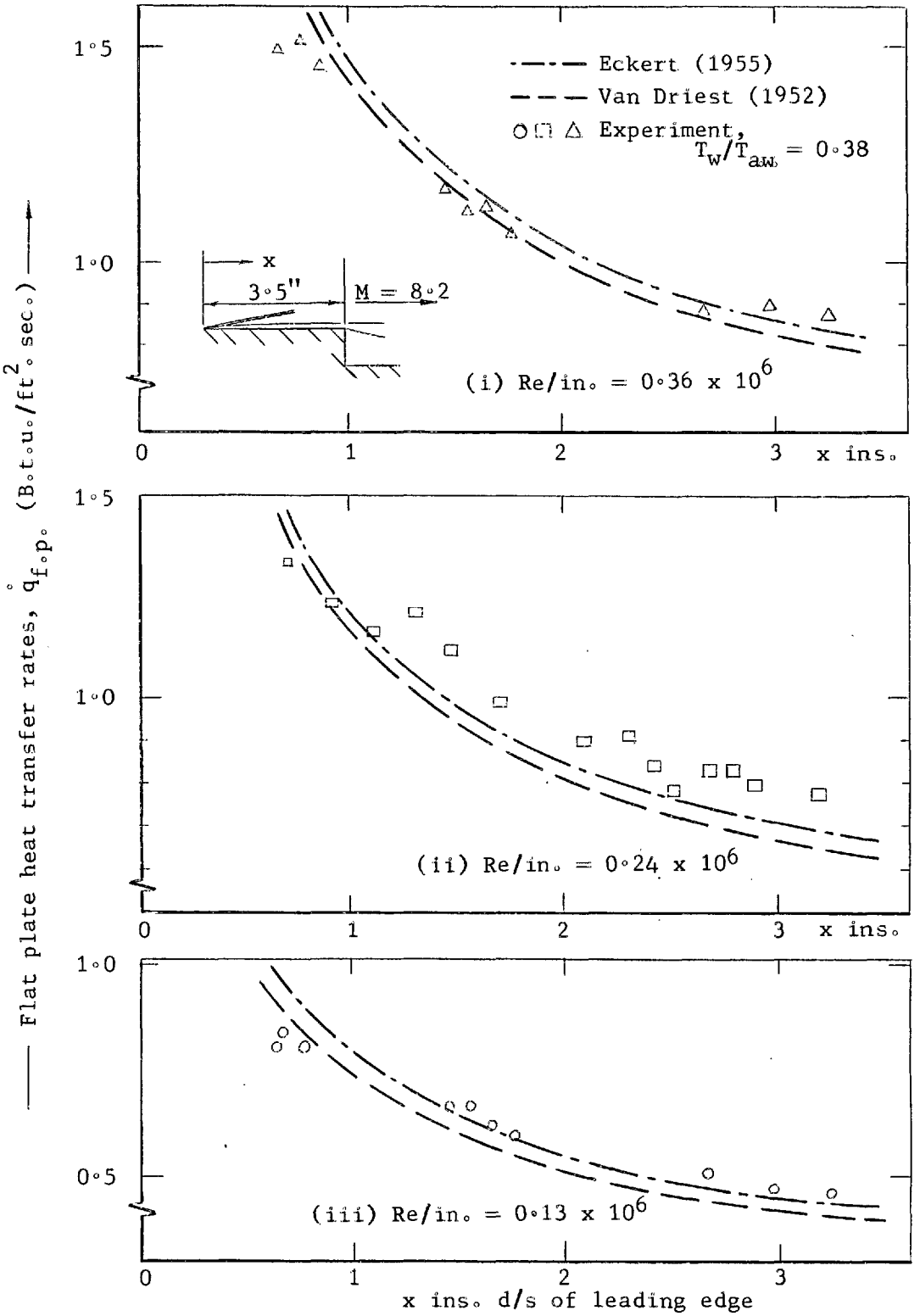

FIG· 39· Flat plate heat transfer distributions in laminar flow and comparison with theory·

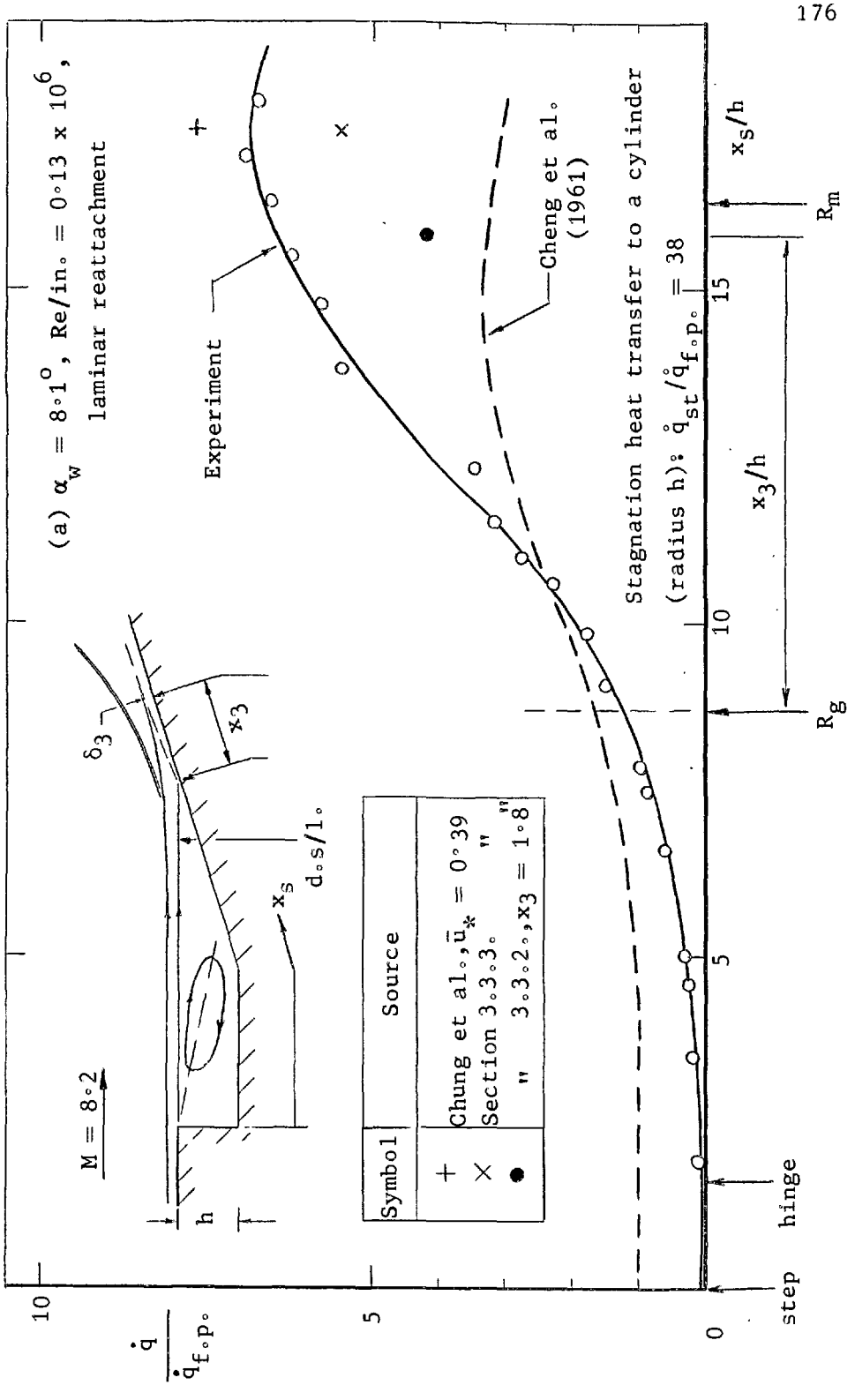

FIG. 40. Reattachment heat transfer distributions for various unit Reynolds numbers and comparison with theory.

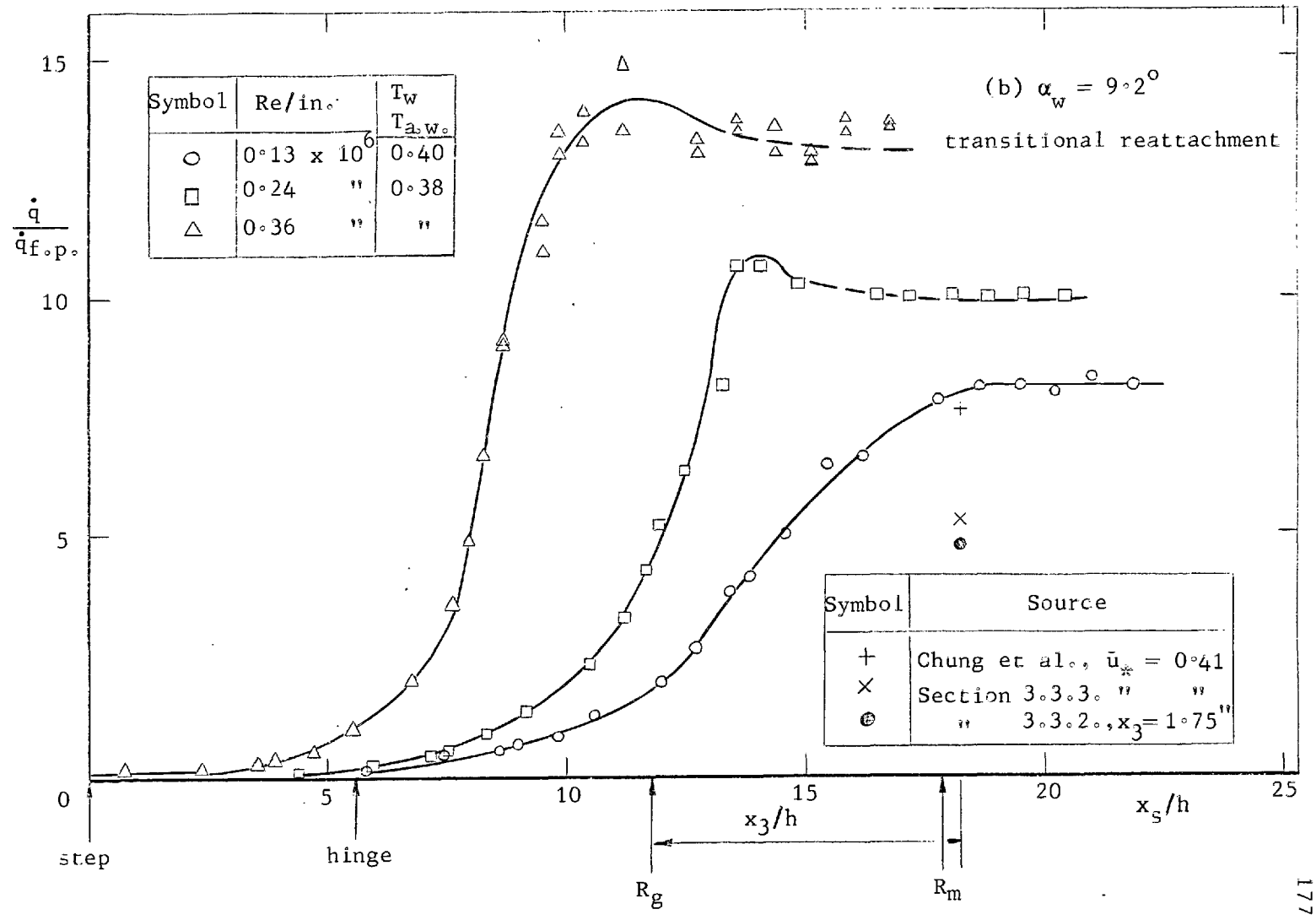

FIG. 40. continued.

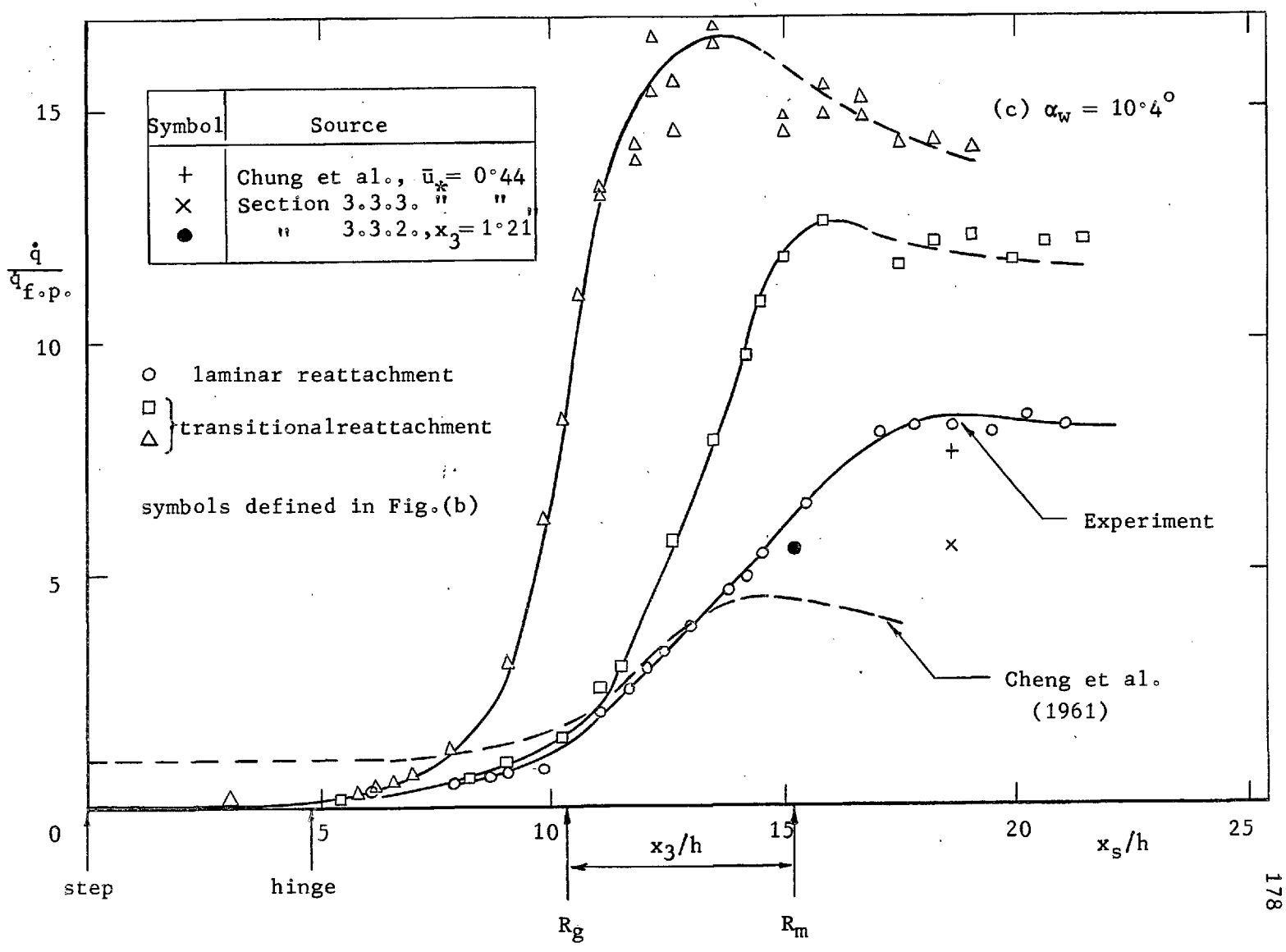

FIG. 40. concluded.

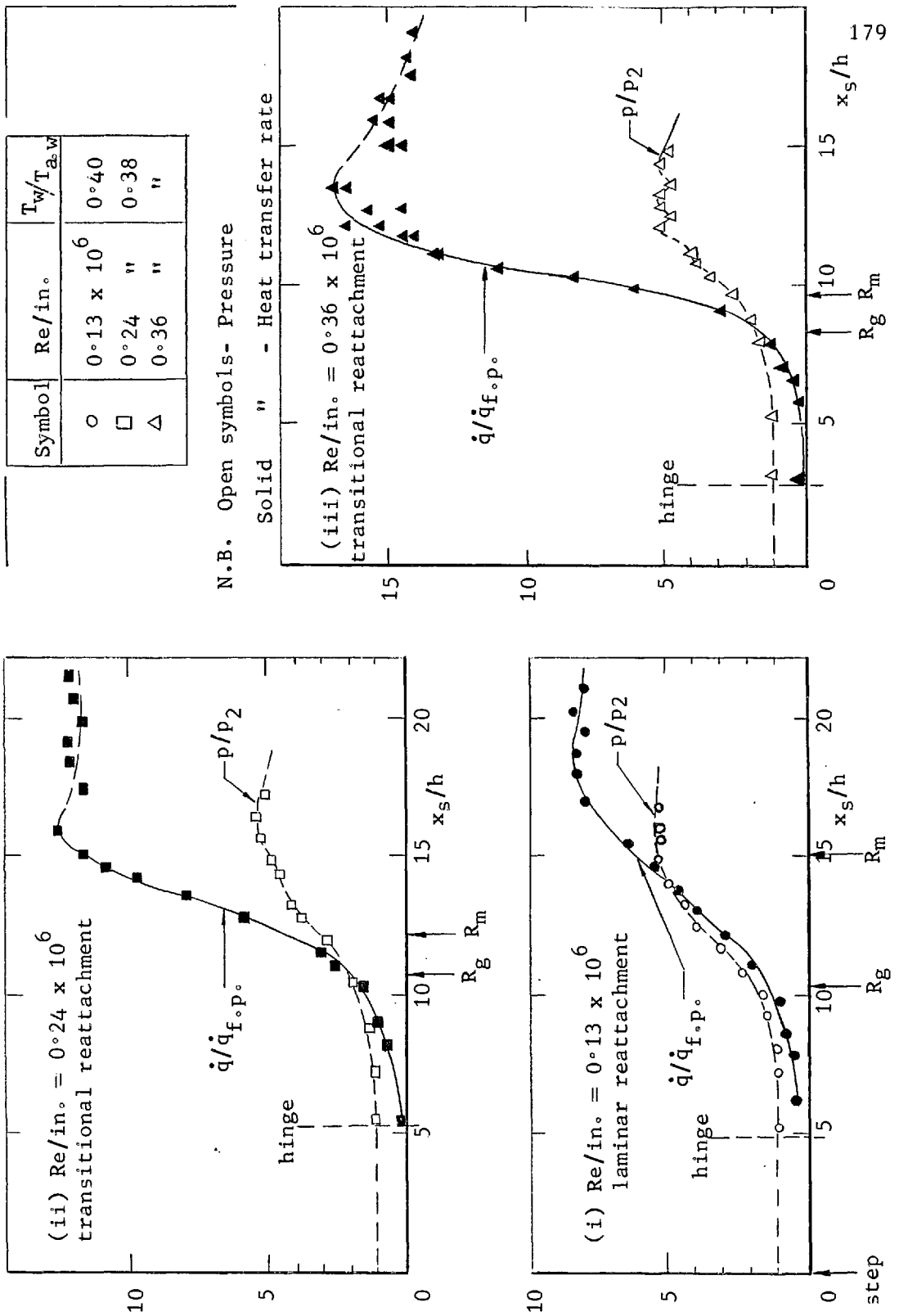

FIG. 41. Comparison of pressure and heat transfer distributions for laminar and transitional reattachments at $\alpha_w = 10{\cdot}4^\circ$.

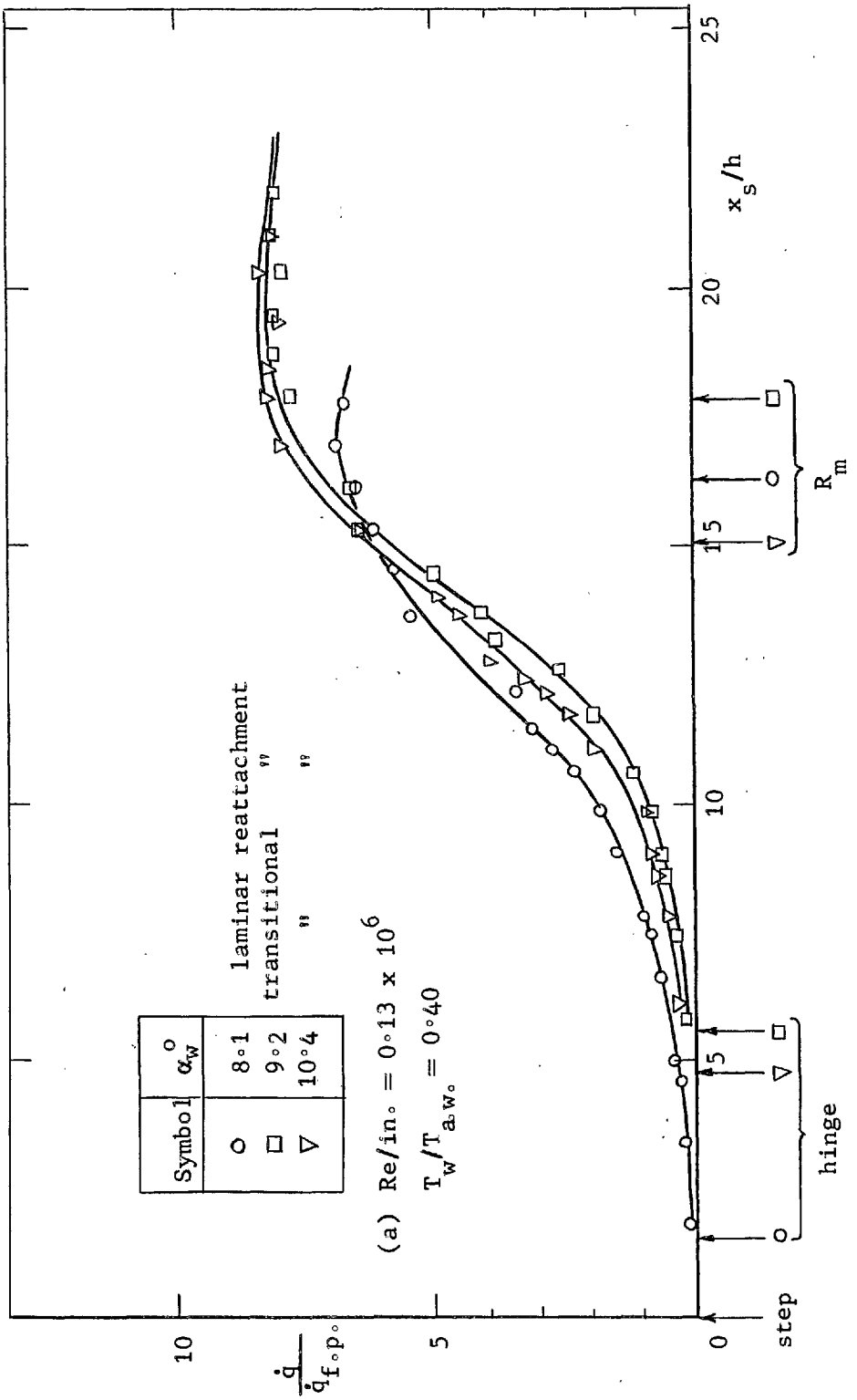

FIG. 42. Effect of flap angle on the reattachment heat transfer distribution at M = 8·2.

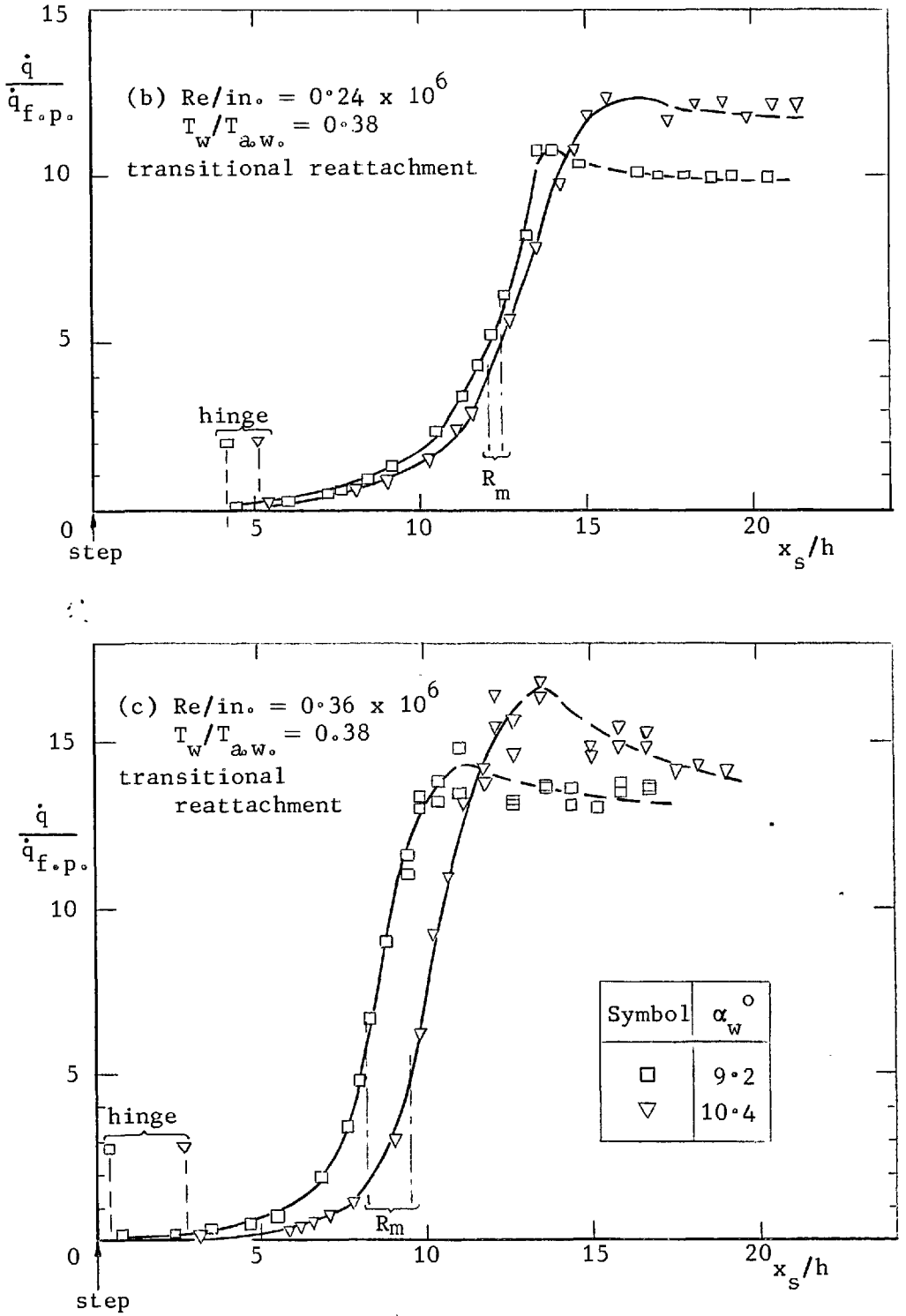

FIG. 42. concluded.

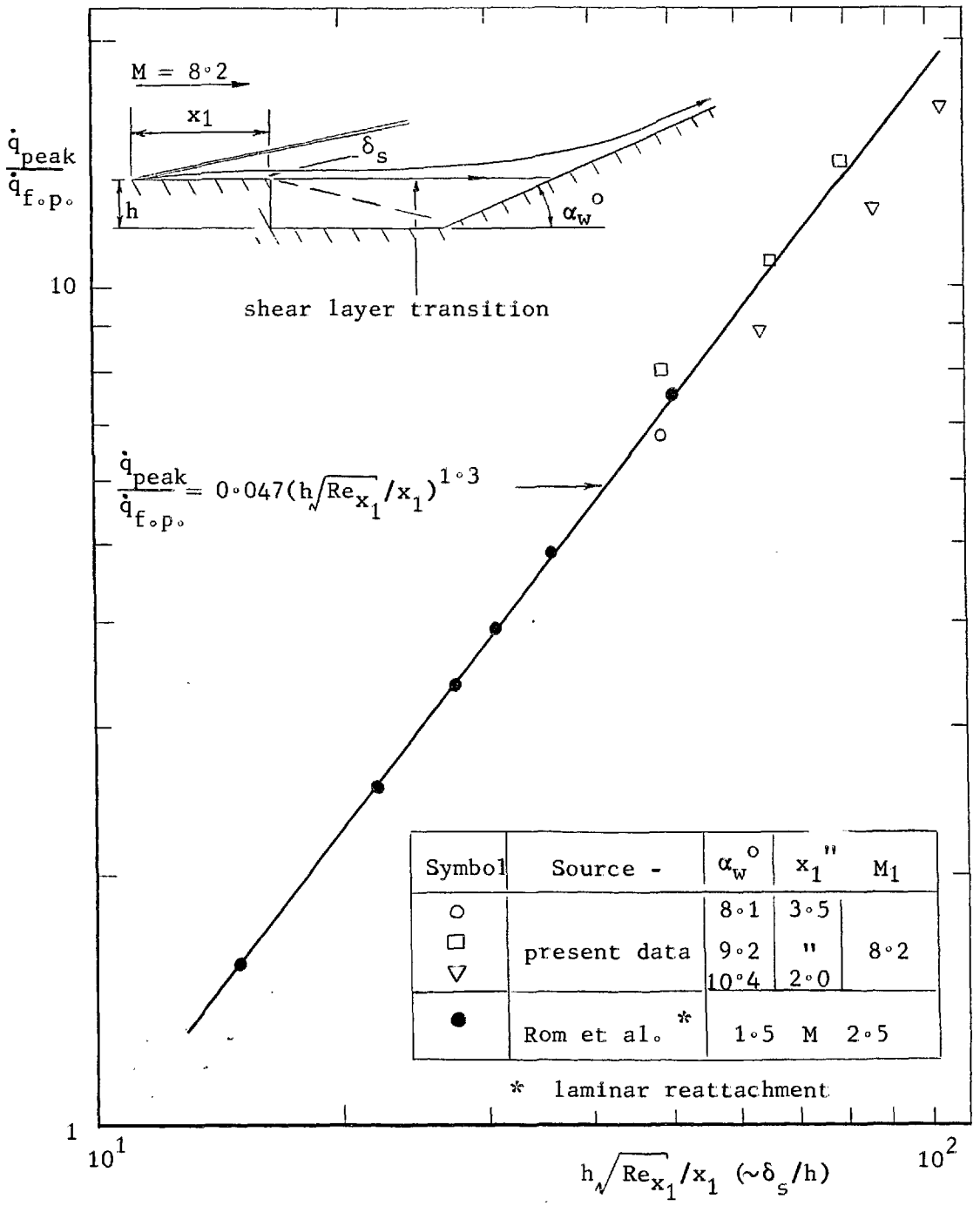

FIG. 43. Correlation of the reattachment peak heat transfer rate with the boundary layer thickness at separation.